# Mechanically-activated assembly of monodisperse metal-based nanoparticles: a novel, simple and sustainable means to access chalcogenide nanoparticles

A thesis submitted to McGill University
in partial fulfillment of the requirements of the
Degree of Master's in Chemistry

by

Michael Yossef Malca

Department of Chemistry

McGill University

Montreal, Quebec, Canada

May 2017

## Abstract

As sustainable practices become increasingly relevant in chemistry, and the realm of nanomaterial synthesis rapidly expands, efforts have been made to develop greener methods to access these valuable materials with fine control over size, monodispersity, shape and surface chemistry, while opening access to large-scale syntheses. While high-quality nanomaterials are presently accessed mostly by solution methods, these are not compatible with sustainable manufacturing due to large solvent and energy input. This thesis describes a unique, unprecedented synthesis of select metal-based nanoparticles (NPs) in the solid state through mechanically-activated spontaneous assembly, without requiring bulk solvents or heat. We first explore the possibility of accessing bismuth sulfide NPs and found that through this method of synthesis, highly monodisperse 2 nm nanoparticles formed systematically regardless of the grinding time, method of grinding, or amount of ligand present. These are the smallest NPs of bismuth sulfide ever reported, suggesting a distinct mechanism of nucleation and growth of NPs under solid-state conditions from that of solution-based methods, and therefore the possibility of accessing novel nanomaterials through this method. By varying the type of ligand, both organo- and water-suspendable products could be accessed, and the latter showed a significant radiodensity for their application as contrast agents in Computed Tomography imaging. We also show that PEGylation of these nanoparticles can be achieved *in situ* without additional steps post-synthesis. Next, we explore whether other metal-sulfide nanoparticles can be accessed via this route and turn to accessing nanoparticles of cadmium sulfide and zinc sulfide, which have numerous applications in optical-based devices and medical diagnostics. Once again, highly monodisperse nanoparticles were obtained in both cases (2.8-3.6 nm and 2.4-2.8 nm, respectively), and both showed fluorescent activity in the blue-range indicative of ultra-small quantum dots. In all cases, the reaction could be linearly scaled-up with ease in a planetary mill to achieve gram-scale quantities of product. Finally, given the increasing relevance of PEGylation in nanomedicine and drug development, we explored the possibility of accessing $\gamma$-functionalized derivatives in solid-state, eschewing the need for a solvent milieu. We find that –OTs, -Br, -SH, -$NH_2$ and –COOH terminated PEG can be obtained rapidly and in

good to quantitative yields with minimal mechanical input. With these results in mind, we hope that our promising results establish further research in accessing monodisperse nanomaterials through mechanochemistry as well as mechanistic elucidation of NP nucleation and growth under solid-state conditions.

## Résumé

Le développement de réactions chimiques dans le cadre de la chimie verte s'accélère, notamment pour la synthèse de nanomatériaux. En plus de l'aspect environnemental, une grande exigence au niveau de la taille, la monodispersité, la forme géométrique et la surface chimique de ces matériaux est requise. Tandis que les réactions en phase liquide permettent de produire des nanomatériaux de haute qualité, l'utilisation de grandes quantités de solvants et d'apport énergétique limitent leur utilisation dans les procédés de fabrication à grande échelle. Ainsi, nous avons choisi d'explorer la synthèse en phase solide de nanomatériaux.

Ce mémoire décrit la synthèse unique et inédite de nanoparticules (NPs) à base de métaux en phase solide s'assemblant spontanément suite à un apport minimal d'énergie mécanique, cela sans utiliser de solvant ou de chaleur. Nous avons tout d'abord exploré la possibilité d'obtenir des NPs de sulfure de bismuth et nous avons obtenu des nanoparticules de 2 nm extrêmement monodispersées, indépendamment du temps ou des méthodes de broyage ou de la quantité de ligand présent. Ce sont les plus petites NPs de sulfure de bismuth reportées dans la littérature, et les résultats suggèrent un mécanisme de nucléation et de croissance des NPs qui soit distinct des méthodes en phase liquide. Cela ouvre par conséquent la possibilité d'obtenir de nouveaux nanomatériaux grâce à cette méthode. En modifiant le type de ligand, des produits dispersables dans des solvants organiques ou dans l'eau peuvent être obtenus, et ces derniers présentent une radiodensité significative dans leur application en tant qu'agents de contraste en imagerie tomographique. Nous avons aussi montré que la PEGylation de ces nanoparticules pouvait être réalisée *in situ* sans aucune étape supplémentaire. Par la suite, nous avons découvert que des nanoparticules de sulfure de cadmium ou de sulfure pouvaient être obtenues via cette méthode, qui ont de nombreuses applications en instrumentation optique et en diagnostic médical. Là aussi, des nanoparticules hautement monodispersées ont été obtenues dans les deux cas (2.8-3.6 et 2.4-2.8 nm respectivement) et les deux possèdent une activité fluorescente dans la gamme du bleu, ce qui est caractéristique des points quantiques de petite taille. Dans tous les cas, les particules peuvent être produites à l'échelle du gramme avec un broyeur planétaire à billes. Finalement, vu l'importance du

PEGylation dans le développement pharmaceutique et nano-médecine, nous avons explore la possibilité d'accéder les dérivés $\gamma$-fonctionnalisés à l'état solide, ce qui évite le besoin d'un milieu liquide. Les PEG termines par –OTs, -Br, -SH, -$NH_2$ et –COOH peuvent être synthétises sure une échelle de rendement allant de bon a quantitatif utilisant une force mécanique minimale. Nous espérons que nos résultats prometteurs inciteront à plus de recherches sur la synthèse mécanochimique de nanomatériaux monodispersés, ainsi qu'à l'élucidation du mécanisme de nucléation et de croissance en phase solide des NP.

To my mother, may she be blessed

“And if you don’t know, now you know”

- Biggie Smalls

## Acknowledgements

I would like to begin by thanking Dr. Audrey Moores, not only for her remarkable support and shaping me into the scientist I am today, but also for helping me grow into the man I am. You have always been a mentor to me; the greatness you have achieved and the well of knowledge you possess has been a light of inspiration throughout my studies. You gave me the opportunity to explore, to learn, cultivate and utilize my strengths, and challenged me to become a better person overall, and for this I will always be grateful.

Dr. Tomislav Friščić, thank you for everything you've done for me and for the many stimulating conversations we've have. You've given me incredible guidance when most needed, and your unwavering cheerful demeanor and humor always made me feel light on my feet. I'm very lucky to have gotten to work with you.

Dr. Joseph Matt Kinsella, it was such a great opportunity to work with you. You taught me a great deal during the time we worked together. Your multidisciplinary skillset, and the ease in which you can relate to the people around you are some of your many qualities I admire greatly and learned from.

I would also like to thank the silent leaders I have met over the course of my stay at McGill that I have consulted with and learned from, and were friends at integral parts of my academic career. To name a few: Dr. Dusica Maysinger, Dr. Hanadi Sleiman, Dr. Mark Andrews, Dr. Terry Hebert and Dr. Ursula Stochaj.

There are several funding agencies and programs that have been important to my research: Green Chemistry NSERC Collaborative Research and Training Experience (CREATE), Hydro-Quebec, Centre for Green Chemistry and Catalysis (CGCC), JCF Montreal and the McGill Chemistry Department. Thank you Dr. Audrey Moores, Dr. Tomislav Friščić, and Dr. Joseph Matt Kinsella for additional funding for travel and conferences throughout my studies.

To my fellow lab mates, past and present - Alain (JTB), Alexandra, Allen, Andreanne, Blaine, Hava, Huizhi, Julio, Luis Carlos, Madhu, Mary, Mikel, Mitra, Monika, Olivia, Paul, Pierre-Olivier, Thomas and Yuting - I am blessed to have had the chance to worked alongside you guys.

To the Friščić Group: you guys have all been awesome, extremely helpful, and a pleasure to be around. Shout out to Louis Do for knowing everything about everything.

To my boys – Gad, Jeremie, Jim, Jordan, Kevin, Laurent, Levi, Manu, Mendel, Ovadia and Yair - thank you for helping me build my tolerance. I couldn't have made it through grad school without you. A special thanks to Gabriel for his scientific insight.

To my family: I love you all.

## Contribution of Authors

All chapters presented in this thesis were first drafted by Michael Y. Malca. All chapters were edited by Dr. Audrey Moores and Dr. Tomislav Friščić. All experiments, data collection and analyses were performed by Michael Y. Malca under Dr. Audrey Moores' and Dr. Tomislav Friščić's supervision, unless otherwise specified below.

Chapter 2: the manuscript was additionally edited by Dr. Joseph Matt Kinsella for clarity and for publication purposes. Dr. Huizhi Bao helped with some XPS and TEM analysis, and performed the ICP-MS experiments. She also performed the MALDI-TOF experiments with the sincere assistance of Dr. Nadim Saadé. She also taught me some TEM techniques pertinent for clear imaging. Mr. Thomas Bastaille performed preliminary reactions that are not presented in this thesis, but aided in directing the research.

Chapter 4: Mr. Pierre-Olivier Ferko performed some reactions that are not presented in this thesis, but aided in directing the research.

## Table of Contents

## List of Figures

## List of Schemes

## List of Tables

# Chapter 1 Introduction

## 1.1 Definitions and Theoretical Aspects

Mechanochemistry is a field of chemistry concerned with reactions performed by input of mechanical energy. Recently, it became a promising route to circumvent the need for bulk solvents and heat-intensive synthetic procedures. The advantages of generating minimal waste with high atom economy, as well as its environmental soundness make this method particularly attractive,[1,2] and its ease of scalability also makes it adaptable to industrial uses, provided the accessibility of equipment.[3,4] Mechanochemistry has found broad application, *e.g.* in making metal-based nanocrystals (oxides[5,6], sulfides[7,8], selenides,[9,10] *etc.*), metal-organic frameworks,[11,12] pharmaceutical co-crystals,[12,13] as well as in organic transformations[14].

The International Union for Pure and Applied Chemistry (IUPAC) defines a mechano-chemical reaction as 'induced by direct absorption of mechanical energy', *e.g.* by grinding, shearing or stretching.[15] These processes can be achieved in several ways, for example by mixer milling (linear grinding) and planetary milling (rotational) but can also be achieved by mortar and pestle grinding in some cases.[16,17] In the laboratory, one or more balls are used as milling media to deliver energy to reactants, prompting their comminution and mixing at a set frequency (usually 25-30 Hz). While a range of ball-to-powder ratios, between 1:1 and 200:1 by weight), have been investigated in the literature, this value can vary depending on the reaction and is commonly kept at $\sim 10:1$[18,19]. Commonly used milling assembly materials are agate, stainless steel, teflon and tungsten carbide.

Mechanistic pathways of mechanochemical reactions have been proposed and refined over the past decades. The term 'mechanochemistry' is claimed to have been introduced by W. Ostwald,[20,21] and received early recognition when it was shown that grinding can lead to different results than heating.[22] However, mechanistic elucidation of mechanochemical reactions has proven difficult. Considerations of frictional heating during milling or grinding led to hot spot theory[23] and the magma-plasma model[18,24] as early mechanistic explanations for mechanochemical transformation. Briefly, the hot-spot theory considers lateral friction between

two surfaces, predicting that temperature jumps exceeding $1000\ \mathrm{K}$ over an area of $1\mu m^2$ can be achieved on the nanosecond scale. The magma-plasma model finds that contact between colliding interfaces can produce local temperatures $>10^3\ \mathrm{K}$, leading to short-lived plasma states. However, such mechanisms should be taken with reserve, as they should also lead to severe decomposition which is hardly ever seen in mechanochemical reactions.[25] This is especially true for reactions by gentle grinding in a mortar, milling under mild conditions (*e.g.* low frequency, or non-metallic milling assemblies). However, frictional heating could lead to bulk heating of the reaction vessel, which may promote the reaction.[19,26] It was shown that bulk temperatures can reach up to $100\ ^\circ C$ and $200\ ^\circ C$ in mixer and planetary mills[27], respectively, but can vary significantly depending on the amount and type of materials used, jar makeup and size, grinding method, and milling frequency. A recent Raman spectroscopy study of the reaction between ZnO and imidazole to form a zeolitic imidazole framework materials ZIF-6 showed little sensitivity to temperature, but was strongly dependent on the milling frequency, which was assumed to be proportional to the frequency of reactive collisions between reactant particles[28]. However, *in situ* powder X-ray diffraction (PXRD) studies of mechanochemical reaction of $CdCl_2$ and cyanoguanidine (cnge) at different temperatures showed a strong temperature dependence of reactions kinetics.[26] Within this context, the physical effects on the precursors should be noted due to their implications in allowing some mechanochemical reactions to occur. Many processes in grinding can contribute to the overall reactivity of a solid such as comminution of bulk materials into smaller sizes and their accompanying increase in surface area, intimate mixing of reactants, defect formation and amorphization, and frictional heating within the reaction chamber[25,29]. Depending on reaction conditions and the choice of materials used, one or more processes can be suspected to be involved in mechanochemical reactions, and at this stage ought to be evaluated on a case-by-case basis.

Mechanical activation is a term coined in 1942 by Smékal, who described it as a process that increases the reaction potential of a substrate without affecting its chemical composition, *i.e.* manifesting through a change in its physical properties.[18] This concept was further detailed to include accumulation of crystal defects, amorphization and formation of metastable polymorphs, which all lead to enhanced reactivity.[18] Lyachov in 1993 regarded mechanical

activation as mediated by structural relaxation, and presented a relaxation curve of activated states as a function of time.[30] Within this context, Balàž *et al.* suggested that one could not influence the reactivity of solids whose relaxation times are shorter than the characteristic time of the reaction itself.[18] Relaxation processes can include formation of new surfaces, aggregation, adsorption, and chemical reaction between nearby particles.[31] In the context of chemical synthesis, milling plays an important role of sequestering products by attrition, exposing fresh reactant surfaces and allowing the reaction to proceed.[32,33]

While mechanochemistry has been used conservatively to define solid-phase reactions, it does not necessarily exclude the participation of small quantities of solvents within the reaction medium[25]. For example, hydrated metal salts can be used in mechanochemical reactions, and moisture from the atmosphere can also contribute to the overall nature of the reaction[25]. Catalytic or substoichiometric amounts of solvent have also been shown to increase, or all-together allow the reaction of precursors in solid-state[34], affording reactions categorized under the term Liquid-assisted grinding (LAG)[35]. For example, Katritzky and his colleagues in 2005 proposed an Aryl N-thiocarbamoyltriazole as a reaction intermediate in the synthesis of a thiourea from aniline and bis(1-benzotriazolyl)methanethione, but could not be isolated from solution due to rapid dissociation into isothiocyanate[36]. Under solid-state conditions by LAG, Štrukil and his colleagues in 2015 were able to identify this intermediate, isolate it and even obtain it in quantitative yields[37]. This exemplifies that mechanochemistry may open access to materials that would otherwise be difficult or even unachievable through solvothermal methods, in which solvation effects direct the reaction to other end-products[38,39,36]. Solvation effects have been sparingly studied within the context of mechanochemical-based nanomaterial synthesis, but have been investigated for co-crystal formation and metal-organic framework syntheses[40,41]. For example, Braga et al. studied the effects of different vapor solvents in accelerating the co-crystal formation between a ferrocenyl complex ([Fe($\eta^2$-$C_5H_4$-$C_5H_4N)_2$]) and pimelic acid, and observed that the solubility of the reactants in the vapor used played a fundamental role in accessing different co-crystal polymorphs[42]. They suggested that this method of "vapor digestion" creates a *solution-like* environment on the grain surfaces whereby the reactants dissolve and the product immediately precipitates out. From this, it suggests that the solvent acts

like a catalyst for interaction between solids. Shan and her colleagues also found that solubility is critical in the acceleration of reaction kinetics in the co-crystal formation between $C_6H_9(COOH)_3$ and 4,7-phenanthroline[43]. As such, solvation may play an important mechanistic role in accessing materials under solid-state conditions[40,44]. On the other hand, it has also been shown that solvent may simply allow a global medium in which the probability of solids 'seeing one another' increases by forming mobile surface layers[45] – given that a reaction between solids is by definition not homogeneous[46] - and in this case would not be dependent on the solubility of the starting materials within the liquid. Friščić suggested the parameter $\eta$ as a quantitative measure to enable comparison of mechanochemical, solvent-mediated and solution techniques. The η parameter is defined as the ratio of added liquid volume to the weight of reactants, expressed in $\mu L/mg$.[45] In that way, reactions can take place by neat grinding ($\eta = 0\ \mu L/mg$), LAG ($\eta = 0 - 1\ \mu L/mg$), a slurrying ($\eta > 1\ \mu L/mg$) or in homogeneous solution ($\eta > 10\ \mu L/mg$)[45].

## 1.2 Mechanical Activation and the Role of Aging

'Aging' a reaction is a long standing concept in history, but has only recently been investigated in further detail within a chemistry paradigm. This chemical process is inspired by natural mineral weathering processes, during which a material slowly reacts with its environment. A relatable example of aging is rusting of iron when exposed to an oxidative atmosphere. Traditionally, aging was performed over a 2-3 month period to produce white lead ($2\ PbCO_3 \cdot Pb(OH)_2$) pigment for oil painting by covering sheets of lead in dung (which evolved $CO_2$ overtime) in the presence of moisture in the air and acetic acid as a catalyst.

From a microscopic perspective, lattice imperfections can allow for reaction of substrates at their interface. For instance, Prout and Tompkins studied the decomposition of $KMnO_4$ and proposed that line dislocations in this material allowed for reaction and product formation (indefinite composition, but comprising $MnO_2$) on the crystal surface, causing strain and cracking of the crystallite, and forming new surfaces in this way[47]. However, as a generalized concept, the time scale in which this process occurs can be long, and assuming no mobile component is involved or spontaneous decomposition occurs, may not progress homogenously or be impeded

by product sequestration[48]. Aging of solid-state reactions has been shown to be accelerated to reasonable times by altering mobility within the solid medium[42], for instance by placing reaction vessels in the presence of water[49,50] or organic vapor[51], which, similar to solvent in LAG, allows for increased mass transfer between solid reagents and can contribute to their defect-mediated interaction. Considering this, a liquid starting material, minimal solvent, intermediate gas evolution or atmospheric conditions, to name a few, can also contribute this acceleration.

### 1.3 Accessing Nanomaterials in Solid-State

Nanoparticle research has become increasingly relevant nowadays to resolve gaps in a number of disciplines, including chemical catalysis[52,53,54], drug delivery[55,56,57], and medical diagnostics and imaging[58,59,60]. Their syntheses generally can be categorized into two methods: the top-down and bottom-up approach[61]. The top-down approach involves the comminution of bulk materials into micro- and nano-clusters. However, it suffers from a number of limitations in terms of product quality, as it affords nanoparticles with a broad distribution of size and shape and surface defects originating from mechanical wear[5,62]. It is however successfully used in applications such as contaminated water remediation[63]. The bottom-up approach involves assembling particles from molecular metal precursors and may happen in the gas phase or in solution. In the former, a number of techniques have been reported following this scheme, such as chemical vapour deposition[64], e-beam[65], thermal[66] and non-thermal plasma[67]. These techniques are effective at providing a variety of nanomaterials, including binary materials and pure metals, formed free, or over a broad range of supports. They do however suffer from limitations, including polydispersity issues and reliance on fairly extreme conditions in terms of temperature, high vacuum or e-beam dependence. Solution-based (or solvothermal) methods are so far the most performant in providing fine control over the nanomaterial features. These methods rely on the use of molecular precursors to the nanomaterial; capping agents to control seeding, direct nanoparticle growth and finely cap the resulting nanomaterial; reducing agent if necessary and a solvent. Under a solution-based bottom up approach, atomic units stochastically associate with one another forming tentative clusters[68]. These clusters are inherently unstable,

and can dissociate back into atomic units, but once they reach a critical radius whereby the bulk energy released compensates for the increase in surface tension, they can nucleate the growth of a nanocrystal with thermodynamic incentive (Figure 1.1)[68]. Equation 1 describes a classical mathematical model of the total free energy associated with nanocrystal growth:

$$\Delta G = 4\pi r^2 \gamma - \frac{4}{3}\pi r^3 \Delta G_v \quad (1)$$

where $\gamma$ is the surface energy per unit area for a nanocrystal of radius r, and $\Delta G_v$ is the free energy of the bulk crystal.

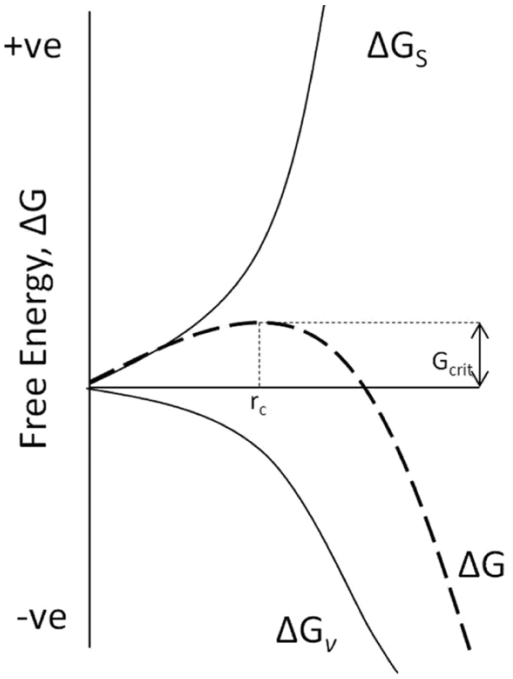


**Figure 1. 1.** Free energy diagram associated with nanocrystal growth. $\Delta G_v$ and $\Delta G_s$ are the bulk and surface free energy of a crowing cluster, respectively. $r_c$ is the critical radius at which $\Delta G_v \geq \Delta G_s$. Adapted from reference 68.

The rate of nucleation can be controlled by several parameters, such as concentration, temperature and surface free energy.[68] The latter depends largely on the choice of ligand used to cap the growing clusters and hinder their growth, enabling control over the size of resulting nanoparticles. More crystalline products tend to be obtained at higher temperatures, due to greater ligand mobility and rectification of defects within the crystal structure.[69] Solvent provides

a medium for which thermal energy can distribute uniformly across the system, allowing greater control over the size, shape, and dispersity of the end product. Typically in such schemes, solvent is used in large excess to ascertain seeding and growth of nanomaterial takes place while limiting the probably of collision between two nanoparticle in formation[70,71].

Given the rapid expansion of this field and its application in a number of different disciplines, efforts have been made to develop more sustainable synthetic methods to access these high-value materials with fine control over size, monodispersity, shape and surface chemistry, while opening access to large scale syntheses[72,73,74]. While solvent-based systems are most convenient in accessing high-quality nanomaterials, the large use of solvents and energy input limits its use in sustainable manufacturing processes. As such, we decided to explore the possibility of accessing nanomaterials under mechanochemical conditions that limit the use of solvent and energy, while opening up the possibility of accessing novel end products. Whereas the mechanism for co-crystal formation and organic reactions under mechanochemical pathways have been more deeply investigated[75,76,77,78], nanomaterial synthesis, particularly nanoparticles for our interest, remains more elusive and is usually generalized under the physical manifestations that grinding inflicts on the starting materials[18,79]. However, this relates more to products that are accessed under the mechanochemical top-down approach that typically yields polydisperse in nature and are not up to par with solvothermal methods for accessing high-quality nanocrystals. On the other hand, accessing monodisperse nanoparticles in the solid state has been much less explored. Our group reported a novel, scalable method of accessing ultra-small monodisperse gold nanoparticles by milling.[80] By making use of solid amine ligands of different chain lengths $(C_{15} - C_{18})$, particles with diameters between 1 nm and 4 nm were selectively obtained,[80] depending on ligand choice and amount. The ability to obtain such surprisingly small NPs can be rationalized in two ways: first, nucleation and growth of nanocrystals in solution are thermodynamically favorable at low temperatures since the dissolution of nanoclusters increase drastically with increasing temperature[69]. High temperatures are employed in solution-based syntheses to overcome kinetic barriers in the formation of successful critical nuclei, and in parallel produce nanoparticles that can be nucleated with smaller radii ($r_c$s)[69]. In the solid state, there is limited or no opportunity for dissolution, potentially

mitigating this need for high temperatures while allowing for smaller clusters to nucleate nanoparticle growth. Therefore, while nanocrystal growth and dissolution are known exothermic processes in solution[69], the latter may not be in the solid state. Second, the restricted mobility of surface-bound ligands and monomer diffusion in the solid state may limit opportunity for Ostwald ripening, coalescence or oriented attachment of crystallographic planes to occur. Altogether, this suggests that smaller nanoparticles (nucleated by smaller $r_c$s) may actually be more favorable under solvent-free conditions when a ligand is employed. Other zero-valent metal nanoparticles (Au, Pd, Ru, Re, Ag) have been synthesized by our group using lignin as a reducing agent.[61] With these results in mind, our goal was to determine if nanoparticles of binary metal sulfides could also be synthesized under mechanochemical conditions. Achieving this would favorably compare with traditional synthetic protocols for nanoparticle synthesis, which generally involve large amounts of solvents, multistep processing, heat and/or often hazardous reagents. In the following chapters, we show for the first time that highly monodisperse $Bi_2S_3$[81], ZnS, and CdS nanoparticles can be accessed via a mechanochemical route in the presence of a capping agent. To the best of our knowledge, the $Bi_2S_3$ nanoparticles formed are the smallest ever reported, and advocates the opportunity to access unique nanomaterials in solid-state. The ease of scalability also makes this process ideal for accessing gram-scale quantities of these nanomaterials in a highly atom-economical and sustainable fashion.

## 1.4 Description of the Thesis

Chapter 2 of this Thesis discusses the synthesis of $Bi_2S_3$ nanoparticles by a mechanical activation and aging methodology, and their potential use as contrast agents in computed tomography imaging. In Chapter 3, we show this methodology is adaptable to accessing ZnS and CdS quantum dots with blue-emitting fluorescent activity. Chapter 4 deals with accessing poly(ethylene glycol) derivatives in the solid state, which may have significant applications in interfacing nanomaterials and medicine. Finally, Chapter 5 offers concluding remarks on the work presented, refinement of the definition of mechanoactivation, and future work.

## 1.5 References


1. Bowmaker, G. A. *Chem. Commun.* **2013**, *49* (4), 334–348.
2. Friščić, T.; James, S. L.; Boldyreva, E. V; Bolm, C.; Jones, W.; Mack, J.; Steed, J. W.; Suslick, K. S. *Chem. Commun. (Camb).* **2015**, *51* (29), 6248–6256.
3. Baig, R. B. N.; Varma, R. S. *Chem. Soc. Rev.* **2012**, *41* (4), 1559–1584.
4. Jiménez-González, C.; Constable, D. J. C.; Ponder, C. S. *Chem. Soc. Rev.* **2012**, *41* (4), 1485–1498.
5. Šepelák, V.; Düvel, A.; Wilkening, M.; Becker, K.-D.; Heitjans, P. *Chem. Soc. Rev.* **2013**, *42* (18), 7507.
6. Yang, H.; Hu, Y.; Zhang, X.; Qiu, G. *Mater. Lett.* **2004**, *58* (3–4), 387–389.
7. Tsuzuki, T.; Ding, J.; McCormick, P. G. *Phys. B Condens. Matter* **1997**, *239* (3–4), 378–387.
8. Balaz, P.; Bastl, Z.; Boldizarova, E. *J. Solid State Chem.* **1999**, *144* (1), 1–7.
9. Achimovičová, M.; Daneu, N.; Rečnik, A.; Ďurišin, J.; Peter, B.; Fabián, M.; Kováč, J.; Šatka, A. *Chem. Pap.* **2009**, *63* (5), 562–567.
10. Klose, E.; Blachnik, R. *Thermochim. Acta* **2001**, *375* (1–2), 147–152.
11. Stock, N.; Biswas, S. *Chem. Rev.* **2012**, *112* (2), 933–969.
12. Friščić, T. *Chem. Soc. Rev.* **2012**, *41* (9), 3493.
13. Braga, D.; Maini, L.; Grepioni, F. *Chem. Soc. Rev.* **2013**, *42* (18), 7638.
14. Boldyreva, E. *Chem. Soc. Rev.* **2013**, *42* (18), 7719.
15. McNaught, A.; Wilkinson, A. *IUPAC Compendium of chemical terminology*, 2nd ed.; Oxford: Blackwell Science, 1997.
16. Adhikari, S.; Ghosh, A.; Mandal, S.; Sahana, A.; Das, D. *RSC Adv.* **2015**, *5* (43), 33878–33884.
17. Takacs, L. *J. Therm. Anal. Calorim.* **2007**, *90* (1), 81–84.
18. Baláž, P.; Achimovičová, M.; Baláž, M.; Billik, P.; Cherkezova-Zheleva, Z.; Criado, J. M.; Delogu, F.; Dutková, E.; Gaffet, E.; Gotor, F. J.; Kumar, R.; Mitov, I.; Rojac, T.; Senna, M.; Streletskii, A.; Wieczorek-Ciurowa, K. *Chem. Soc. Rev.* **2013**, *42* (18), 7571.
19. Suryanarayana, C. *Prog. Mater. Sci.* **2001**, *46* (1–2), 1–184.
20. Oswald, W. *Lehrbuch der Allgemeinen Chemie*, 2nd ed.; Aufgabe: Leipzig, 1886.
21. Baláž, P. *Mechanochemistry in Nanoscience and Minerals Engineering*; Berlin Heidelberg, 2008.
22. Takacs, L. *J. Mater. Sci.* **2004**.
23. Bowden, F.; Yoffe, A. *Initiation and growth of explosion in liquids and solids*; Cambridge University Press: Cambridge, 1952.
24. Thiessen, P. A.; Meyer, K.; Heinicke, G. *Grundlagen der Tribochemie*; Akademie-Verlag: Berlin, 1967.
25. James, S. L.; Adams, C. J.; Bolm, C.; Braga, D.; Collier, P.; Friščić, T.; Grepioni, F.; Harris, K. D. M.; Hyett, G.; Jones, W.; Krebs, A.; Mack, J.; Maini, L.; Orpen, A. G.; Parkin, I. P.; Shearouse, W. C.; Steed, J. W.; Waddell, D. C. *Chem. Soc. Rev.* **2012**, *41* (1), 413–447.
26. Užarević, K.; Štrukil, V.; Mottillo, C.; Julien, P. A.; Puškarić, A.; Friščić, T.; Halasz, I. *Cryst. Growth Des.* **2016**, *16* (4), 2342–2347.
27. Takacs, L.; McHenry, J. S. *J. Mater. Sci.* **2006**, *41* (16), 5246–5249.

28. Ma, X.; Yuan, W.; Bell, S.; James, S. *Chem. Commun.* **2014**.
29. Boldyrev, V. V.; Tkáčová, K. *J. Mater. Synth. Process.* **2000**, *8* (3/4), 121–132.
30. Lyachov, N. Z. *Proceedings of the 1st International Conference on Mechanochemistry*, Vol. 1.; Tkáčová, K., Ed.; Cambridge Interscience Publishing: Cambridge, 1993.
31. Boldyrev, V. V. *Proc. Indian. natn. Sci. Acad.* **1986**, *1* (52), 400–417.
32. Gracin, D.; Štrukil, V.; Friščić, T.; Halasz, I.; Užarević, K. *Angew. Chemie* **2014**, *126* (24), 6307–6311.
33. Kaupp, G. *CrystEngComm* **2003**, *5* (23), 117.
34. Do, J.-L.; Friščić, T. *ACS Cent. Sci.* **2017**, *3* (1), 13–19.
35. Cruz-Cabeza, A.; Karki, S.; Fabian, L.; Friščić, T. *Chemical* **2010**.
36. Katritzky, A. R.; Witek, R. M.; Rodriguez-Garcia, V.; Mohapatra, P. P.; Rogers, J. W.; Janet, C.; Ashraf A. A., A.-F.; Steel‖, P. J. *J. Org. Chem* **2005**, *70*, 7866–7881.
37. Štrukil, V.; Gracin, D.; Magdysyuk, O. V.; Dinnebier, R. E.; Friščić, T. *Angew. Chemie Int. Ed.* **2015**, *54* (29), 8440–8443.
38. Komatsu, K.; Wang, G.-W.; Murata, Y.; Shiro, M. *Nature* **1997**, *387* (6633), 583–586.
39. Tan, D.; Mottillo, C.; Katsenis, A. D.; Štrukil, V.; Friščić, T. *Angew. Chemie* **2014**, *126* (35), 9475–9478.
40. Trask, A. V.; Motherwell, W. D. S.; Jones, W. *Chem. Commun.* **2004**, *0* (7), 890–891.
41. Halasz, I.; Friščić, T.; Kimber, S. a. J.; Užarević, K.; Puškarić, A.; Mottillo, C.; Julien, P.; Strukil, V.; Honkimaki, V.; Dinnebier, R. E. *Faraday Discuss.* **2014**, No. 170, 203–221.
42. Braga, D.; Giaffreda, S. L.; Grepioni, F.; Chierotti, M. R.; Gobetto, R.; Palladino, G.; Polito, M.; Mathre, D. J.; Dormer, P. G.; Euler, D. H.; Ball, R. G.; Ye, Z.; Wang, Y.; Santos, I. *CrystEngComm* **2007**, *9* (10), 879.
43. Shan, N.; Toda, F.; Jones, W. *Chem. Commun. (Camb).* **2002**, No. 20, 2372–2373.
44. Cinčić, D.; Friščić, T.; Jones, W. *J. Am. Chem. Soc.* **2008**, *130* (24), 7524–7525.
45. Friščić, T.; Childs, S.; Rizvi, S.; Jones, W. *CrystEngComm* **2009**.
46. Berry, R.; Rice, S.; Ross, J. *Matter in equilibrium: statistical mechanics and thermodynamics*; Oxford University Press: USA, 2002.
47. Brown, M. E.; Dollimore, D.; Galwey, A. K.; Bamford, C. H.; Tipper, C. F. H. *Comprehensive Chemical Kinetics: Reactions in the Solid State*, 22nd ed.; Elsevier Scientific Pub. Co.: New York, 1980.
48. West, A. R. *Solid state chemistry and its applications*, 2nd ed.; John Wiley & Sons: Chichester, 2014.
49. Cliffe, M. J.; Mottillo, C.; Stein, R. S.; Bučar, D.-K.; Friščić, T.; Nowell, H.; Allan, D. R.; Poliakoff, M.; Schröder, M.; Liu, X.; DuChene, J. S.; Zhang, H.; Zhang, Q.; Chen, X.; Ma, J.; Loo, S. C. J.; Wei, W. D.; Yang, Y.; Hupp, J. T.; Huo, F. *Chem. Sci.* **2012**, *3* (8), 2495.
50. Mottillo, C.; Lu, Y.; Pham, M.-H.; Cliffe, M. J.; Do, T.-O.; Friščić, T.; Shimizu, G. K. H.; Shankland, K.; Brammer, L.; Liu, X.; DuChene, J. S.; Zhang, H.; Zhang, Q.; Chen, X.; Ma, J.; Loo, S. C. J.; Wei, W. D.; Yang, Y.; Hupp, J. T.; Huo, F. *Green Chem.* **2013**, *15* (8), 2121.
51. Braga, D.; Grepioni, F.; Maini, L.; Mazzeo, P. P.; Ventura, B. *New J. Chem.* **2011**, *35* (2), 339–344.
52. Turner, M.; Golovko, V.; Vaughan, O.; Abdulkin, P. *Nature* **2008**.
53. Zeng, T.; Chen, W.; Cirtiu, C.; Moores, A.; Song, G. *Green* **2010**.
54. Hudson, R.; Li, C.; Moores, A. *Green Chem.* **2012**.

55. Cho, K.; Wang, X.; Nie, S.; Shin, D. *Clin. cancer Res.* **2008**.
56. Irvine, D. J. *Nat. Mater.* **2011**, *10* (5), 342–343.
57. Wang, A. Z.; Langer, R.; Farokhzad, O. C. *Annu. Rev. Med.* **2012**, *63* (1), 185–198.
58. Georganopoulou, D. G.; Chang, L.; Nam, J.-M.; Thaxton, C. S.; Mufson, E. J.; Klein, W. L.; Mirkin, C. A. *Proc. Natl. Acad. Sci. U. S. A.* **2005**, *102* (7), 2273–2276.
59. Cormode, D. P.; Naha, P. C.; Fayad, Z. A. *Contrast Media Mol. Imaging* **2014**, *9* (1), 37–52.
60. Kodiha, M.; Hutter, E.; Boridy, S.; Juhas, M.; Maysinger, D.; Stochaj, U. *Cell. Mol. Life Sci.* **2014**, *71* (21), 4259–4273.
61. Rak, M. J.; Friščić, T.; Moores, A. *Faraday Discuss.* **2014**, *170* (0), 155–167.
62. Šepelák, V.; Bégin-Colin, S.; Le Caër, G. *Dalt. Trans.* **2012**, *41* (39), 11927.
63. Grieger, K. D.; Fjordbøge, A.; Hartmann, N. B.; Eriksson, E.; Bjerg, P. L.; Baun, A. *J. Contam. Hydrol.* **2010**, *118* (3), 165–183.
64. Palgrave, R. G.; Parkin, I. P. *J. Am. Chem. Soc.* **2006**, *128*, 1587–1597.
65. Mendes, P. M.; Jacke, S.; Critchley, K.; Plaza, J.; Chen, Y.; Nikitin, K.; Palmer, R. E.; Preece, J. A.; Evans, S. D.; Fitzmaurice, D. *Langmuir* **2004**, *20*, 3766–3768.
66. Ren, G.; Hu, D.; Cheng, E. W. C.; Vargas-Reus, M. A.; Reip, P.; Allaker, R. P. *Characterisation of copper oxide nanoparticles for antimicrobial applications*; 2009; Vol. 33.
67. Moreno-Couranjou, M.; Monthioux, M.; Gonzalez-Aguilar, J.; Fulcheri, L. *Carbon N. Y.* **2009**, *47* (10), 2310–2321.
68. Thanh, N. T. K.; Maclean, N.; Mahiddine, S. *Chem. Rev.* **2014**, *114* (15), 7610–7630.
69. Van Embden, J.; Mulvaney, P. *Langmuir* **2005**, *21* (22), 10226–10233.
70. Alexandridis, P. *Chem. Eng. Technol.* **2011**, *34* (1), 15–28.
71. Laurent, S.; Forge, D.; Port, M.; Roch, A.; Robic, C.; Vander Elst, L.; Muller, R. N. *Chem. Rev.* **2008**, *108* (6), 2064–2110.
72. Jennifer A. Dahl; Bettye L. S. Maddux, A.; Hutchison, J. E. *Chem. Rev.* **2007**, *107* (6), 2228–2269.
73. Eckelman, M. J.; Zimmerman, J. B.; Anastas, P. T. *J. Ind. Ecol.* **2008**, *12* (3), 316–328.
74. Murphy, C. J. *J. Mater. Chem.* **2008**, *18* (19), 2173.
75. Rothenberg, G.; Downie, A. P.; Raston, C. L.; Scott, J. L. *J. Am. Chem. Soc.* **2001**, *123* (36), 8701–8708.
76. Friščić, T.; Jones, W. *Cryst. Growth Des.* **2009**, *9* (3), 1621–1637.
77. Kuroda, R.; Higashiguchi, K.; Hasebe, S. *CrystEngComm* **2004**, *6* (76), 464–469.
78. Chadwick, K.; Davey, R.; Cross, W. *CrystEngComm* **2007**.
79. Opoczky, L. *Powder Technol.* **1977**.
80. Rak, M. J.; Saadé, N. K.; Friščić, T.; Moores, A. *Green Chem.* **2014**, *16* (1), 86–89.
81. Malca, M. Y.; Bao, H.; Bastaille, T.; Saade, N. K.; Kinsella, J. M.; Friščić, T.; Moores, A. *Submitted for Publication* **2017**.

# Chapter 2 Mechanically activated synthesis of ultrasmall organo- and water-suspendable $Bi_2S_3$ nanoparticles and their use as contrast agents in Computed Tomography imaging


## Abstract

Nanosized $Bi_2S_3$ particles are one of the most promising nanomaterials for biomedical imaging, due to a unique combination of low toxicity and high electron count of bismuth. However, the study and use of nano-$Bi_2S_3$ have been prevented by major synthetic challenges, including sensitivity to air and harsh solvothermal conditions. Herein, we describe a novel, surprisingly simple pathway, based on solid-state self-assembly, to access the elusive $Bi_2S_3$ nanoparticles functionalized with surface ligands that allow dispersion in either organic or aqueous media. This one-pot, room-temperature synthesis utilizes mechanical activation in the solid state, either by milling or even manual grinding, to induce the spontaneous assembly of monodisperse 2 nm diameter nanoparticles applicable for CT imaging in physiological media. This solvent-free methodology, which utilizes simple and readily available precursors, provides unprecedented one-step access to monodisperse nano-$Bi_2S_3$ in multi-gram amounts, including poly (ethylene glycol)-coated nanoparticles, without the need for controlled atmospheres or solvothermal treatment.

## 2.1. Introduction

The impressive and exciting properties of nanomaterials have made them attractive candidates for solving some of the most daunting scientific problems in the domains of energy, health and electronics.[1-4] In recent years, efforts have been made to find routes to access molecules and materials in a more efficient and sustainable fashion,[5-7] with particular focus on the reduction of waste and energy input, and the use of safe reagents.[8-9] Nanoparticle (NP) synthesis is intrinsically complicated by their metastable nature, necessitating the use of high dilution and capping ligands to achieve uniform sample features, *e.g.* size and shape.[10-13] These constraints imply that the development of large-scale syntheses of NPs with well-defined features remains a challenge for low waste and energy-efficient synthesis.[14-16] Recently, however, we demonstrated that low-energy mechanochemistry can be used to access highly monodisperse gold NPs through galvanic reduction of $HAuCl_4$ in presence of terminal monoalkylamines as capping agents.[18] By employing lignin as a reducing and surface-capping agent, this approach was readily adapted for the production of supported noble metal (*e.g.* Au, Ag, Pd, Ru and Re) NPs from their corresponding salts.[17, 21] Whereas solvent-free mechanochemistry has previously been used to access diverse advanced materials, including supported metal NPs,[17, 21-25] metal oxide, nitride and sulfide NPs,[26-29] carbon-based NPs,[30-32] and porous nanocomposites,[33-34] as well as microporous metal–organic materials,[35-36] and shows significant improvements in atom- and energy-economy.[17-20], such work has been largely based on a top-down mechanochemical route, through energy-demanding comminution of bulk materials.[37-38]

Bismuth sulfide ($Bi_2S_3$) is a V-VI semiconductor that has attracted much attention for applications in photoconducting materials[39-40], lithium ion batteries[41-42], solar cells[43-44], electrochemical hydrogen storage[45-46], and thermoelectric devices[47-48]. Due to the large atomic number of bismuth and its surprisingly low toxicity in biological systems, $Bi_2S_3$ NPs are also well suited as contrast agents in Computed Tomography (CT) and have shown equal or superior efficacy compared to currently used iodinated CT compounds.[49-51] However, the development of bismuth-based CT contrast agents has been hampered by synthetic challenges.[52] Hydrothermal methods, which are commonly employed in $Bi_2S_3$ NP syntheses, typically require high temperatures, extended heating period, inert

atmospheres and copious amounts of solvents in order to access monodisperse nanomaterials.[49, 51, 53-54] In all cases, these approaches lead to the synthesis of nanomaterials readily suspendable in organic solvent, implying that, for any biological or medicinal application, an extra functionalization step is required to render them water suspendable. One solvent-free room-temperature synthesis of $Bi_2S_3$ NPs has also been reported by Dutkova *et al.*[38], and it relies on a top-down approach, using as starting materials metallic bismuth and sulfur powder under argon atmosphere, affording polydisperse products.

We now describe a completely novel, surprisingly simple synthesis of $Bi_2S_3$ NPs suitable for CT imaging applications, by quick mechanical activation followed by an aging period. Remarkably, the whole procedure is performed at room temperature in air, yielding gram amounts of NPs with well-defined average diameters that can be modulated between 2 and 8 nm, depending on the reaction conditions. The approach directly yields NPs capped by either oleylamine (OA) or 6-aminohexanoate (AHA). The OA-modified $Bi_2S_3$ NPs are readily suspended in organic solvent, while using AHA gives access to NPs compatible with aqueous media. In further demonstration of this new, simple technique for making complex and biologically compatible nanomaterials, we demonstrate a one-step, solvent-free procedure for the synthesis of $Bi_2S_3$ NPs modified by poly(ethylene glycol)-methyl-ether-amine (mPEG-$NH_2$, M.W. = 5000 g/mol), a polymer typically used to functionalize bio-targeted agents.[49] The methodology was easily scaled-up to generate grams of NP materials that were suitable as bioimaging contrast agents, as demonstrated by evaluating the radiodensity of the AHA-capped NPs, as well as their PEGylated counterparts in physiological buffer medium.

## 2.2 Results and discussion

### 2.2.1 Organo-suspendable $Bi_2S_3$ nanoparticles

We first explored the possibility to mechanochemically access $Bi_2S_3$ NPs by mixer mill ball milling (MM) of $Bi(NO_3)_3{\cdot}5H_2O$ and L-cysteine[55] as sources of bismuth and sulfur,

respectively, in the presence of oleyamine (OA) as the capping agent. After 90 min milling, TEM analysis of the resulting pale yellow paste did not reveal any sign of NP formation. However, it was observed that the sample after milling began to darken without external manipulation, so we decided to leave it to age in air at room temperature. After 12 hours, the paste became completely black and was then purified through several washing and centrifugation cycles (Scheme 2.1). For different experiments, the bismuth-to-sulfur ratio in all cases was chosen to match the stoichiometry of $Bi_2S_3$, while the OA to bismuth stoichiometric ratio was set to either 5:1 (sample **5OA@$Bi_2S_3$-90-MM**) or 10:1 (sample **10OA@$Bi_2S_3$-90-MM**) (Table 2.1). The resulting materials were readily suspendable in hexanes and toluene.

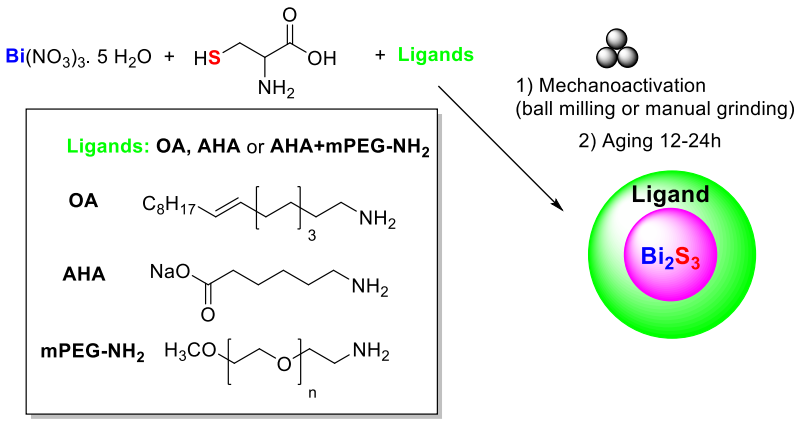


**Scheme 2. 1.** Overview of herein developed synthesis of $Bi_2S_3$ NPs capped with oleylamine (OA), sodium 6-aminohexanoate (AHA) and poly-(ethylene glycol)-methyl-ether-amine (mPEG-NH2 M.W.=5000 g/mol). All steps are performed at ambient conditions in air.

| Samples ***x*Ligand@NP-*t*-Milling$^{H2O}$** | Ligand[a] | Ligand: Bismuth molar ratio | Milling time (min) | Milling Method[c] | Water (µL) | Mean diameter (nm) |
|---|---|---|---|---|---|---|
| **5OA@$Bi_2S_3$-90-MM** | OA | 5:1 | 90 | MM | - | 2.09±0.29 |
| **10OA@$Bi_2S_3$-90-MM** | OA | 10:1 | 90 | MM | - | 2.08±0.32 |
| **5OA@$Bi_2S_3$-5-MM** | OA | 5:1 | 5 | MM | - | 2.09±0.31 |
| **5OA@$Bi_2S_3$-GM** | OA | 5:1 | N/A[b] | MG | - | 1.96±0.24 |
| **5OA@$Bi_2S_3$-90-PM** | OA | 5:1 | 90 | PM | - | 1.88±0.27 |
| **5AHA@$Bi_2S_3$-90-MM$^0$** | AHA | 5:1 | 90 | MM | - | NA |
| **5AHA@$Bi_2S_3$-90-MM$^{50}$** | AHA | 5:1 | 90 | MM | 50 | 7.9±2.1 |
| **10AHA@$Bi_2S_3$-90-MM$^{50}$** | AHA | 10:1 | 90 | MM | 50 | 8.2±2.3 |
| **5AHA@$Bi_2S_3$-90-MM$^{100}$** | AHA | 5:1 | 90 | MM | 100 | 7.6±4.0 |
| **10AHA@$Bi_2S_3$-90-MM$^{100}$** | AHA | 10:1 | 90 | MM | 100 | 7.8±1.9 |
| **5AHA@$Bi_2S_3$-90-PM** | AHA | 5:1 | 90 | PM | 2000[d] | 3.0±0.41 |
| **5AHA&PEG@ $Bi_2S_3$-90-MM$^{50}$** | AHA and mPEG-$NH_2$ | 4.5:1 and 0.5:1 | 90 | MM | 50 | 2.9±1.2 |

**Table 2. 1.** Summary of synthetic parameters and mean particle diameters for resulting $Bi_2S_3$ NP samples. [a]. OA: oleylamine; AHA: sodium 6-aminohexanoate; mPEG-$NH_2$: poly-(ethylene glycol)-methyl-ether-amine. [b]. Manual grinding was performed until the reaction mixtures appeared homogenous. [c]. MM: mixer ball milling; PM: planetary ball milling; MG: manual grinding. [d]. 2 mL water was added to the PM scale-up vessel, equivalent to 75 µL of water in the MM procedure.

Purified **5OA@$Bi_2S_3$-90-MM** and **10OA@$Bi_2S_3$-90-MM** samples were first analysed by X-ray photoelectron spectroscopy (XPS, Figures S2.1 and S2.2, and detailed characterization in Supplementary Information), which revealed the presence of Bi, S, O, N, and C. Detection of N confirms the presence of a ligand shell surrounding the NPs. The appearance of O is attributed to either reaction with atmospheric $O_2$ or adsorbed moisture. No carbonyl peak is observed in the C1s of both samples, confirming the absence of L-cysteine at the surface of the particles (Figure S2.18). In the two samples, the Bi4f$_{7/2}$, Bi4f$_{5/2}$ , Bi4d$_{5/2}$ and Bi 4d$_{3/2}$, signals were all consistent with $Bi^{3+}$ ions, while the S2p and S2s signals matched $S^{2-}$. The Bi4f$_{7/2}$ binding energy found at 158.4 eV in all the samples is ca. 1.0 eV lower than that of $Bi_2O_3$,[56] signifying the formation of $Bi_2S_3$. The

integration of Bi4d and S2s signals indicated an average Bi:S atomic ratio between 0.5 and 0.6, thus implying a slight excess of sulfur.

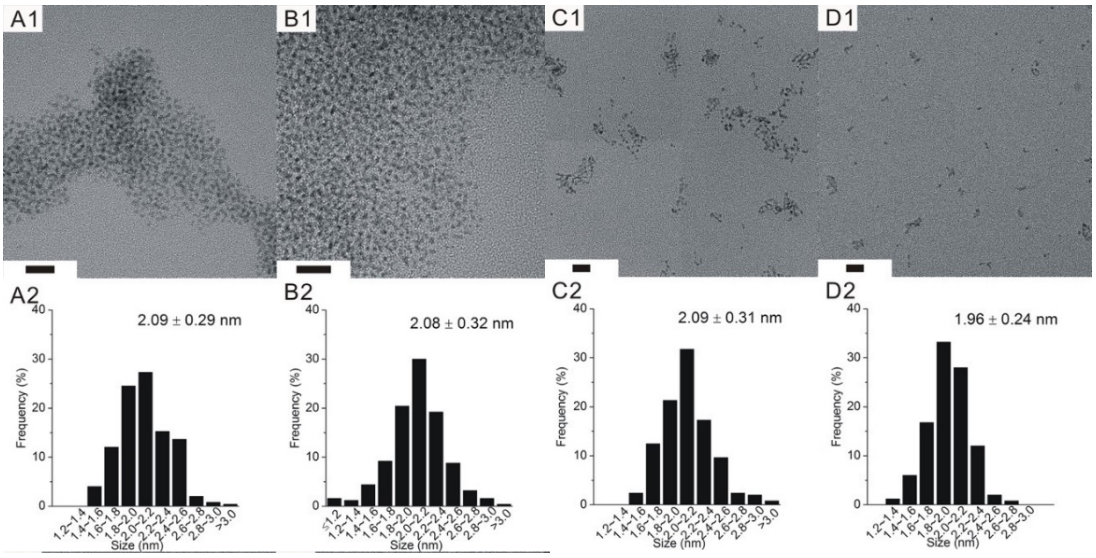


**Figure 2. 1.** TEM images and size distribution histograms of OA-capped $Bi_2S_3$ NPs: (A1&A2) 5OA@$Bi_2S_3$-90-MM (n=250); (B1&B2) 10OA@$Bi_2S_3$-90-MM (n=250); (C1&C2) 5OA@$Bi_2S_3$-5-MM (n=250); (D1&D2) 5OA@$Bi_2S_3$-MG (n=250). Scale bars represent 20 nm.

Structures of **5OA@$Bi_2S_3$-90-MM** and **10OA@$Bi_2S_3$-90-MM** were further analyzed by transmission electron microscopy (TEM, Figure 2.1-A, -B). In both cases, NPs with narrow size distributions, independent of the OA:bismuth ratio, were observed. Ratios of both 5:1 and 10:1 gave NPs with average diameters of 2.09±0.29 nm and 2.08±0.32 nm, respectively. Overall, these results indicate that our method successfully affords $Bi_2S_3$ NPs, despite the absence of inert atmosphere which is required in most syntheses.[38, 49]

Next, thermogravimetric analysis (TGA) was performed on samples **5OA@$Bi_2S_3$-90-MM** and **10OA@$Bi_2S_3$-90-MM** in order to gain insight into the organic ligand shell. Increasing the ligand: bismuth stoichiometric ratio during synthesis from 5:1 to 10:1 afforded no significant change in the OA surface coating (Figure S2.3), and the loss of organic matter upon thermolysis of the final product was very similar in both cases (17.5% and 17.6% of by weight, respectively). These results indicate that the NP surface is already

saturated with organic ligand at the 5:1 stoichiometric ratio, and that any additional ligand will likely be washed away during work up. We also tested the possibility to produce NPs using a 3:1 stoichiometric ratio of the OA and bismuth, respectively, but these attempts failed to produce NPs even after 5 days of aging.

Surprisingly, milling time did not have a notable effect on the resulting material, indicating that the principal role of milling treatment is mechanical activation. For example, the XPS and TEM analysis results are virtually identical for **5OA@$Bi_2S_3$-5-MM**, obtained using a milling period of 5 min and featuring NPs of a 2.09±0.31 nm mean diameter, and for **5OA@$Bi_2S_3$-90-MM** (2.09±0.29 nm), which was obtained after 90 min of milling and 12 hours of aging (Figure S2.1 and 2.1-C). To further investigate the ability to assemble uniform $Bi_2S_3$ NPs with minimum mechanical activation, we explored manual grinding (MG), using a mortar and pestle, which generated the sample **5OA@$Bi_2S_3$-MG**. In this case again, TEM revealed an average NP diameter of 1.96±0.24 nm (Figure 2.1-D), and XPS showed binding energies similar to those for **5OA@$Bi_2S_3$-90-MM** (Figure S2.1). Consequently, using OA as the capping agent leads to reproducible assembly of $Bi_2S_3$ NPs with a preferred size of ca. 2 nm, as long as intimate mixing is achieved.

PXRD analysis of all samples involving OA, prepared either by milling or manual grinding revealed only broad, featureless diffractograms (Figure S4), indicating either very small particle sizes and/or amorphous nature. PXRD patterns of annealed samples confirmed the absence of $Bi_2O_3$ in the produced samples (Supplementary information)

Characterization was completed by mass spectrometry, a method previously used in analysis of nanoclusters and small-sized nanocrystals.[18, 57-61] Matrix-assisted laser desorption ionization-time of flight mass spectroscopy (MALDI-TOF MS) characterization of $Bi_2S_3$ NPs revealed clear fragmentation patterns of Bi and S loss, with peaks separated by 209.2 and 32.0 units, respectively (Figures 2.2, S2.5, S2.6, Table S2.1), consistent with the laser beam-induced decomposition of $Bi_2S_3$ NPs into $Bi_n$ and $Bi_nS_m$ clusters (n = 3-7, m

= 1-4). The peaks of highest Bi mass were measured as 1463.6 for all the OA-capped samples, corresponding to bare $Bi_7$ clusters (Table S1). No oxygen species were detected, validating the formation of $Bi_2S_3$ under aerobic synthetic conditions. No characteristic peak could be identified under 627 AMUs (range: 420 ~ 1600 m/z).

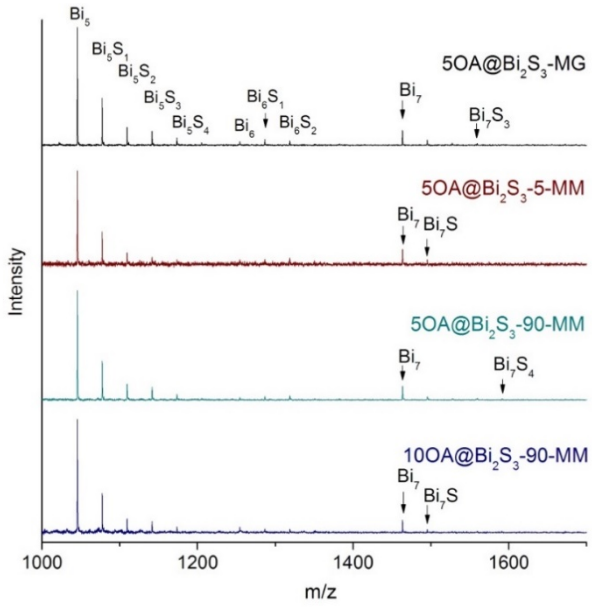


**Figure 2. 2.** MALDI-TOF MS measurements for the OA-capped $Bi_2S_3$ NPs obtained using the mechanically-activated aging approach. The spectra demonstrate the fragmentation of NPs into $Bi_n$ and $Bi_nS_m$ clusters (n = 3-7, m = 1-4). Importantly, no oxygen-containing species were detected.

### 2.2.2 Water-suspendable $Bi_2S_3$ nanoparticles

While the NPs produced in presence of OA are readily suspendable in a poorly polar solvent such as toluene, consistent with the presence of NPs capped with hydrophobic long chain amine ligands,[54, 62] direct functionalization of $Bi_2S_3$ NPs with water-compatible ligands would be critical for their use as *in vivo* injectable contrast agents. In classic syntheses, an extra phase-transfer reaction step is required to reach such species.[49] Consequently, we explored the possibility of synthesizing monodisperse and water-soluble $Bi_2S_3$ NPs by replacing OA with the sodium salt of 6-aminohexanoic acid in the milling procedure. However, attempts to synthesize such NPs by 90 min milling of $Bi(NO_3)_3{\cdot}5H_2O$, L-cysteine and sodium 6-aminohexanoate (AHA), followed by aging up to 5 days, were not successful. Next, we turned to liquid-assisted grinding (LAG), a technique

that utilizes catalytic, substoichiometric amounts of liquid to facilitate mechanochemical transformations.[20] Milling in the presence of 50 µL water (sample **nAHA@$Bi_2S_3$-90-MM$^{50}$**, with the AHA:Bi ratios *n*=5 and 10) provided, after 24 hours aging at room temperature, highly uniform NPs of 7.6 nm - 8.2 nm in diameter (Figure 2.3, Table 2.1). The XPS spectra revealed similar binding energies for each element as previously seen for OA-capped NPs (Figures S2.7 and S2.8). Just like the OA-capped NPs, the as-prepared AHA-functionalized samples diffracted poorly (Figure S2.9). The amount of water introduced into the reaction mixture in LAG also did not significantly affect the final NP size, although doubling the amount of water additive from 50 to 100 µL allowed for a shorter aging time of 12 hours.[20]

The use of AHA provided larger NPs than with OA, which may be explained by the relative sizes of the two capping agents, the aliphatic chain of AHA being 3 times shorter than that in OA. Indeed, the earlier study on mechanosynthesis of gold NPs showed that longer chain lengths lead to smaller NP sizes,[18] due to a more limited access of precursors to the NP surface protected by larger capping agents. The result suggests that nanoparticle stabilization models based on micellar arrangements [63] cannot be applied for the reported particles made under mechanochemical conditions.

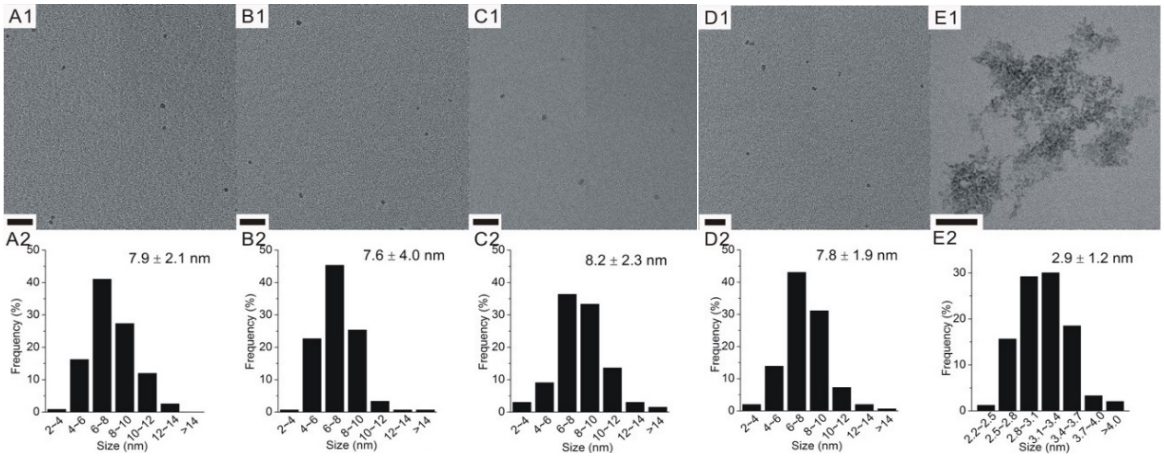


**Figure 2. 3.** TEM images and size distribution histograms of **AHA-capped $Bi_2S_3$ NPs**: (A1&2) **5AHA@$Bi_2S_3$-90-MM$^{50}$** (n=120); (B1&2) **5AHA@$Bi_2S_3$-90-MM$^{100}$** (n=150); (C1&2) **10AHA@$Bi_2S_3$-90-MM$^{50}$** (n=75); (D1&2) **10AHA@$Bi_2S_3$-90-MM$^{100}$** (n=150); (E1&2) **5AHA/PEG@$Bi_2S_3$-90-MM$^{50}$** (n=250). Scale bars represent 50 nm.

### 2.2.3 Multigram scale synthesis of OA- and AHA-capped $Bi_2S_3$ NPs

The described mechanical activation and aging approach to monodisperse $Bi_2S_3$ NPs is readily scalable to multi-gram scales. Both the **5OA@$Bi_2S_3$** and **5AHA@$Bi_2S_3$** syntheses were linearly scaled-up (using 2.5 g and 2.0 g of reactant $Bi(NO_3)_3{\cdot}5H_2O$, respectively) by 90 minutes mechanical activation in a planetary ball mill (PM) operating at 500 rpm. Sample analysis by TEM demonstrated the formation of uniform NPs of 1.88±0.27 nm and 3.0±0.41 nm in diameter, for **5OA@$Bi_2S_3$-90-PM** and **5AHA@$Bi_2S_3$-90-PM**, respectively, after milling and 48 hours aging (Figure S2.10). Switching from a mixer to a planetary mill resulted in limited size change for OA-derived materials (1.88±0.27 nm for **5OA@$Bi_2S_3$-90-PM** *vs*. 2.09±0.29 nm for **5OA@$Bi_2S_3$-90-MM**), while a marked drop in average NP diameter from 7.9 nm (**5AHA@$Bi_2S_3$-90-MM**[50]) to 3.0 nm (**5AHA@$Bi_2S_3$-90-PM**) was observed with AHA samples. 1.70 g and 0.936 g of purified product were obtained for the OA and AHA samples, corresponding to a respective yield in bismuth of 95% and 72% (based on TGA analysis, Figure S2.3 and S2.11). Besides being done in the absence of hazardous solvents or external heating, these syntheses are also economically efficient, with the cost for scale-up reactions being approximately 2.61 $ CDN per gram of purified **5OA@$Bi_2S_3$-90-PM** and 4.56 $ CDN per gram of purified **5AHA@$Bi_2S_3$-90-PM** (see Supplementary Information for experimental details and cost analysis).

### 2.2.4 Synthesis of PEG-functionalized NPs

Finally, we explored another strategy to obtain water-soluble biocompatible $Bi_2S_3$ NPs through milling and aging, by direct surface ligand conjugation with poly(ethylenecglycol) (PEG) polymers. Namely, PEG polymers are often used to make NPs pharmaceutically relevant by reducing surface protein adsorption,[64-66] avoiding NP recognition by the mononuclear phagocyte system and increasing their circulation time *in vivo*.[64-66] To afford biocompatible, directly mechanochemically PEGylated $Bi_2S_3$ NPs, the amino-terminated polymer mPEG-$NH_2$ (M.W.=5000 mg/mol, 10 mol % $NH_2$-content) was

added into the reaction mixture ahead of a typical AHA-capped $Bi_2S_3$ NP synthesis. TEM images (Figure 2.3-E) of the product revealed NPs 3 nm in diameter, which is ca. half the size of pure AHA-capped $Bi_2S_3$ NPs obtained under the same conditions, suggesting that attachment of the mPEG-$NH_2$ hinders NP growth. An infrared analysis of the synthesized NPs (Figure S2.12) clearly revealed the characteristic adsorption bands of AHA in **5AHA@$Bi_2S_3$-90-MM**[50], while **5AHA&PEG@$Bi_2S_3$-90-MM**[50] exhibited all the characteristic bands of both AHA and mPEG-$NH_2$. We conclude that the synthesized $Bi_2S_3$ NPs are stabilized by a composite of mPEG-$NH_2$ and AHA.

### 2.2.5 $Bi_2S_3$ NPs solubility and μCT analysis

In order to establish that ultrasmall $Bi_2S_3$ NPs produced by mechanical activation would be viable as contrast probes for CT imaging, we explored their solubility and solution μCT contrast generation. Solubility was evaluated in water and phosphate buffered saline (PBS) solution, a physiologically representative buffer used as a solvent for NP intravenous injection formulations.[67] For **5AHA@$Bi_2S_3$-90-MM**[50] and **5AHA&PEG@$Bi_2S_3$-90-MM**[50] saturated suspensions samples in water, the measured concentrations were 14.8 and 24.3 mM, respectively, and were stable for 2-3 hours. In PBS, the corresponding values were 74.7 and 74.7 mM respectively. Importantly, the PBS suspensions were stable for 24 hours and were used to evaluate radiodensity as a function of concentration. The concentration of bismuth in each suspension was evaluated by ICP (Figure 2.4, Table S2.2). Two parallel results were collected for each sample, and the mean concentration of bismuth expressed with corresponding Hounsfield unit (HU) values, calibrated for each dilution by referencing to air (HU = -1000) and PBS (HU = 0). For both **5AHA&PEG@$Bi_2S_3$-90-MM**[50] and **5AHA@$Bi_2S_3$-90-MM**[50] samples, the concentrated samples of 0.075 M showed good radiodensity responses, of 1437±0.0 HU and 1335±33.8 HU respectively, on par with the best reports in the literature.[49] For all explored concentrations, the HU values for both NPs were very close to the concentration values

determined by ICP, demonstrating that the herein generated $Bi_2S_3$ NPs can be reliably used as PBS-suspended contrast agents over an order of magnitude of concentrations.

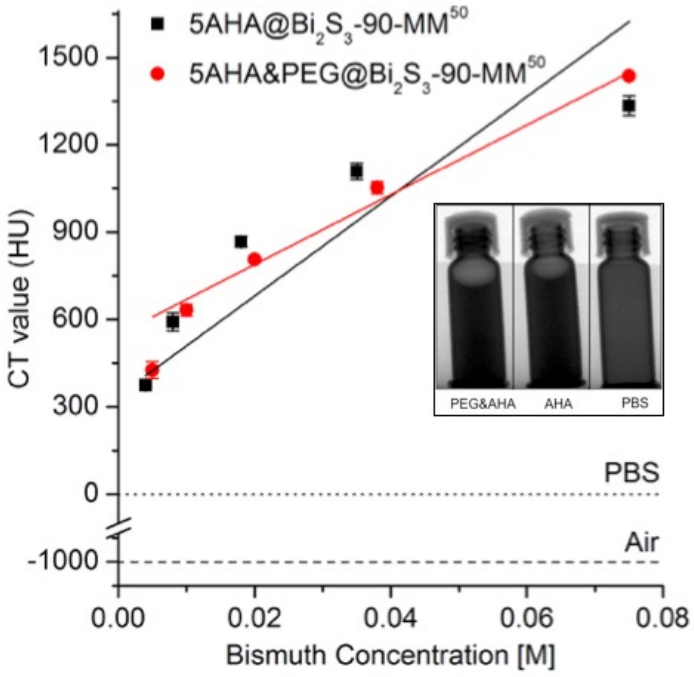


**Figure 2. 4.** Experimental radiodensity for the $Bi_2S_3$ NP samples **5AHA@$Bi_2S_3$-90-MM[50]** and **5AHA&PEG@$Bi_2S_3$-90-MM[50]** as a function of bismuth concentration (M) measured by ICP. Error bars represent standard deviation of the CT value (in Hounsfield Units) for 20 random measurements (circular regions of 2r = 3.0 mm, 11.1 pixels/mm) about the μCT images of each sample. Opacities of PBS and air were calibrated to HU = 0 and HU = -1000, respectively. Inset: μCT images of 0.075 M **5AHA@$Bi_2S_3$-90-MM[50]** and **5AHA&PEG@$Bi_2S_3$-90-MM[50]** samples with PBS for comparison.

## 2.3 Conclusions

Mechanical activation enabled unprecedented, solvent-free and room-temperature assembly of small, monodisperse $Bi_2S_3$ NPs from solid reagents. This operationally simple process enabled the synthesis of a variety of $Bi_2S_3$ NPs, differently functionalized for suspension in either organic, aqueous or physiological media. Thorough characterization by XPS, TEM, MALDI-TOF and XRD revealed that the pure $Bi_2S_3$ NPs with well-defined, monodisperse sizes, ranging from 2 to 8 nm in diameter were easily accessed, in contrast to previous mechanochemical techniques that led to NP sizes in the range 100 nm-300 nm, with a mean crystallite size of 26 nm. [38] The effect of the ligand

nature, the milling duration, the ligand:bismuth ratio and the grinding technique (mixer milling, planetary milling or manual grinding) were extensively studied, and the use of planetary milling devices enabled the scale-up to yield multi-gram quantities of each product. To further distinguish this methodology from those conventionally employed to generate similar NPs, all syntheses were performed without hazardous solvents, heating, and in aerobic conditions. This, combined with demonstrated excellent X-ray attenuation properties of selected NP systems in physiological media, provides a clear illustration how unconventional, solvent-free approaches can lead to unprecedentedly inexpensive, clean, as well as materials- and energy-efficient routes to advanced nanomaterials. Future research will focus on the use of these materials for *in vivo* applications. In particular, the behavior of the produced nanoparticles in suspension, potential formation of aggregates and their ability to cross or not biological barriers will be thoroughly evaluated. While this method is so far unique for $Bi_2S_3$, we believe it may develop into a novel, more general pathway to access ultrasmall and monodisperse metal chalcogenides and binary species.

## 2.4 References


1. Q. Zhang, E. Uchaker, S. L. Candelaria and G. Cao, *Chem. Soc. Rev.*, 2013, **42**, 3127-3171.
2. R. Weissleder, M. Nahrendorf and M. J. Pittet, *Nat. Mater.*, 2014, **13**, 125-138.
3. D. Jariwala, V. K. Sangwan, L. J. Lauhon, T. J. Marks and M. C. Hersam, *Chem. Soc. Rev.*, 2013, **42**, 2824-2860.
4. A. Kamyshny and S. Magdassi, *Small*, 2014, **10**, 3515-3535.
5. J. A. Dahl, B. L. Maddux and J. E. Hutchison, *Chem. Rev.*, 2007, **107**, 2228-2269.
6. C. J. Murphy, *J. Mater. Chem.*, 2008, **18**, 2173-2176.
7. M. J. Eckelman, J. B. Zimmerman and P. T. Anastas, *J. Ind. Ecol.*, 2008, **12**, 316-328.
8. H. Duan, D. Wang and Y. Li, *Chem. Soc. Rev.*, 2015, **44**, 5778-5792.
9. S. Iravani, *Green Chem.*, 2011, **13**, 2638-2650.
10. S. Xie, X. Y. Liu and Y. Xia, *Nano Res.*, 2015, **8**, 82-96.
11. P. Alexandridis, *Chem. Eng. Technol.*, 2011, **34**, 15-28.
12. S. Laurent, D. Forge, M. Port, A. Roch, C. Robic, L. Vander Elst and R. N. Muller, *Chem. Rev.*, 2008, **108**, 2064-2110.
13. M. Niederberger and N. Pinna, *Metal oxide nanoparticles in organic solvents: synthesis, formation, assembly and application*, Springer Science & Business Media, 2009.
14. M. Shigeta and A. B. Murphy, *J. Phys. D: Appl. Phys.*, 2011, **44**, 174025.
15. S. A. Galindo-Rodríguez, F. Puel, S. Briançon, E. Allémann, E. Doelker and H. Fessi, *Eur. J. Pharm. Sci.*, 2005, **25**, 357-367.

16. C. J. Tighe, R. Q. Cabrera, R. I. Gruar and J. A. Darr, *Ind. Eng. Chem. Res.*, 2013, **52**, 5522-5528.
17. M. J. Rak, T. Friščić and A. Moores, *Faraday Discuss.*, 2014, **170**, 155-167.
18. M. J. Rak, N. K. Saadé, T. Friščić and A. Moores, *Green Chem.*, 2014, **16**, 86-89.
19. C. Xu, S. De, A. M. Balu, M. Ojeda and R. Luque, *Chem. Comm.*, 2015, **51**, 6698-6713.
20. S. L. James, C. J. Adams, C. Bolm, D. Braga, P. Collier, T. Friščić, F. Grepioni, K. D. Harris, G. Hyett and W. Jones, *Chem. Soc. Rev.*, 2012, **41**, 413-447.
21. M. J. Rak, T. Friščić and A. Moores, *RSC Adv.*, 2016, **6**, 58365-58370.
22. U. Kamolphop, S. F. Taylor, J. P. Breen, R. Burch, J. J. Delgado, S. Chansai, C. Hardacre, S. Hengrasmee and S. L. James, *ACS Catal.*, 2011, **1**, 1257-1262.
23. S. A. Kondrat, G. Shaw, S. J. Freakley, Q. He, J. Hampton, J. K. Edwards, P. J. Miedziak, T. E. Davies, A. F. Carley and S. H. Taylor, *Chem. Sci.*, 2012, **3**, 2965-2971.
24. B. Mohan, J. C. Park and K. H. Park, *ChemCatChem*, 2016.
25. M. s. e. al., *Green Chem.*, 2016.
26. C. Shifu, C. Lei, G. Shen and C. Gengyu, *Chem. Phys. Lett.*, 2005, **413**, 404-409.
27. R. Zhang, A. Villanueva, H. Alamdari and S. Kaliaguine, *J. Catal.*, 2006, **237**, 368-380.
28. Y. Xue, X. Jin, Y. Fan, R. Tian, X. Xu, J. Li, J. Lin, J. Zhang, L. Hu and C. Tang, *Polym. Compos.*, 2014, **35**, 1707-1715.
29. D. Liu, W. Lei, S. Qin, L. Hou, Z. Liu, Q. Cui and Y. Chen, *J. Mater. Chem. A*, 2013, **1**, 5274-5278.
30. T. Xing, J. Sunarso, W. Yang, Y. Yin, A. M. Glushenkov, L. H. Li, P. C. Howlett and Y. Chen, *Nanoscale*, 2013, **5**, 7970-7976.
31. O. Y. Posudievsky, O. A. Khazieieva, V. G. Koshechko and V. D. Pokhodenko, *J. Mater. Chem.*, 2012, **22**, 12465-12467.
32. R. V. Salvatierra, S. H. Domingues, M. M. Oliveira and A. J. Zarbin, *Carbon*, 2013, **57**, 410-415.
33. R. Hosseinpour, A. Pineda, A. Garcia, A. A. Romero and R. Luque, *Catal. Comm.*, 2014, **48**, 73-77.
34. M. Ojeda, A. Pineda, A. A. Romero, V. Barrón and R. Luque, *ChemSusChem*, 2014, **7**, 1876-1880.
35. W. Yuan, T. Friščić, D. Apperley and S. L. James, *Angew. Chem. Int. Ed.*, 2010, **122**, 4008-4011.
36. P. J. Beldon, L. Fábián, R. S. Stein, A. Thirumurugan, A. K. Cheetham and T. Friščić, *Angew. Chem. Int. Ed.*, 2010, **49**, 9640-9643.
37. V. Šepelák, S. Bégin-Colin and G. Le Caër, *Dalton Trans.*, 2012, **41**, 11927-11948.
38. E. Dutková, L. Takacs, M. J. Sayagués, P. Baláž, J. Kováč and A. Šatka, *Chem. Eng. Sci.*, 2013, **85**, 25-29.
39. M. Aresti, M. Saba, R. Piras, D. Marongiu, G. Mula, F. Quochi, A. Mura, C. Cannas, M. Mureddu and A. Ardu, *Adv. Funct. Mater.*, 2014, **24**, 3341-3350.
40. R. Suarez, P. Nair and P. V. Kamat, *Langmuir*, 1998, **14**, 3236-3241.
41. Y. Zhao, D. Gao, J. Ni, L. Gao, J. Yang and Y. Li, *Nano Res.*, 2014, **7**, 765-773.
42. Z. Zhang, C. Zhou, H. Lu, M. Jia, Y. Lai and J. Li, *Mater. Lett.*, 2013, **91**, 100-102.
43. A. K. Rath, M. Bernechea, L. Martinez and G. Konstantatos, *Adv. Mater.*, 2011, **23**, 3712-3717.

44. L. Martinez, M. Bernechea, F. de Arquer and G. Konstantatos, *Adv. Energy Mater.*, 2011, **1**, 1029-1035.
45. L. Li, N. Sun, Y. Huang, Y. Qin, N. Zhao, J. Gao, M. Li, H. Zhou and L. Qi, *Adv. Funct. Mater.*, 2008, **18**, 1194-1201.
46. B. Zhang, X. Ye, W. Hou, Y. Zhao and Y. Xie, *J. Phys. Chem. B*, 2006, **110**, 8978-8985.
47. Q. Yang, C. Hu, S. Wang, Y. Xi and K. Zhang, *J. Phys. Chem. C*, 2013, **117**, 5515-5520.
48. Z.-H. Ge, B.-P. Zhang, P.-P. Shang and J.-F. Li, *J. Mater. Chem.*, 2011, **21**, 9194-9200.
49. J. M. Kinsella, R. E. Jimenez, P. P. Karmali, A. M. Rush, V. R. Kotamraju, N. C. Gianneschi, E. Ruoslahti, D. Stupack and M. J. Sailor, *Angew. Chem. Int. Ed.*, 2011, **50**, 12308-12311.
50. O. Rabin, J. M. Perez, J. Grimm, G. Wojtkiewicz and R. Weissleder, *Nat. Mater.*, 2006, **5**, 118-122.
51. K. Ai, Y. Liu, J. Liu, Q. Yuan, Y. He and L. Lu, *Adv. Mater.*, 2011, **23**, 4886-4891.
52. Y. Liu, K. Ai and L. Lu, *Acc. Chem. Res.*, 2012, **45**, 1817-1827.
53. M. Ibáñez, P. Guardia, A. Shavel, D. Cadavid, J. Arbiol, J. R. Morante and A. Cabot, *J. Phys. Chem. C*, 2011, **115**, 7947-7955.
54. R. Malakooti, L. Cademartiri, Y. Akçakir, S. Petrov, A. Migliori and G. A. Ozin, *Adv. Mater.*, 2006, **18**, 2189-2194.
55. P. Baláž, M. Baláž, M. Čaplovičová, A. Zorkovská, Ľ. Čaplovič and M. Psotka, *Faraday Discuss.*, 2014, **170**, 169-179.
56. J. Chastain, R. C. King and J. Moulder, *Handbook of X-ray photoelectron spectroscopy: a reference book of standard spectra for identification and interpretation of XPS data*, Physical Electronics Eden Prairie, MN, 1995.
57. A. Dass, A. Stevenson, G. R. Dubay, J. B. Tracy and R. W. Murray, *J. Am. Chem. Soc.*, 2008, **130**, 5940-5946.
58. B. Guan, W. Lu, J. Fang and R. B. Cole, *J. Am. Chem. Soc.*, 2007, **18**, 517-524.
59. G. A. Khitrov and G. F. Strouse, *J. Am. Chem. Soc.*, 2003, **125**, 10465-10469.
60. B. H. Kim, K. Shin, S. G. Kwon, Y. Jang, H.-S. Lee, H. Lee, S. W. Jun, J. Lee, S. Y. Han and Y.-H. Yim, *J. Am. Chem. Soc.*, 2013, **135**, 2407-2410.
61. Y. Levi-Kalisman, P. D. Jadzinsky, N. Kalisman, H. Tsunoyama, T. Tsukuda, D. A. Bushnell and R. D. Kornberg, *J. Am. Chem. Soc.*, 2011, **133**, 2976-2982.
62. X. Lu, H. Y. Tuan, B. A. Korgel and Y. Xia, *Chem. Eur. J.*, 2008, **14**, 1584-1591.
63. K. L. Luska and A. Moores, *Can. J. Chem.*, 2011, **90**, 145-152.
64. R. Gref, M. Lück, P. Quellec, M. Marchand, E. Dellacherie, S. Harnisch, T. Blunk and R. Müller, *Colloids Surf., B*, 2000, **18**, 301-313.
65. D. Bazile, C. Prud'homme, M. T. Bassoullet, M. Marlard, G. Spenlehauer and M. Veillard, *J. Pharm. Sci.*, 1995, **84**, 493-498.
66. D. E. Owens and N. A. Peppas, *Int. J. Pharm.*, 2006, **307**, 93-102.
67. S. A. Kulkarni and S.-S. Feng, *Pharm. Res.*, 2013, **30**, 2512-2522.

## 2.5 Appendix – Supporting Information

### 2.5.1 Materials and Methods

**Materials:** $Bi(NO_3)_3 \cdot 5H_2O$ (≥98%), oleylamine (OA, 70%), L-cysteine (97%), and 6-aminohexanoic acid (≥98.5%) were purchased from Sigma-Aldrich and used without further purification. Poly-(ethylene glycol)-methyl-ether-amine (mPEG-$NH_2$, mw=5000 g/mol) was purchased from Lysan Bio. NaOH pellets (≥97%) were purchased from ACS Reagents. Water was purified through Milli Q system prior to use.

**Mechanochemical experiments:** Milling was performed with a Retsch Mixer Mill MM400 (MM) using 10 ml Retsch stainless steel grinding jars (01.462.0236). An agate mortar and pestle was used for manual grinding (MG). Scale-up syntheses were performed with a Retsch S100 centrifugal ball mill (PM), using a Retsch 50 ml stainless steel grinding jar (01.462.0149).

***n*OA@$Bi_2S_3$-*m*-MM:** (*n*=5 or 10, *m* = 5 or 90): $Bi(NO_3)_3 \cdot 5H_2O$ (0.103 mmol, 50.0 mg), L-cysteine (0.155 mmol, 18.8 mg) and OA (0.515 mmol, 137.8 mg for n=5; 1.03 mmol, 275.6 mg for n=10) were placed in a 10 mL stainless steel milling jar with a 10 mm stainless steel ball and milled in a mixer mill (MM) for *m* minutes at 29.5 Hz. The resulting yellow mixtures, with the Bi:S:OA stoichiometric ratio of 1:1.5:*n*, were kept sealed in the milling jars and aged for 12 hours in ambient conditions. The resulting black paste was then washed three times with a 3:1:1 v/v mixture of pentane, ethanol, and acetone three times, and centrifuged at 9000 rpm (5 min) after each wash. The samples were dried under vacuum overnight.

**5OA@$Bi_2S_3$-MG**: $Bi(NO_3)_3 \cdot 5H_2O$ (0.103 mmol, 50.0 mg), L-cysteine (0.155 mmol, 18.8 mg) and OA (0.515 mmol, 137.8 mg) were manually ground (MG) with an agate mortar and pestle. The yellow paste was then transferred to a closed glass vial, and aged for 12 hours in ambient conditions. The resulting black pastes, with a Bi:S:OA stoichiometric ratio of

1:1.5:5, were washed with a 3:1:1 v/v mixture of pentane, ethanol, and acetone three times, and centrifuged at 9000 rpm (5 min) after each wash. The samples were dried under vacuum overnight.

**5OA@$Bi_2S_3$-PM:** Linear scale-up was performed as follows: $Bi(NO_3)_3{\cdot}5H_2O$ (5.15 mmol, 2.50 g), L-cysteine (7.73 mmol, 0.937 g) and OA (25.8 mmol, 6.89 g) were placed in a 50 ml stainless steel jar loaded with two 15 mm, four 10 mm and six 7 mm stainless steel balls, and milled in a planetary mill (PM) operating at 500 rpm for 90 min. The direction of jar motion was set to periodically alternate every 30 seconds. The mixture was then aged in the milling jar for 24 hours and the resulting black paste, with a Bi:S:OA stoichiometric ratio of 1:1.5:5, was washed three times with a 3:1:1 v/v mixture of pentane, ethanol, and acetone, and centrifuged at 9000 rpm (5 min) after each wash. The samples were dried under vacuum overnight.

**Synthesis of sodium 6-aminohexanoate (AHA)**: 6-aminohexanoic acid (1.52 mmol, 200.0 mg) and NaOH (1.52 mmol, 61.0 mg) were placed in a 10 mL Teflon milling jar with a 10 mm Teflon ball and milled in a mixer mill (MM) for 30 min at 29.5 Hz.. The resulting powder was used as prepared in the synthesis of **nAHA@$Bi_2S_3$-90-MM$^x$.**

**nAHA@$Bi_2S_3$-90-MM$^x$:** (*n*=5 or 10, *x*= 50 or 100): $Bi(NO_3)_3{\cdot}5H_2O$ (0.154 mmol, 75.0 mg for n=5; 0.103 mmol, 50 mg for n=10), L-cysteine (0.232 mmol, 28.1 mg for *n*=5; 0.155 mmol, 18.8 mg for *n*=10) and AHA (0.773 mmol, 118.4 mg for *n*=5; and 1.03 mmol, 157.8 mg for *n*=10) were placed in a 10 mL stainless steel milling jar along with one stainless steel ball of 10 mm diameter and *x* µL of water. The mixture was then milled in a mixer mill (MM) for 90 minutes at 29.5 Hz. The yellow reaction mixture was then aged for 24 hours in the jar, and the resulting black product washed twice with water, once with ethanol, and centrifuged at 9000 rpm (5 min) after each wash. The samples were dried under vacuum overnight.

**5AHA&PEG@$Bi_2S_3$-90-MM**[50]: $Bi(NO_3)_3 \cdot 5H_2O$ (0.0412 mmol, 20.0 mg), L-cysteine (0.0619 mmol, 7.50 mg), AHA (0.186 mmol, 28.50 mg), mPEG-$NH_2$ (0.0206 mmol, 103.0 mg) and 50 µL water were placed in a 10 mL stainless steel milling jar along with a stainless steel ball of 10 mm diameter. The mixture was then milled in a mixer mill (MM) for 90 min at 29.5 Hz. The yellow mixture was then aged for 24 hours in the jar, and the resulting black product washed twice with water, once with ethanol, and centrifuged at 9000 rpm (5 min) after each wash. The samples were dried under vacuum overnight.

**5AHA@$Bi_2S_3$-90-PM:** Linear scale-up was performed as follows. First, 6-aminohexanoic acid (20.6 mmol, 2.70 g) and NaOH pellets (20.6 mmol, 0.825 g) were placed in a 50 ml stainless steel jar loaded with two 15 mm, four 10 mm and six 7 mm stainless steel balls, and the mixture milled in a planetary mill (PM) for 30 min, operating at 500 rpm, with the jar motion M, alternating clockwise-counterclockwise periodically. The produced AHA that stuck to the sides and lid of the jar were gently scraped off into the middle with the help of 2 ml of water. Next, $Bi(NO_3)_3 \cdot 5H_2O$ (4.12 mmol, 2.00 g) and L-cysteine (6.18 mmol, 0.75 g) were added to the jar, and the mixture was milled for 90 min at 500 rpm, with the direction of jar rotation alternating periodically. The yellow reaction mixture was then aged for 24 hours, the resulting black product washed twice with water, once with ethanol, and centrifuged at 9000 rpm (5 min) after each wash. The samples were dried under vacuum overnight.

### 2.5.2 Characterization

**Transmission Electron Microscopy (TEM):** In order to observe their morphology and size, OA-capped and AHA-capped samples were dispersed in toluene and water, respectively. A droplet of the suspension was put onto the Cu grid and subsequently dried under vacuum overnight. High-resolution TEM images were obtained using a FEI Tecnai G2 F20 Cryo-scanning transmission electron microscope at an acceleration voltage of 200 kV. The mean sizes of the NPs were obtained by measuring the largest diameters using imageJ (data are expressed as mean ± standard deviation).

**Powder X-Ray Diffraction (PXRD):** The phase and structural analysis of the samples were carried out using a Bruker D2 Phaser X-Ray Diffractometer equipped with a Cu Kα source (λ=1.54184 Å) operating at 30 kV and 10 mA.

**X-ray Photoelectron Spectroscopy (XPS):** Measurements were performed on a Thermo Scientific K-Alpha X-Ray photoelectron spectrometer with an excitation source of Al Kα= 1486.6 eV. The binding energies were corrected by referencing the C 1s line to 284.80 eV. The samples were dried overnight in an Isotemp Vacuum Oven (model 281A) at room temperature prior to XPS analysis.

**Thermogravimetric Analysis (TGA):** Surface coating of the nanoparticles was determined using a TA instruments thermogravimetric analyzer Q500; the samples were heated to 800 °C at a rate of 20 °C/min and the atmosphere was switched from nitrogen to oxygen at 100 °C.

**Electrospray Ionization Mass Spectrometry (ESI-MS):** Reaction intermediates were resolved, using a Bruker maXis Impact quadrupole time-of-flight mass spectrometer equipped with an electrospray ionization source, using sodium formate as a calibration standard.

**Matrix-Assisted Laser Desorption/Ionization Time-of-Flight Mass Spectrometry (MALDI-TOF MS):** Mass spectra of the OA-capped $Bi_2S_3$ NPs were carried out using an Bruker Auto Flex MALDI-TOF MS, with 2, 5-dihydroxybenzoic acid or dithranol as the matrix. A single droplet of matrix solution (5-dihydroxybenzoic acid with 1:1 molar ratio acetone-acetonitrile; dithranol in 1:1 molar ratio dichloromethane-methanol) was spotted onto a stainless steel target plate and dried at room temperature. Next, the NPs were dispersed in the acetone-acetonitrile solution, and a drop of the suspension was placed over the plated matrix. Desorption and ionization of the samples was achieved by irradiation using

a pulsed nitrogen laser (337 nm, 180 µJ/pulse, 4 ns pulses). MS were measured with the laser at 58% full power in positive mode. The accelerating voltage was set at 20 kV. Data were collected using the Reflex control software and processed with the Bruker Flex Analysis software.

**Micro-CT:** The radiodensity of the **5AHA@$Bi_2S_3$-90-MM$^{50}$** and **5AHA&PEG@$Bi_2S_3$-90-MM$^{50}$** samples as a function of bismuth concentration were evaluated using a SkyScan 1178 high-throughput micro-CT with a source voltage of 50 kV, and source current of 615 µA. Images were taken of the samples at various dilutions in phosphate buffered saline (PBS), and the CT value, in Hounsfield Units (HU), were obtained by referencing PBS and air to HU= 0 and HU = -1000, respectively. Water provided an equivalent CT value to that of PBS.

**Inductively Coupled Plasma-Optical Emission Spectra (ICP-OES):** $Bi_2S_3$ NPs' suspendibility in water and PBS were evaluated by measuring the bismuth concentration of different dilutions using a Thermo Scientific iCAP Q ICP-MS equipped with an autosampler. Excess of each sample were added to 500 µL water or PBS, and well suspended by ultra-sonicating for 30 min. The suspensions were left idle for 30 min, and then 100 µL was pipetted from the very top of the suspension into digestion tubes. The suspensions were digested with 0.5 mL nitric acid (68 wt%) and 0.5 mL $H_2O_2$ (30 wt%), and the calculated amount of water or PBS was added to have 10 mL dilute solutions. Dilutions and ICP analysis were done in duplicate for reproducibility purposes. The average was given as the final data.

**Infrared Spectrometry:** An infrared spectra was performed on the samples, **5AHA@$Bi_2S_3$-90-MM$^{50}$** and **5AHA&PEG@$Bi_2S_3$-90-MM$^{50}$,** using a PerkinElmer FT-IR spectroscopy 400 (4 $cm^{-1}$ resolution) equipped with GladiATR sampling device (Pike technology) in order to identify the surface bound ligands.

### 2.5.3 Sample annealing, followed by PXRD analysis

PXRD analysis of all samples produced with OA and AHA revealed that no crystalline material was present in the sample. However, in order to further establish that the samples were solely composed of $Bi_2S_3$ and exclude the presence of any $Bi_2O_3$, we performed the following experiments: all OA and AHA-containing samples, after aging, were annealed under vacuum at 275 °C for 6 hours and re-examined by PXRD. As displayed in Figure S11 and S12 for OA and for AHA, the positions and relative intensities of all X-ray reflections are in excellent agreement with those expected for the orthorhombic $Bi_2S_3$ (JCPDS No. 017-0320). All reflections in the X-ray diffractogram were readily assigned to the known $Bi_2S_3$ structure, indicating the absence of any crystalline impurities, notably $Bi_2O_3$ NPs, which would have appeared if the original samples had contained such an impurity, either crystalline or amorphous. The TEM images (Figure S13) of the annealed sample revealed significant increase in the size of nanoparticles upon annealing, with lattice fringes of $Bi_2S_3$ readily visible. Additionally, the annealed sample of **5OA@$Bi_2S_3$-5-MM** was analyzed by XPS (Figure S14) and was compared to its as-prepared counterparts (Figure 1) to ascertain the presence of $Bi_2S_3$ *ab initio*. No significant binding energy shifts are observed for each element peak, signifying chemical state of the NP core is not affected by the annealing. Importantly, there was no difference in binding energies measured by XPS for freshly prepared and annealed **5AHA@$Bi_2S_3$-90-MM**[50] NPs (Figure S15), except for Bi4f spectra in which annealing induced the appearance of two series of peaks with a splitting of 1.0 eV. While the signal at 159.4 eV is attributed to $Bi_2O_3$,[1] likely formed by partial oxidation during annealing process, signal at 158.4 eV corresponds to $Bi_2S_3$, signifying that $Bi_2S_3$ was formed *ab initio*.

### 2.5.4 Synthesis Cost Analysis

**5OA@$Bi_2S_3$-PM:**

- $Bi(NO_3)_3 \cdot 5H_2O$ (≥98%, Sigma Aldrich): 50.20 $ CAD per 100 g bottle (2.50 g ~ 1.26 $ CAD)
- L-cysteine (97%, Sigma Aldrich): 80.90 $ CAD per 100 g bottle (0.937 g ~ 0.76 $ CAD)
- Oleylamine (70%, Sigma Aldrich): 35.00 $ CAD per 100 g bottle (6.89 g ~ 2.41 $ CAD)

**4.43 $ CAD / 1.53 g yield; ~ 2.61 $ CAD / g of 5OA@$Bi_2S_3$-PM**

**5AHA@$Bi_2S_3$-90-PM:**

- $Bi(NO_3)_3 \cdot 5H_2O$ (≥98%, Sigma Aldrich): 50.20 $ CAD per 100 g bottle (2.0 g ~ 1.00 $ CAD)
- L-cysteine (97%, Sigma Aldrich): 80.90 $ CAD per 100 g bottle (0.75 g ~ 0.61 $ CAD)
- 6-aminohexanoic acid (≥98.5%, Sigma Aldrich): 94.70 $ CAD per 100g bottle (2.70 g ~ 2.56 $ CAD)
- NaOH pellets (≥97%, ACS Reagents): 120.00 $ CAD per 1 Kg bottle (0.825 g ~ 0.10 $ CAD)

**4.27 $ CAD / 0.936 g yield; ~ 4.56 $ CAD / g of 5AHA@$Bi_2S_3$-90-PM**

### 2.5.5 Additional Figures

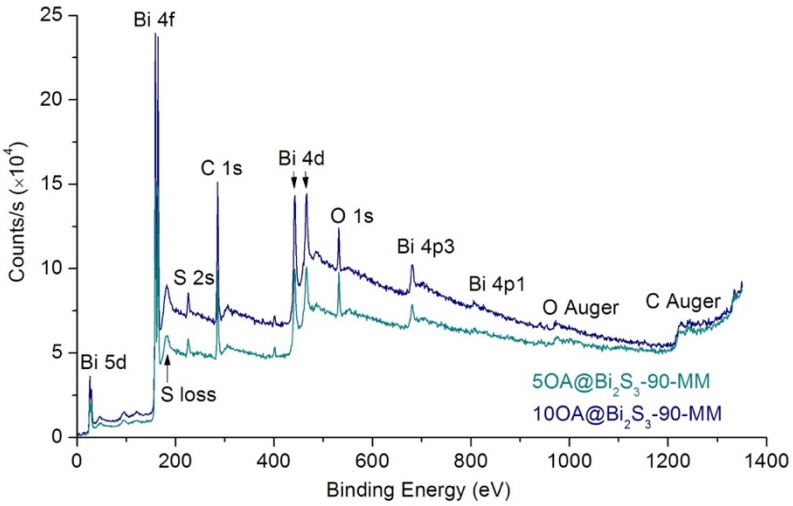


**Figure S2. 1.** Survey XPS spectra of OA-capped $Bi_2S_3$ NPs.

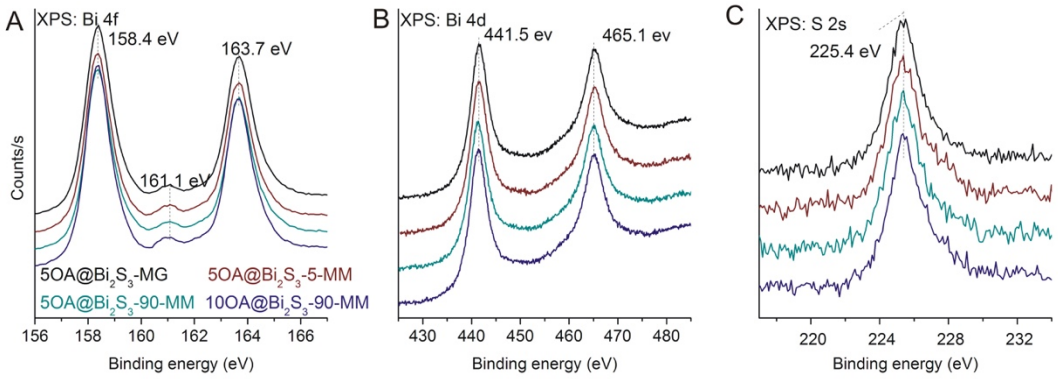


**Figure S2. 2.** High-resolution XPS spectra of Bi 4f (A), Bi 4d (B) and S 2s (C) of OA-capped $Bi_2S_3$ NPs.

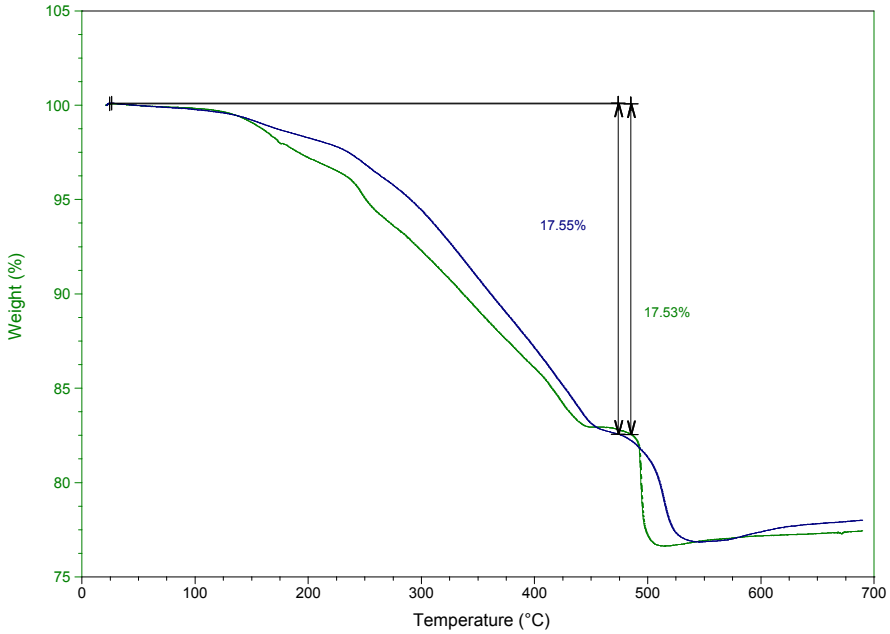


**Figure S2. 3.** TGA of **5OA@$Bi_2S_3$-90-MM** (green) and **10OA@$Bi_2S_3$-90-MM** (blue) samples, showing a 17.53% and 17.55% mass loss, respectively.

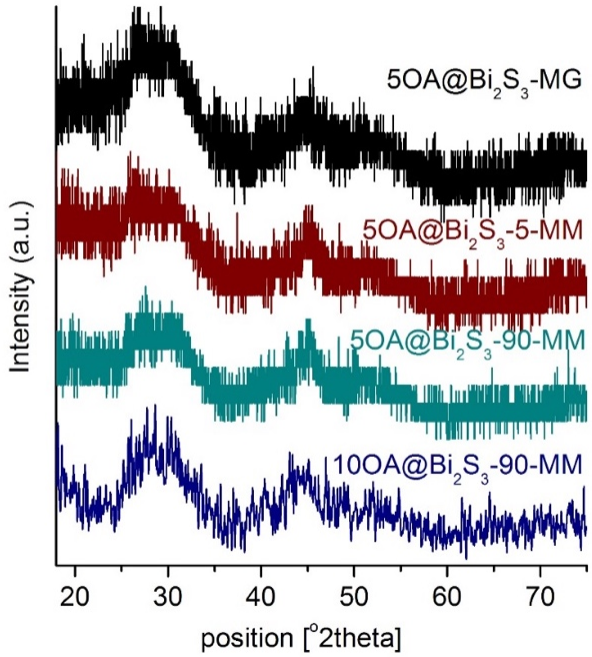


**Figure S2. 4.** PXRD of the OA-capped $Bi_2S_3$ NPs after 5/90 min mixer ball milling and manual grinding at 5:1 or 10:1 ligand-to-bismuth ratios.

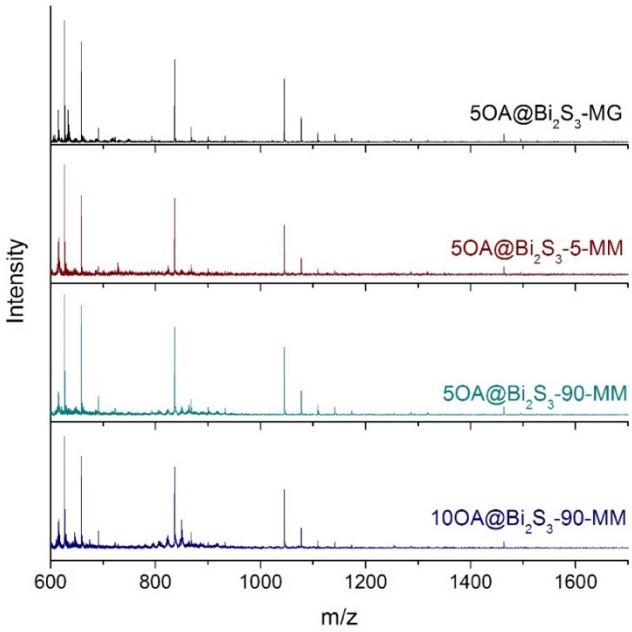


**Figure S2. 5.** Expanded window of MALDI-TOF MS spectra for OA-capped $Bi_2S_3$ NPs using 5-dihydroxybenzoic acid as the matrix.

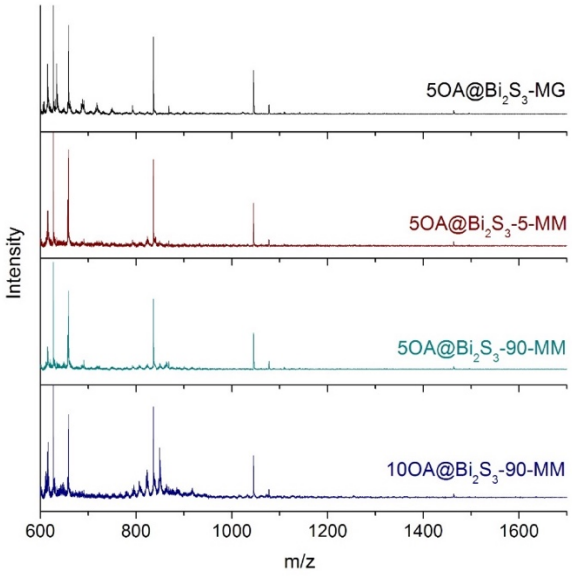


**Figure S2. 6.** Expanded MALDI-TOF MS spectra for OA-capped $Bi_2S_3$ NPs using dithranol as the matrix.

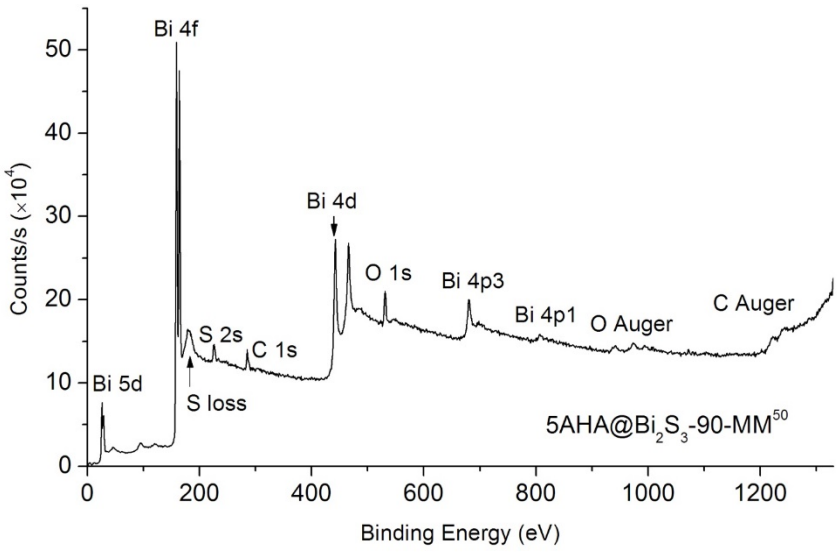


**Figure S2. 7.** Survey XPS spectra of the **5AHA@$Bi_2S_3$-90-MM$^{50}$** sample.

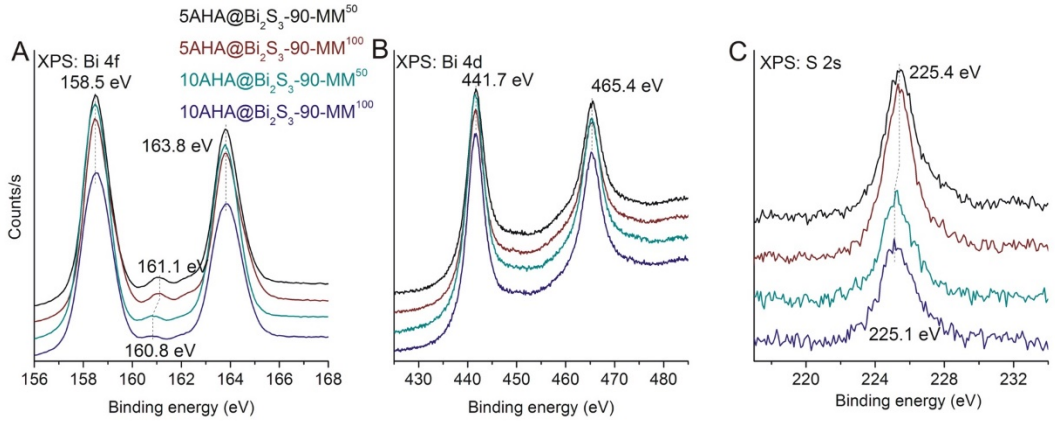


**Figure S2. 8.** High-resolution XPS spectra of Bi 4f (A), Bi 4d (B) and S 2s (C) of the AHA-capped $Bi_2S_3$ NP samples.

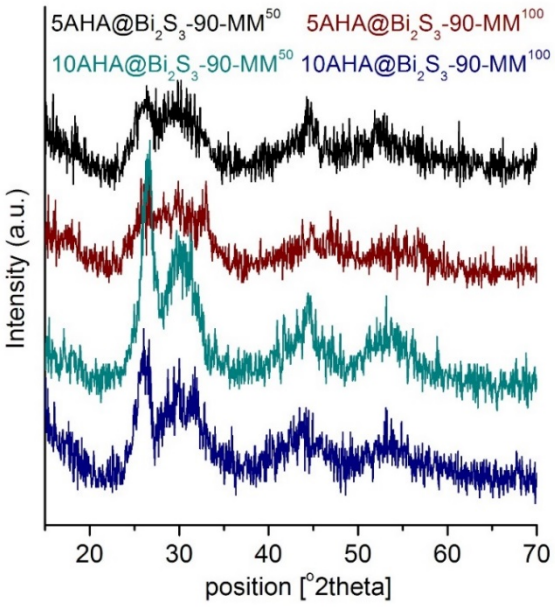


**Figure S2. 9.** PXRD of the AHA-capped $Bi_2S_3$ NPs after 90 min mixer ball milling at various ligand-to-bismuth ratios (5:1 or 10:1) and water contents (50 or 100 µL).

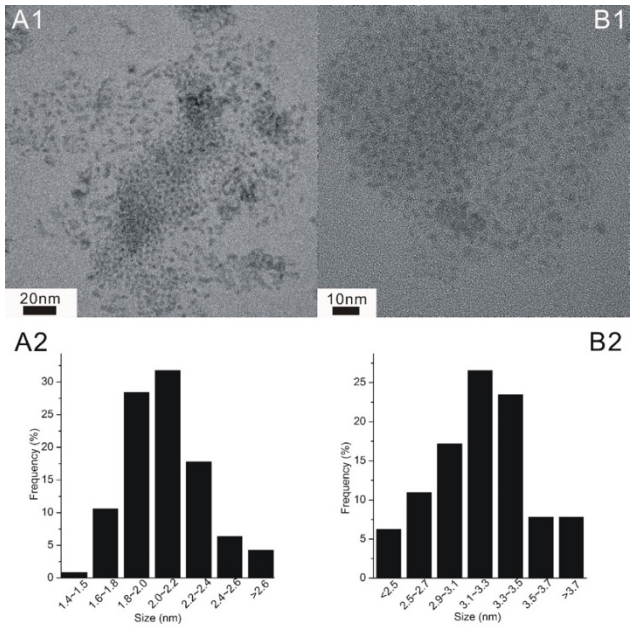


**Figure S2. 10.** TEM images and size distribution histograms of scale-up $Bi_2S_3$ nanoparticles: (A1&2) **5OA@$Bi_2S_3$-90-PM** (n=235); (B1&2) **5AHA@$Bi_2S_3$-90-PM** (n=75).

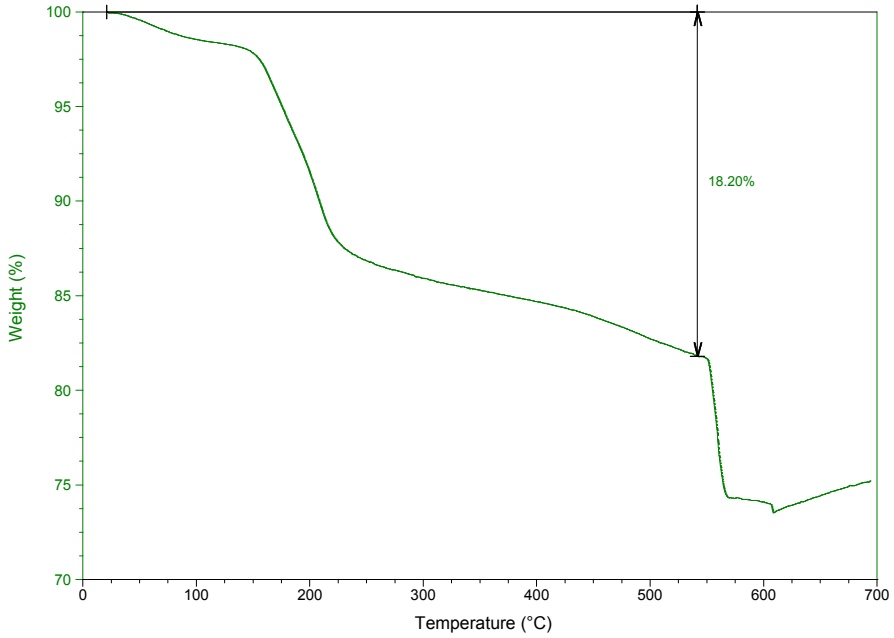


**Figure S2. 11.** TGA of **5AHA@$Bi_2S_3$-90-PM** showing a 18.20% mass loss.

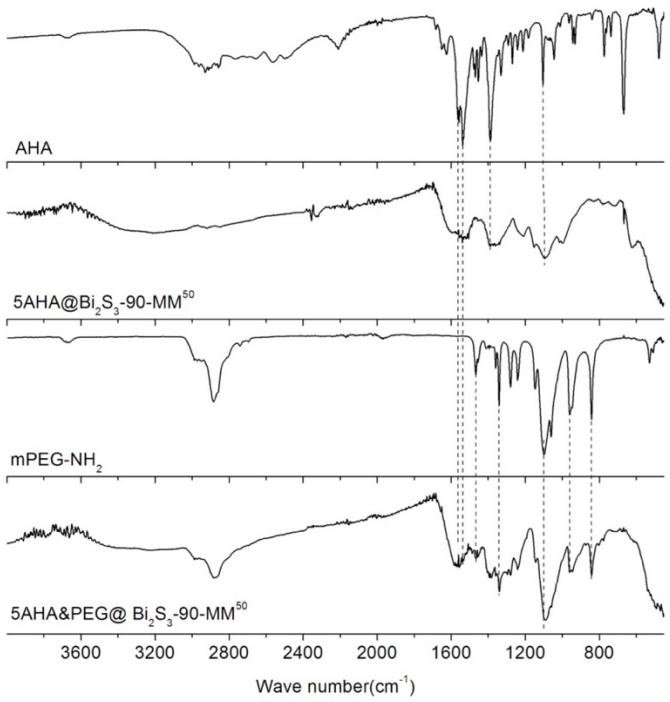


**Figure S2. 12.** Infrared spectra of pure ligands and the corresponding ligand-capped $Bi_2S_3$ NPs.

| Ligands | Wavenumber ($cm^{-1}$) | Assignments[ref.] |
|---|---|---|
| $mPEG\text{-}NH_2$ | 2883 | -CH stretching[2] |
| | 1467 | -CH bending[3] |
| | 1341 | C-O-C asymmetric stretching[2] |
| | 1278, 1059 | -CO stretching[3] |
| | 1099 | C-O-C symmetric stretching[2] |
| | 956 | -CH out-of-plane bending[2] |
| AHA | 2926, 2853 | -C-H stretching [4] |
| | 1650,1625 | C=O stretching [4-6] |
| | 1557 | $COO^-$ asymmetric stretching, overlapped with amine II [4, 5] |
| | 1538 | $COO^-$ symmetric stretching, overlapped with Amine II [5]<br>Amine II [6] |
| | 1453 | $CH_2$ bending deformation [4] |
| | 1386 | C-O symmetric stretching of $COO^-$ [6]<br>-CN stretching [5]<br>-OH deformation [4] |

**Table S2. 1.** Corresponding IR stretches and their assignments.

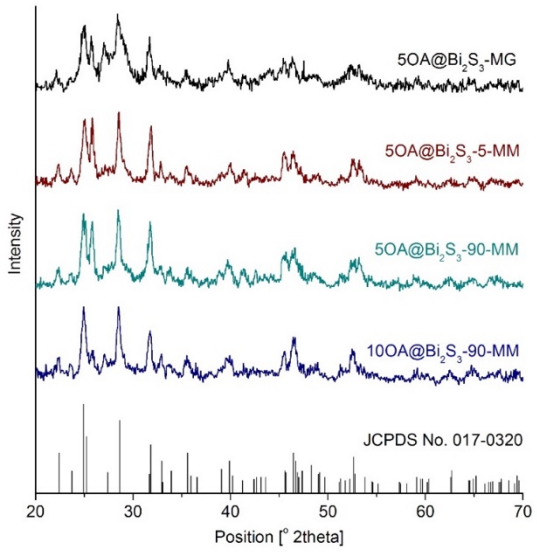


**Figure S2. 13.** PXRD of the OA-capped NPs after annealing at 275 °C under vacuum for 6 hours. All peaks are in good agreement with the orthorhombic crystal structure of $Bi_2S_3$ (JCPDS No. 017-0320).

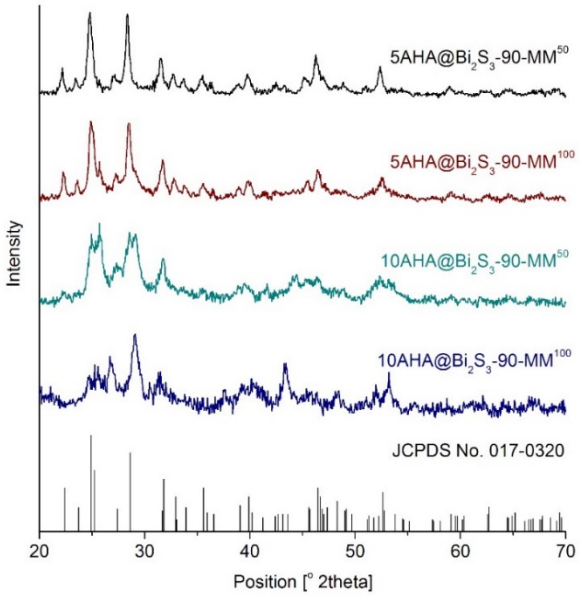


**Figure S2. 14.** PXRD of the AHA-capped NPs after annealing at 275 °C under vacuum for 6 hours. All peaks are in good agreement with the orthorhombic crystal structure of $Bi_2S_3$ (JCPDS No. 017-0320).

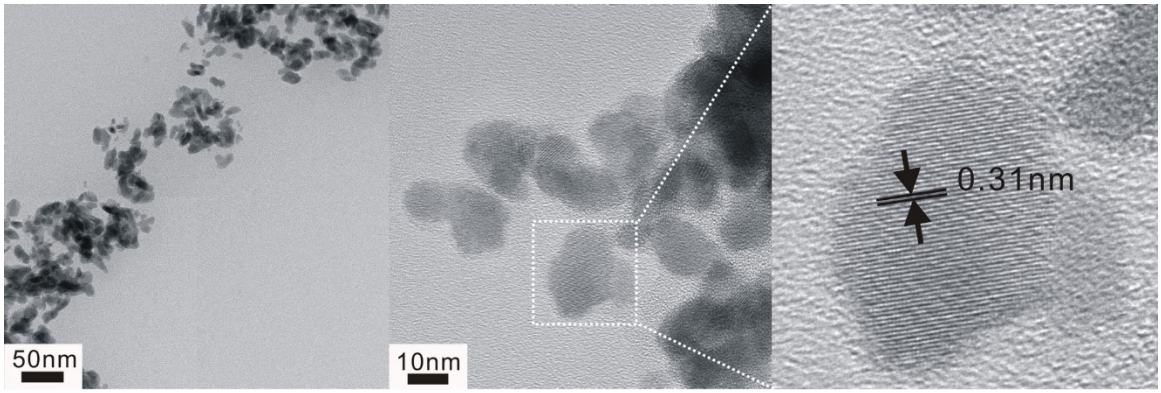


**Figure S2. 15.** TEM images of **5OA@$Bi_2S_3$-5-MM** annealed at 275 °C under vacuum for 6 hours. High-resolution TEM image (right) shows lattice fringes of 0.31 nm, corresponding to the (211) plane of orthorhombic $Bi_2S_3$ structure.

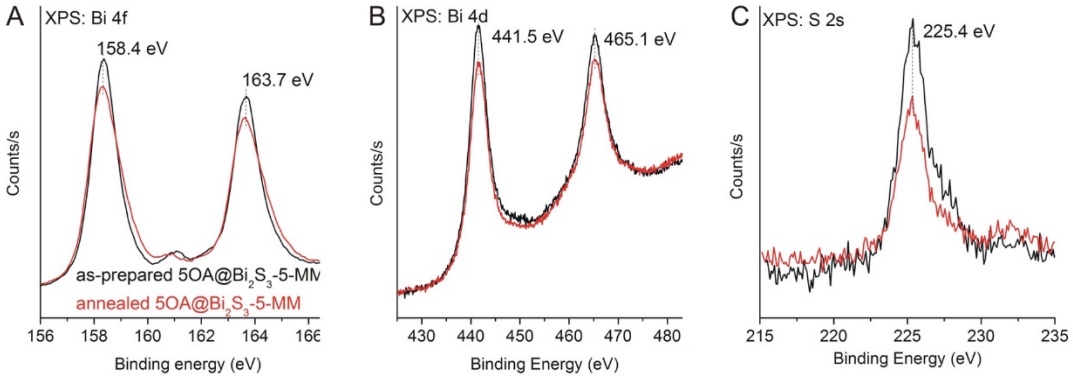


**Figure S2. 16.** High-resolution XPS spectra of Bi 4f (A), Bi 4d (B) and S 2s (C) of **5OA@$Bi_2S_3$-5-MM** before (black) and after (red) annealing.

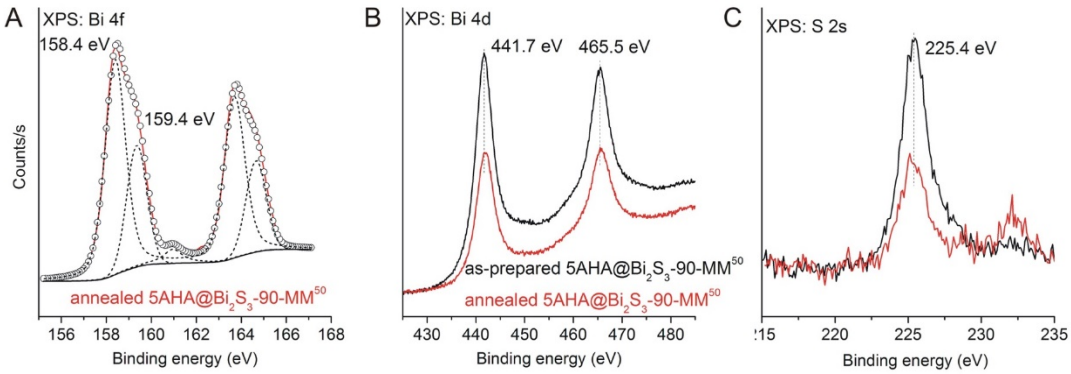


**Figure S2. 17.** High-resolution XPS spectra of Bi 4f (A), Bi 4d (B) and S 2s (C) of **5AHA@$Bi_2S_3$-90-MM**[50] before (black) and after (red) annealing under vacuum. Solid lines: experimental data; circles and dash lines: fitting data. Bi 4f spectrum of annealed sample shows two fitting peaks at 158.4 and 159.4 eV, which are assigned to $Bi_2S_3$ and $Bi_2O_3$, respectively. The sample was partially oxidized during annealing.

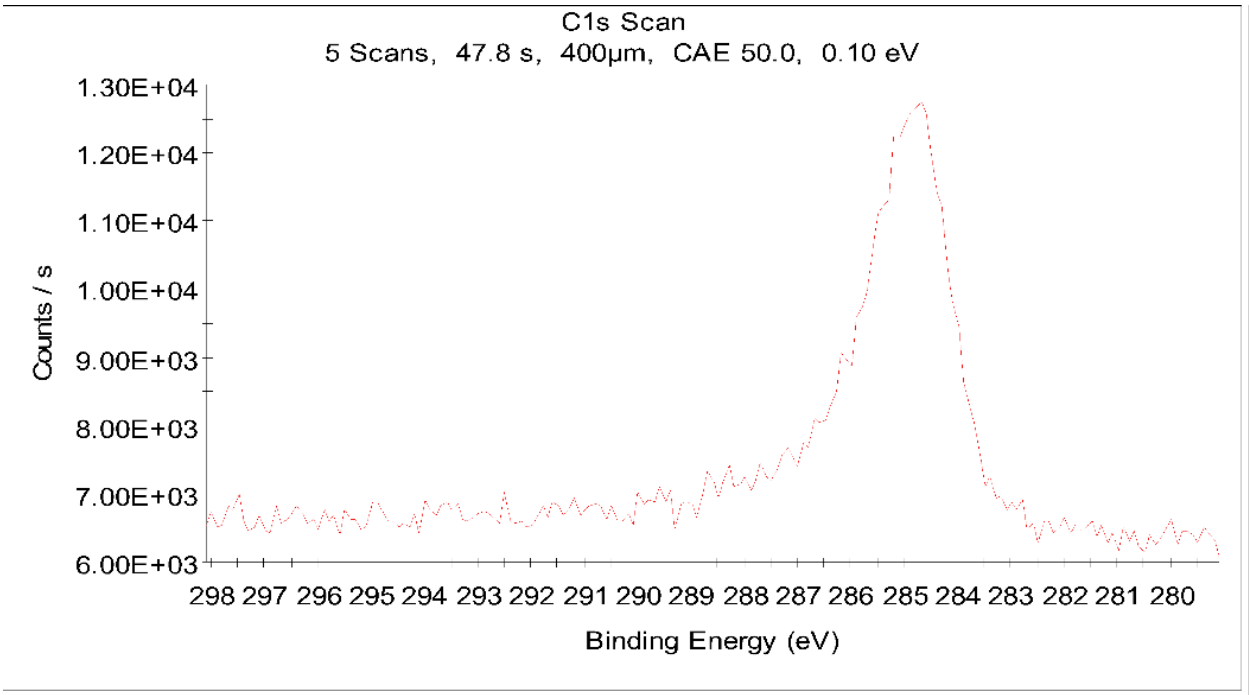


**Figure S2. 18.** High-resolution XPS C1s spectrum of **5OA@$Bi_2S_3$-90-MM** showing absence of C=O peak.

### 2.5.6 Supplementary Tables

| 5-Dihydroxybenzoic Acid | | | | Dithranol | | | |
|---|---|---|---|---|---|---|---|
| **5OA@$Bi_2S_3$-MG** | **5OA@$Bi_2S_3$-5-MM** | **5OA@$Bi_2S_3$-90-MM** | **10OA@$Bi_2S_3$-90-MM** | **5OA@$Bi_2S_3$-MG** | **5OA@$Bi_2S_3$-5-MM** | **5OA@$Bi_2S_3$-90-MM** | **10OA@$Bi_2S_3$-90-MM** |
| 626.957 | 626.945 | 626.940 | 626.948 | 626.948 | 626.896 | 626.980 | 626.945 |
| 658.995 | 658.991 | 658.996 | 659.002 | 659.016 | 659.038 | 659.038 | 659.008 |
| 691.036 | 690.939 | 691.041 | 690.899 | 691.100 | 690.939 | 687.838 | 836.253 |
| 723.062 | 727.758 | 723.037 | 723.037 | 719.817 | 836.243 | 691.107 | 1045.567 |
| 754.992 | 836.265 | 836.273 | 807.041 | 749.858 | 868.206 | 836.353 | 1077.517 |
| 836.270 | 868.311 | 868.274 | 836.253 | 792.693 | 1045.483 | 868.409 | 1463.903 |
| 868.319 | 1045.464 | 900.301 | 863.252 | 836.304 | 1077.438 | 1045.651 | |
| 900.267 | 1077.411 | 932.316 | 868.284 | 868.138 | 1463.753 | 1077.671 | |
| 932.278 | 1109.428 | 1045.488 | 886.243 | 868.364 | | 1110.068 | |
| 964.295 | 1141.365 | 1077.486 | 900.347 | 900.485 | | 1463.954 | |
| 1045.443 | 1173.548 | 1109.475 | 932.304 | 1045.533 | | 1496.604 | |
| 1077.429 | 1318.358 | 1141.486 | 1045.465 | 1077.570 | | | |
| 1109.412 | 1463.627 | 1173.600 | 1077.490 | 1109.479 | | | |
| 1141.372 | 1495.465 | 1255.064 | 1109.530 | 1110.001 | | | |
| 1173.389 | | 1286.584 | 1141.440 | 1141.691 | | | |
| 1205.382 | | 1318.877 | 1173.460 | 1463.823 | | | |
| 1254.551 | | 1463.624 | 1254.509 | 1495.590 | | | |
| 1286.534 | | 1495.986 | 1285.549 | 1496.005 | | | |
| 1318.419 | | 1527.506 | 1286.482 | | | | |
| 1463.579 | | 1559.724 | 1318.475 | | | | |
| 1495.497 | | 1591.523 | 1463.583 | | | | |
| 1527.326 | | | 1495.709 | | | | |
| 1527.750 | | | | | | | |
| 1527.805 | | | | | | | |
| 1559.455 | | | | | | | |

**Table S2. 2.** Peak lists of MALDI-TOF MS spectra in Figure S4 and S5.

| | **Mean Bismuth Concentration (M)** | **Mean CT Value (HU) ±SD** |
|---|---|---|
| **5AHA&PEG@$Bi_2S_3$-90-MM[50]** | 0.0747 | 1437±0.0 |
| | 0.0381 | 1053±20.6 |
| | 0.0201 | 806±7.4 |
| | 0.0099 | 633±19.9 |
| | 0.0050 | 426±28.7 |
| **5AHA@$Bi_2S_3$-90-MM[50]** | 0.0747 | 1335±33.8 |
| | 0.0351 | 1109±28.1 |
| | 0.0181 | 867±17.0 |
| | 0.0084 | 592±31.4 |
| | 0.0043 | 374±6.2 |

**Table S2. 3.** Experimental radiodensity, bismuth concentration determined by ICP for **5AHA@$Bi_2S_3$-90-MM[50]** and **5AHA&PEG@$Bi_2S_3$-90-MM[50]** samples in PBS buffer.

### 2.5.7 Supplementary Information References


1. J. F. Moulder, *Handbook of X-ray photoelectron spectroscopy: a reference book of standard spectra for identification and interpretation of XPS data*, Perkin-Elmer, Eden Prairie, MN, 1992.
2. C. Yue-Jian, T. juan, X. Fei, Z. Jia-Bi, G. Ning, Z. Yi-Hua, D. Ye and G. Liang, *Drug Dev. Ind. Pharm.*, 2010, **36**, 1235-1244.
3. K. Shameli, M. Bin Ahmad, S. D. Jazayeri, S. Sedaghat, P. Shabanzadeh, H. Jahangirian, M. Mahdavi and Y. Abdollahi, *Int. J. Mol. Sci.*, 2012, **13**, 6639.
4. A. Phadke, C. Zhang, B. Arman, C.-C. Hsu, R. A. Mashelkar, A. K. Lele, M. J. Tauber, G. Arya and S. Varghese, *Proc. Natl. Acad. Sci. U.S.A*, 2012, **109**, 4383-4388.
5. J. D. Patel, F. Mighri and A. Ajji, *Mater. Sci. Appl.*, 2012, **3**, 125-130.
6. R. Barbucci, M. Casolaro and A. Magnani, *Die Makromolekulare Chemie*, 1989, **190**, 2627-2638.

# Chapter 3 Mechanically-activated assembly of blue-emitting CdS and ZnS quantum dots

**Abstract**

---

Semiconductor nanomaterials have become increasingly relevant to researchers in the domains of optics, biomedical imaging, and catalysis. Herein we describe a facile mechanically activated self-assembly of monodisperse ZnS and CdS quantum dots of 2.4-3.6 nm in diameter that proceeds spontaneously in air with minimal intervention. This method is low-energy consuming, eschews added solvent, and can be linearly scaled up with ease to afford gram-scale quantities of both nanomaterials, which is unprecedented in forgoing literature. Both products are blue-emitting with narrow photoluminescent emissions. The synthesized ZnS nanoparticles have shown to have stable absorbance and emission shifts for over a month. The mechanism through which this reaction proceeds is briefly discussed.

---

## 3.1 Introduction

Semiconductor quantum dots have attracted much attention for their unique optical and electronic properties that are absent in their bulk counterparts[1,2]. An interesting property of semiconductors is their band gap energy, which is the minimum energy required to excite an electron from the valence band to a vacant conduction band, and for these materials lie between that of a metal and insulator. Excitation of an electron creates a hole in the valence band, leading to an electrostatically bound electron-hole pair known as an *exciton*[3]. Exciton relaxation can result in the emission of a photon in a process known as radiative recombination[3]. The electron-hole pair inter-distance is defined by the Bohr radius ($r_B$). If the size of the semiconductor nanocrystal becomes smaller than $r_B$, the exciton becomes spatially confined, raising its energy, and leading to quantum confinement, according to the equation:

$$\Delta E_g = {E_g}^{nano} - {E_g}^{bulk} = \frac{\hbar^2 \pi^2}{2MR^2}$$

where $\Delta E_g$ is the change in band-gap energy, $\hbar$ is the reduced plank constant, M is the effective mass of the electron-hole pair, and R is the radius of the nanocrystal, assuming a perfect sphere[2]. From this, we see that the optical and electronic properties of these nanocrystal become dependent on their size below $r_B$ and can be tuned accordingly to absorb and emit at certain wavelengths reminiscent of discrete electronic transitions. This affords a means to manipulate their optical properties through varying reaction conditions[3].

ZnS and CdS nanoparticles (NP) are among the semiconductor materials studied in this domain due to their high chemical- and photo-stability[4], making them candidates for many optical based devices[5,6] and medical diagnostic tools[7]. Furthermore, their emissions can also be tuned by controlling their shape[8], surface chemistry[9] or introducing metal dopants within the nanocrystal lattice[10], unlike organic fluorophores, which are more constrained to their nature. Their high surface area also makes them attractive materials for photocatalysis[11]. ZnS is a II-VI semiconductor that has a wide band gap of 3.72 - 3.77 eV[12] and a Bohr exciton radius of around 2.5 nm[13]. It usually exists in two main crystal phases: cubic (spalerite) and hexagonal (wurtzite).

CdS has a direct band gap of 2.42 eV with a Bohr exciton radius of about 2.85 nm[14,15]. Bulk CdS adopts a hexagonal structure but can exist in a cubic phase when nano-sized[14]. Their size, shape and environment are important factors in determining their chemical and physical properties. For example, as a bulk material, ZnS adopts a cubic structure at room temperature, while being more stable as hexagonal at temperatures above 1293 K[16]. However, the interfacial energy of nano-sized (< 7nm) cubic ZnS has been suggested to be greater than that of the hexagonal phase[17,18], which explains why low-temperature NP syntheses often yield hexagonal products[19].

Several preparations of ZnS and CdS nanostructures have been previously reported[20,21,11,22,23]. However, their multi-gram syntheses are inherently challenging due to the protocols employed that would require tedious methods to achieve comparable products to that of small-scale ones. For example, under the most commonly used hot-injection protocols, major issues arise in achieving uniform distribution of sulfur and thermal energy across the reaction mixture (provided the large injected volume, differential mass transfer profiles, and the strong dependence on temperature throughout the reaction) as well as making reproducible protocols to avoid polydisperse end-products[24,25]. Mechanochemistry has very recently become an emerging technique at the forefront of nanomaterial synthesis. This method allows the reaction of molecular precursors in solid state, circumventing the need of a solvent medium and thermal energy, and accordingly may afford novel materials that may not be accessible under solution-based conditions[26,27]. In ball milling, mechanical forces prompt the intimate mixing of molecular precursors, allowing reactivity between reactant in the solid phase[28,29]. Since the use of solvent and energy is drastically reduced by this method, it would be particularly attractive if it can be amended to large-scale or industrial syntheses of nanomaterials.

Previously, Baláž *et al.* and Godočíková *et al.* were able to prepare ZnS and CdS nanocrystals *via* by high-energy ball milling of zinc acetate and sodium sulfide under inert atmosphere[30,31]. Lu et al. synthesized ZnS nanocrystals by milling zinc acetate and thioacetamide, followed by thermal reaction at temperatures varying from 100-300 °C[32]. $Cd_xZn_{1-x}S$ nanostructures have also been synthesized by high-energy planetary milling[33]. However, among

other mechanochemical procedures, all result in irregular, polydisperse particles. Our group recently described a facile, mechanically activated synthesis of highly monodisperse bismuth sulfide nanoparticles[34], of sizes ranging from 2 to 8 nm depending on the reaction conditions, in which the use of stabilizing agent was key in controlling the final NP size. Interestingly the reaction proceeded *via* a short mechanoactivation (ball milling for 5 min or grinding by mortar and pestle) followed by an aging period of 12 to 24 hrs, where the premised-precursors were allowed to assemble spontaneously to afford the final product. This is inherent of a "bottom-up" approach, which involves assembling particles from metal precursors in the presence of a capping agent, and to the best of our knowledge is the first documented case of synthesizing monodisperse metal calcogenide NPs via this route. We have shown that this method is ideal for synthesizing uniform products with high atom economy. Herein, we demonstrate the adaptability of our method to synthesize small, monodisperse ZnS and CdS quantum dots in a green and simple fashion. The ease of scalability makes this method particularly appealing for synthesizing gram-scale quantities of these materials. The materials produced were characterized using high-resolution transmission electron microscopy (HRTEM), X-ray photoelectron spectroscopy (XPS), powder X-ray diffraction (PXRD), UV-Vis spectroscopy and photoluminescence spectroscopy (PL-Spec).

### 3.2 Results and Discussion

To access ZnS and CdS NPs, $Zn(NO_3)_2 \cdot 6\ H_2O$ or $Cd(NO_3)_2 \cdot 4\ H_2O$ were ball-milled with L-cysteine (sulfur source) in a mixer mill (MM), in the presence of oleylamine (OA) as a capping agent (Scheme 3.1, see supporting information for procedure). After 90 min of milling, the samples were left to age at room temperature for 24 hours. They were then purified through several washing and centrifugation cycles. L-cysteine was added in slight excess (~1.2 eq) above the stoichiometry of ZnS and CdS and the metal-to-OA ratio was set to 5:1 in both cases, producing the samples **OA@ZnS-MM** and **OA@CdS-MM**. The resulting materials could be readily suspended in hexanes and toluene.

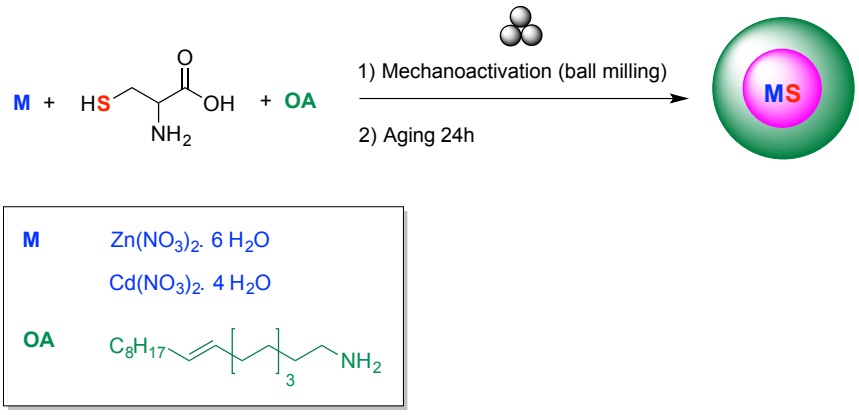


**Scheme 3. 1.** Overview of developed synthesis of CdS and ZnS NPs. M = metal precursor; OA = oleylamine.

### 3.2.1 OA@CdS-MM Results

HRTEM imaging of OA@CdS-MM were taken to assess their structure and size (Figure 3.1). Small NPs were observed, with a narrow size distribution of $3.6 \pm 0.31$ nm. Clear lattice fringes could be seen in the sample, and the d-spacing (0.352 nm) is most consistent with the (1 0 0) plane of hexagonal CdS (see inset). The NPs produced are visually spherical in morphology. EDS was also performed (Figure S3.1), confirming the presence of primarily Cd and S in the sample.

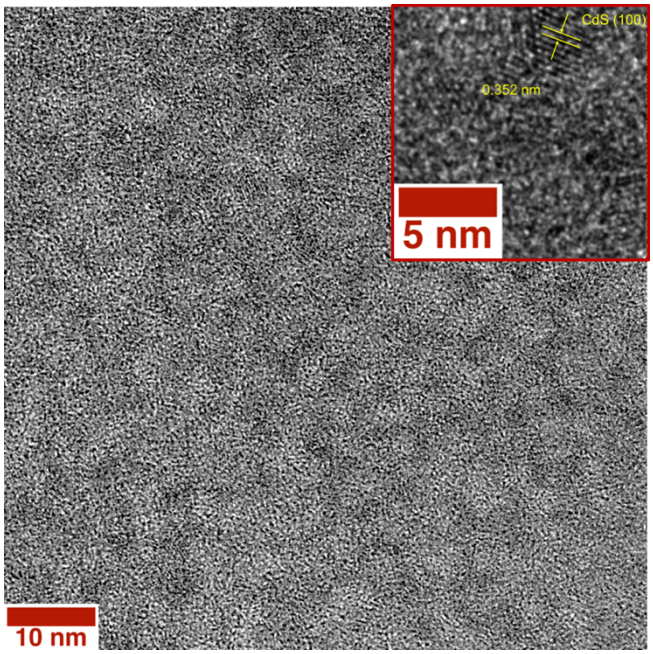

**Figure 3. 1.** HRTEM image of synthesized OA@CdS-MM. The lattice spacing of 0.352 nm corresponds to the (1 0 0) plane of hexagonal CdS (see inset).

Purified OA@CdS-MM was further studied by PXRD (Fig. S3.2). Only broad featureless peaks were observed and no clear assignment could be made. PXRD could not provide conclusive evidence on the crystallinity of the sample. As seem by TEM, the particles are crystalline, as seen be clearly visible lattice spacing, but are too small to sufficiently diffract.

Next, the OA@CdS-MM sample was analyzed by X-ray photoelectron spectroscopy (XPS), which revealed the presence of Cd, S, O, N, and C (Fig S3.3). Detection of N confirms the presence of the oleylamine ligand at the surface of the NPs. The O 1s peak centered about 531.8 eV can be ascribed to chemisorbed $O_2$ on the XPS copper tape film surface (Fig S3.4)[35]. $\mathrm{Cd}\ 3\mathrm{d}_{3/2}$ and $\mathrm{Cd}\ 3\mathrm{d}_{5/2}$ peaks at 411.9 eV and 405.1 eV, respectively, are consistent with $\mathrm{Cd}^{2+}$ ions in CdS, while the $\mathrm{S}\ 2\mathrm{p}$ signal matched $\mathrm{S}^{2-}$ (S 2p3/2: 161.4 eV, S2p ½: 162.6 eV)[35] (Figure 3.2). The integration of Cd 3d and S 2p signals indicated an average Cd:S atomic ratio of 1.01, signifying roughly equivalent amounts of Cd and S within the produced nanocrystals. This result reveals a complementary association of counter ions, even though the sulfur source was added in excess, validating the strong self-assembly nature of the precursors during the aging process. Given that the relative amounts of metal to sulfur can disturb the optical properties of the nanocrystals formed, these results were promising in having produced high-quality nanocrystals.

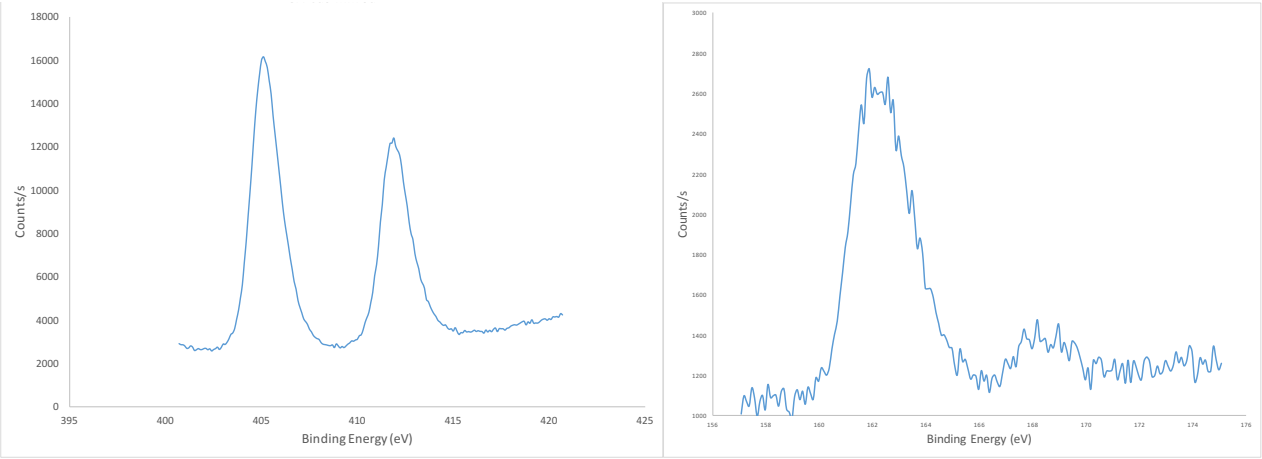


**Figure 3. 2.** XPS of OA@CdS-MM showing Cd 3d (left) and S2p (right) spectra.

UV-Vis and PL spectra of the OA@CdS-MM sample is shown in Figure 3.3. The sample exhibits an absorption edge at 364 nm that is blue-shifted with respect to bulk CdS[15], due to quantum confinement effects within the nanocrystals. A sharp emission peak at 427 nm can be seen with a full width half-maximum (FWHM) of 68 nm. A fine shoulder centered about 411 nm and 450 nm can be attributed to surface-defect emissions. The sample reveals an overall Stokes shift of 83 nm.

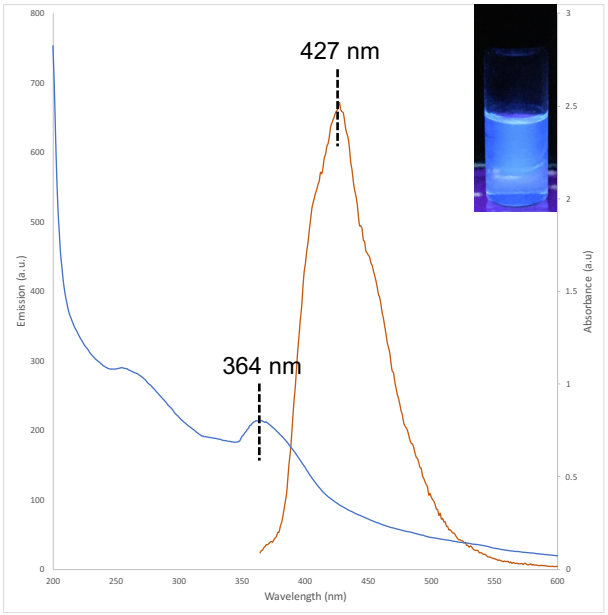


**Figure 3. 3.** UV-Vis (blue) and PL-Spectra (orange) of OA@CdS-MM suspension in hexanes.

### 3.2.2 OA@ZnS-MM Results

HRTEM imaging of OA@ZnS-MM were taken to assess their structure and size (Figure 3.4). Like with Cd, very small NPs were observed, with a narrow size distribution of $2.8 \pm 0.35$ nm. Clear lattice fringes could be seen in some regions of the sample, and the d-spacing (0.31 nm) can be ascribed to the (1 1 1) plane of cubic ZnS (see inset). EDS was also performed (Figure S3.5), confirming the presence of primarily Zn and S in the sample. While low-temperature syntheses of ZnS tend to produce hexagonal-phase products, the kinetics of nanocrystal nucleation and growth under solid-state conditions may be different, since these processes may not be influenced as much by solvation effects in achieving a global energy minimum across the sample. However, this result may not reflect the totality of the sample, and a mixture of both phases may have been produced.

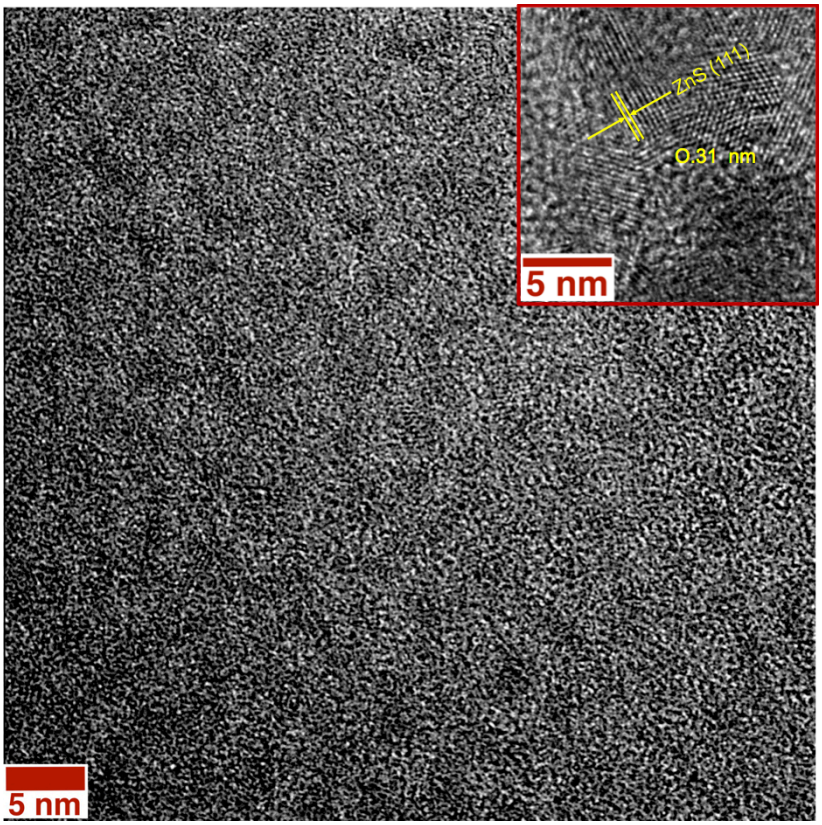


**Figure 3. 4.** HRTEM image of synthesized OA@ZnS-MM. The lattice spacing of 0.31 nm corresponds to the (1 1 1) plane of cubic ZnS (see inset).

Purified OA@ZnS-MM was next studied by PXRD (Figure S3.5). Most peaks were too broad for assessment, and like with Cd, the particle are likely too small to reach a definitive conclusion. Interestingly, the most defined peak at 2 θ of 28.6 is in agreement with the (1 1 1) plane of cubic ZnS that is most evident under HRTEM imaging.

The OA@ZnS-MM sample was analyzed by XPS, which revealed the presence of Zn, S, O, N, and C (Fig S3.7). Detection of N confirms the presence of a ligand shell surrounding the NPs. The O1s peak centered about 531.9 eV can be ascribed to chemisorbed $O_2$ on the XPS copper tape film surface (Fig S3.8)[36]. Zn2p 3/2 and ½ peaks at 1021.9 eV and 1044.8 eV are consistent with $Zn^{2+}$ ions in ZnS, while the S2p signal matched $S^{2-}$ (S 2p3/2: 161.7 eV; S 2p ½: 162.8 eV)[36] (Figure 3.5). The integration of Zn 2p and S2p signals indicated an average Zn:S atomic ratio of 1.00, indicating equivalent amounts of Zn and S integrated within the nanocrystals.

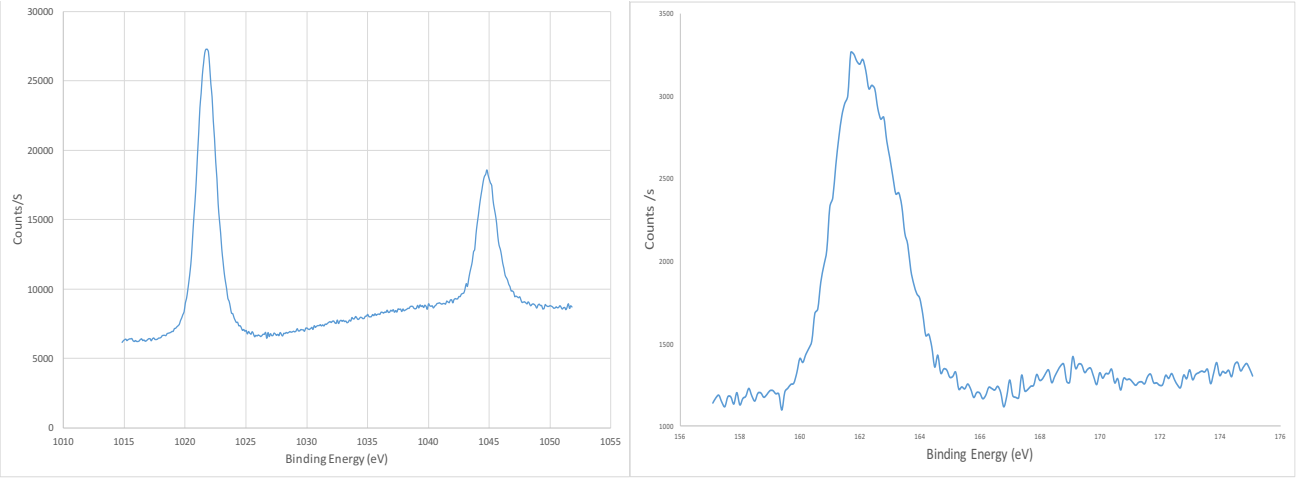


**Figure 3. 5.** XPS of OA@ZnS-MM showing Zn 2p (left) and S2p (right) spectra.

Next, we decided to study the optical properties of the produced ZnS NPs and the effect aging has on them. Fig. 6 shows the UV-Vis and PL spectra evolution of the course of aging the reaction for 24 h, 72 h and 1 month. An absorbance band can be seen at 278 nm with a bulk exciton emission fixed at 293 nm and a surface emission max centered about 402-404 nm (Table 3.1). All samples have a FWHM of around 85 nm. The absorbance and emission intensities

gradually increase with aging time from 0.27 a.u and 30 a.u (24 h) to 0.44 a.u and 44 a.u (1 month), respectively.

Since the radius of the NPs is related to its absorbance, this persistence in shift suggest that magic-sized NPs were formed, that is, particles that undergo nucleation without any further growth[37]. This has been suggested by Kudera and his colleagues to be due to stability of the small particles formed, which do not re-dissolve and contribute to Oswald ripening of the larger ones[38]. This increase in absorption as a function of reaction time had previously been seen with 'magic-sized' ZnS nanocrystals[39] of size ~3.5 nm in diameter, though on the scale of minutes under solvothermal conditions. Interestingly, as shown in Figure 3.6, we the see the evolution on the time scale of days/weeks. Provided the sample maintains its PL emission shift and breadth over 1 month of bench-top aging, this implies that the NP size is stable for at least this long, without the need for annealing or high temperature reaction conditions. However, TEM over the course of a month would need to be performed to confirm this notion. With regard to the slow increase in absorbance/emission intensity, we believe this is due to the NPs becoming more organized over time – either increased crystallinity within the lattice and/or increased ligand passivation of the crystal facets. It is still possible that unreacted precursors are assembling into NPs over this time scale, thereby increasing the optical response of the sample. However, we would expect growth of already made particle to supersede this thermodynamically. Nevertheless, it is possible under solid-state conditions, in which mass transfer is limited, that decreased mobility of surface ligands may prevent further growth.

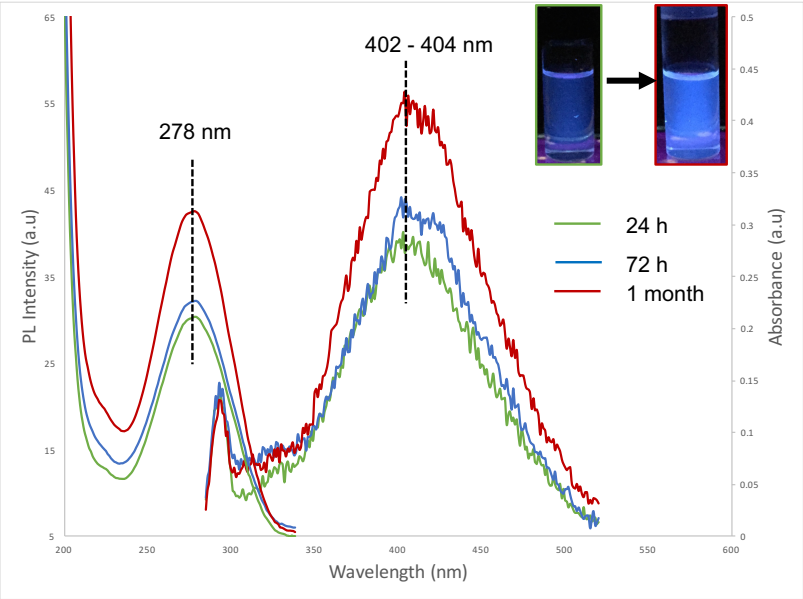


**Figure 3. 6.** UV-Vis (left) and PL-Spectra (right) of OA@ZnS-MM in hexanes after 24 h (green), 72 h (blue) and 1 month (red) of aging.

| Aging Time | Absorbance Max (nm) | Bulk Emission Max (nm) | Surface Emission Max (nm) |
|---|---|---|---|
| 24 hours | 278 | 293 | 403 |
| 72 hours | 278 | 293 | 402 |
| 1 month | 278 | 293 | 404 |

**Table 3. 1.** Photophysical properties of OA@ZnS-MM samples after 24 h, 72 h and 1 month of aging.

### 3.2.3 Multigram scale synthesis of OA@ZnS and OA@CdS NPs

Both syntheses were linearly scaled-up (1.5 grams of metal precursor) by 90 minutes of mechanical grinding using a planetary ball mill (PM) operating at 450 RPM, followed by 12 hours of aging, yielding the samples **OA@ZnS-PM** and **OA@CdS-PM**. TEM analysis showed the formation of NPs of $2.4 \pm 0.22$ nm and $2.8 \pm 0.31$ nm in diameter, respectively, with the same morphology seen in the MM reactions (Figure 3.7). The smaller diameters obtained can be accounted for by the increased energy of the planetary mill condition; the aging time of both

reactions seemed to decrease under PM conditions, most likely indicating the nucleation and growth of more NPs earlier in the aging process. However, given that the aging was terminated at half the time compared to the MM reactions, it could be that the PM reactions were aborted earlier in the nanocrystal growth.

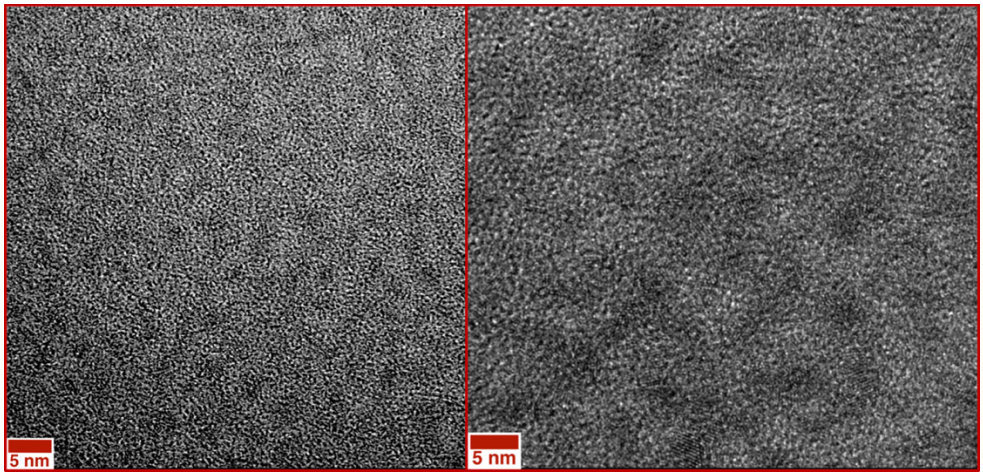


**Figure 3. 7.** TEM images of OA@ZnS-PM (left) and OA@CdS-PM (right).

## 3.3 Conclusion

In this paper, we show that precursors can be induced to assemble into nanoparticles through mechanical activation. Both the CdS and ZnS nanoparticles are fluorescently active and blue-emitting. In adjunct to our previously reported synthesis of ultra-small monodisperse bismuth sulfide NPs, we define this method of synthesis as mechanical activation (or mechanoactivation), whereby the energy supplied by mechanical perturbation stimulates the spontaneous assembly of these precursors overtime (i.e. aging the reaction), as opposed to the direct absorption of mechanical energy to surpass associated energy barriers and reach the final product. The reasons are as follows: (a) the nanoparticles form only after aging and not after milling; (b) the method of grinding (ball milling, planetary milling or manual grinding) or grinding time was previously shown to not significantly affect the final product size at similar aging intervals; (c) changing the amount of ligand was previously shown to not affect the size distribution of the product obtained and (d), the relative ratios of metal and sulfur in the produced nanomaterials are equivalent even though the sulfur precursor was added in excess,

suggesting a complementary association of ions during the aging process. To date, we have established these results for Bi, Zn and Cd as metals, in the context of the production of sulfide. The generality of this method for more material still needs to be studied. However, the advantages of this method are numerous, being solvent-free, low energy consuming, spontaneous after a small mechanical energy input, and can be linearly scaled up with ease to gram-scale quantities, which is a feat that proves to be challenging via conventional methods.

## 3.4 References


1. Alivisatos, A.; Science. *Science (80).* **1996**, *271* (5251), 933–937.
2. Kayanuma, Y. *Phys. Rev. B* **1988**, *38* (14), 9797–9805.
3. Smith, A. M.; Nie, S. *Acc. Chem. Res.* **2010**, *43* (2), 190–200.
4. Khalkhali, M.; Liu, Q.; Zeng, H.; Zhang, H. *Sci. Rep.* **2015**, *5*, 14267.
5. Li, Y.; Chen, J.; Zhu, C.; Wang, L.; Zhao, D.; Zhuo, S.; Wu, Y. *Spectrochim. Acta Part A Mol. Biomol. Spectrosc.* **2004**, *60* (8–9), 1719–1724.
6. Tan, Z.; Zhang, F.; Zhu, T.; Xu, J.; Wang, A. Y.; Dixon, J. D.; Li, L.; Zhang, Q.; Mohney, S. E.; Ruzyllo, J. *Nano Lett.* **2007**, *7* (12), 3803–3807.
7. Bruchez Jr., M.; Moronne, M.; Gin, P.; Weiss, S.; Alivisatos, A. P. *Science (80-. ).* **1998**, *281* (5385), 2013–2016.
8. La Porta, F. A.; Andrés, J.; Li, M. S.; Sambrano, J. R.; Varela, J. A.; Longo, E. *Phys. Chem. Chem. Phys.* **2014**, *16* (37), 20127–20137.
9. Chen, W.; Wang, Z.; Lin, Z.; Lin, L. *Appl. Phys. Lett.* **1997**, *70*, 1465.
10. Liu, M.; Yao, W.; Li, C.; Wu, Z.; Li, L. *RSC Adv.* **2015**, *5* (1), 628–634.
11. Zhao, Q.; Xie, Y.; Zhang, Z.; Bai, X. *Cryst. Growth Des.* **2007**, *7* (1), 153–158.
12. Fang, X.; Bando, Y.; Gautam, U. K.; Ye, C.; Golberg, D. *J. Mater. Chem.* **2008**, *18* (5), 509–522.
13. Gayou, V. L.; Salazar-Hernández, B.; Macuil, R. D.; Zavala, G.; Santiago, P.; Oliva, A. I. *J. Nano Res.* **2010**, *9*, 125–132.
14. Banerjee, R.; Jayakrishnan, R.; Banerjee, R.; Ayyub, P. *J. Phys. Condens. Matter* **2000**, *12* (50), 10647–10654.
15. Kumar, P.; Saxena, N.; Chandra, R.; Gupta, V.; Agarwal, A.; Kanjilal, D. *Nanoscale Res. Lett.* **2012**, *7* (1), 584.
16. Li, S.; Yang, G. W. *J. Phys. Chem. C* **2010**, *114* (35), 15054–15060.
17. Wang, Z.; Daemen, L. L.; Zhao, Y.; Zha, C. S.; Downs, R. T.; Wang, X.; Wang, Z. L.; Hemley, R. J. *Nat. Mater.* **2005**, *4* (12), 922–927.
18. Zhang, H.; Huang, F.; Gilbert, B.; Banfield, J. F. *J. Phys. Chem. B* **2003**, *107*, 13051–13060.
19. La Porta, F. A.; Ferrer, M. M.; de Santana, Y. V. B.; Raubach, C. W.; Longo, V. M.; Sambrano, J. R.; Longo, E.; Andrés, J.; Li, M. S.; Varela, J. A. *J. Alloys Compd.* **2013**, *556*, 153–159.
20. Vossmeyer, T.; Katsikas, L.; Gienig, M.; Popovic, I. G.; Diesner, K.; Chemseddine, A.;

Eychmiiller, A.; Weller, H. *J. Phys. Chem* **1994**, *98*, 7665–7673.
21. Kuzuya, T.; Tai, Y.; Yamamuro, S.; Hihara, T. *Mater. Trans.* **2004**, *45* (8), 2650–2652.
22. Zhao, Y.; Zhang, Y.; Zhu, H.; Hadjipanayis, G. C.; Xiao, J. Q. *J. Am. Chem. Soc.* **2004**, *126*, 6874–6875.
23. Pradhan, N.; Katz, B.; Efrima, S. *J. Phys. Chem. B.* **2003**, *107*, 13843–13854.
24. van Embden, J.; Chesman, A. S. R.; Jasieniak, J. J. *Chem. Mater.* **2015**, *27*, 2246–2285.
25. Van Embden, J.; Mulvaney, P. *Langmuir* **2005**, *21* (22), 10226–10233.
26. Komatsu, K.; Wang, G.-W.; Murata, Y.; Shiro, M. *Nature* **1997**, *387* (6633), 583–586.
27. Štrukil, V.; Gracin, D.; Magdysyuk, O. V.; Dinnebier, R. E.; Friščić, T. *Angew. Chemie Int. Ed.* **2015**, *54* (29), 8440–8443.
28. Do, J.-L.; Friščić, T. *ACS Cent. Sci.* **2017**, *3* (1), 13–19.
29. James, S. L.; Adams, C. J.; Bolm, C.; Braga, D.; Collier, P.; Friščić, T.; Grepioni, F.; Harris, K. D. M.; Hyett, G.; Jones, W.; Krebs, A.; Mack, J.; Maini, L.; Orpen, A. G.; Parkin, I. P.; Shearouse, W. C.; Steed, J. W.; Waddell, D. C. *Chem. Soc. Rev.* **2012**, *41* (1), 413–447.
30. Baláž, P.; Boldižárová, E.; Godočí, E.; Briančin, J. *Mater. Lett.* **2003**, *57* (9–10), 1585–1589.
31. Godočíková, E.; Baláž, P.; Gock, E.; Choi, W. S.; Kim, B. S. *Powder Technol.* **2006**, *164* (3), 147–152.
32. Lu, H.-Y.; Chu, S.-Y.; Tan, S.-S. *J. Cryst. Growth* **2004**, *269* (2–4), 385–391.
33. Dutková, E.; Baláž, P.; Pourghahramani, P.; Nguyen, A. V.; Šepelák, V.; Feldhoff, A.; Kováč, J.; Šatka, A. *Solid State Ionics* **2008**, *179* (21–26), 1242–1245.
34. Malca, M. Y.; Bao, H.; Bastaille, T.; Saade, N. K.; Kinsella, J. M.; Friščić, T.; Moores, A. *Submitted for Publication* **2017**.
35. Gasparottocinzia, D. B.; Tondello, M.; Barreca, D.; Gasparotto, A.; Maragno, C.; Tondello, E. *Surf. Sci. Spectra* **2002**, *9* (46).
36. Gasparotto, D. B.; Maragno, C.; Tondellotrevor, E.; Spalding, R.; Barreca, D.; Gasparotto, A.; Tondello, E.; Spalding, T. R. *Surf. Sci. Spectra* **2002**, *9* (54).
37. Yu, K.; Hu, M. Z.; Wang, R.; Le Piolet, M.; Frotey, M.; Badruz Zaman, M.; Wu, X.; Leek, D. M.; Tao, Y.; Wilkinson, D.; Li, C. *J. Phys. Chem. C* **2010**, *114*, 3329–3339.
38. Kudera, S.; Zanella, M.; Giannini, C.; Rizzo, A.; Li, Y.; Gigli, G.; Cingolani, R.; Ciccarella, G.; Spahl, W.; Parak, W. J.; Manna, L. *Adv. Mater.* **2007**, *19* (4), 548–552.
39. Mandal, A.; Dandapat, A.; De, G. *Analyst* **2012**, *137* (3), 765–772.

## 3.5 Appendix – Supporting Information

### 3.5.1 Materials and Methods

**Chemicals:** $Cd(NO_3)_2 \cdot 4\,H_2O$ (98%), $Zn(NO_3)_2 \cdot 6\,H_2O$ (≥98%), oleylamine (98%), and L-cysteine (97%) were purchased from Sigma-Aldrich and used without further purification. All experiments were performed under atmospheric conditions.

**Mechanochemical experiments:** Milling reactions were performed with a Retsch Mixer Mill MM400 (MM) using 10 ml teflon milling jars loaded with one 10 mm zirconia ball (purchased from FORM-TECH Scientific). Scale-up syntheses were performed with a Retsch S100 centrifugal ball mill (PM), using a 50 ml zirconia jar loaded with ten 10 mm zirconia balls (from Retsch).

**Synthesis of OA@CdS-MM:** 1:1.2:5 molar equivalents of CN (30.0 mg, 0.097 mmol); Cys (14.2 mg, 0.117 mmol) and OA (130.1 mg, 0.486 mmol) were placed in a Teflon milling jar loaded with a zirconia ball and ground together in a *Retsch MM400* for 90 minutes at 30 Hz. After milling, the mixtures were kept sealed in the jars and left to age for 24 hours. The resulting pastes were washed with a 3:1:1 v/v solution of hexanes:ethanol:acetone three times and centrifuged at 3500 rpm (5 min) after each wash to obtain the precipitated **OA@CdS-MM**.

**Synthesis of OA@ZnS-MM:** 1:1.2:5 molar equivalents of ZN (30 mg, 0.101 mmol); Cys (14.7 mg, 0.121 mmol) and OA (134.9 mg, 0.504 mmol) were placed in a Teflon milling jar loaded with a zirconia ball and ground together in a *Retsch MM400* for 90 minutes at 30 Hz. After milling, the mixtures were kept sealed in the jars and left to age for 24 hours. The resulting paste was washed with a 3:1:1 v/v solution of hexanes:ethanol:acetone three times and centrifuged at 3500 rpm (5 min) after each wash to obtain the precipitated **OA@ZnS-MM**.

**Synthesis of OA@CdS-PM:** Linear scale-up was performed as follows: 1:1.2:5 molar equivalents of CN (1.50 g, 4.86 mmol); Cys (0.707 g, 5.84 mmol) and OA (6.50 g, 24.31 mmol) were placed in a 50 mL zirconia jar loaded with ten 10 mm zirconia balls and milled at 450 RPM for 90 min. The direction of jar motion was set to periodically alternate every 30 seconds. After milling, the mixtures were kept sealed in the zirconia jar and left to age for 12 hours. The resulting pastes were washed with a 3:1:1 v/v solution of hexanes:ethanol:acetone three time and centrifuged at 3500 rpm (5 min) after each wash to obtain **OA@CdS-PM**.

**Synthesis of OA@ZnS-PM:** Linear scale-up was performed as follows: 1:1.2:5 molar equivalents of ZN (1.50 g, 5.04 mmol), Cys (0.733 g, 6.05 mmol) and OA (6.74 g, 25.21 mmol) were placed in

a 50 mL zirconia jar loaded with ten 10 mm zirconia balls and milled at 450 RPM for 90 min. The direction of jar motion was set to periodically alternate every 30 seconds. After milling, the mixtures were kept sealed in the zirconia jar and left to age for 12 hours. The resulting pastes were washed with a 3:1:1 v/v solution of hexanes:ethanol:acetone three and centrifuged at 3500 rpm (5 min) after each wash to obtain **OA@ZnS-PM.**

### 3.5.2 Characterization

**Transmission Electron Microscopy (TEM):** In order to observe their morphology and size, all samples were dispersed in hexanes, placed on a Cu grid and subsequently dried in a desiccator overnight. High-resolution TEM images were obtained using a FEI Tecnai G2 F20 Cryo-scanning transmission electron microscope at an acceleration voltage of 200 kV, and equipped with an AMETEK EDAX detector (for EDS measurements). The mean sizes of the NPs were obtained by measuring the largest diameters using imageJ (data are expressed as mean ± standard deviation).

**Powder X-Ray Diffraction (PXRD):** The phase and structural analysis of the samples were carried out using a PROTO MANUFACTURING AXRD Benchtop Powder equipped with a Cu Kα source (λ=1.54184 Å) operating at 30 kV and 20 mA.

**X-ray Photoelectron Spectroscopy (XPS):** Measurements were performed on a Thermo Scientific K-Alpha X-Ray photoelectron spectrometer with an excitation source of Al Kα= 1486.6 eV. The binding energies were corrected by referencing the C 1s line to 284.80 eV. The samples were dried overnight under vacuum at room temperature prior to XPS analysis.

**UV-VIS Spectroscopy:** Measurements were performed using a Varian Cary 300 bio UV-Visible Spectrophotometer. The samples were dispersed in hexanes and filtered through a 0.22 µm nylon pore filter prior to analysis.

**Fluorescence Spectroscopy:** Measurements were carried out using a Varian Cary Eclipse Fluorescence Spectrophotometer operating at 600 V with an excitation slit size of 5nm and an

emission slit size of 10 nm. The samples were dispersed in hexanes and filtered through a 0.22 µm nylon pore prior to analysis. The OA@CdS-MM and OA@ZnS-MM samples were excited with an incident wavelength of 350 nm and 270 nm, respectively.

### 3.5.3 Additional Figures

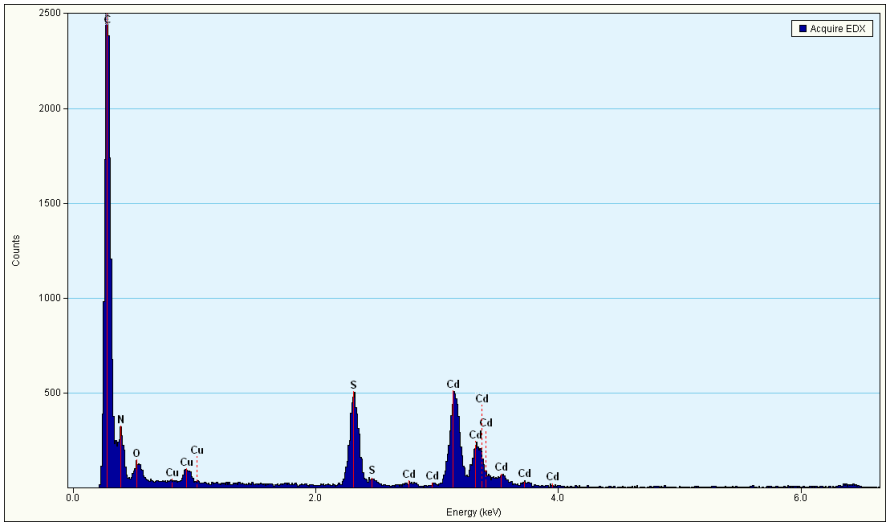


**Figure S3. 1.** EDS Spectra of OA@CdS-MM.

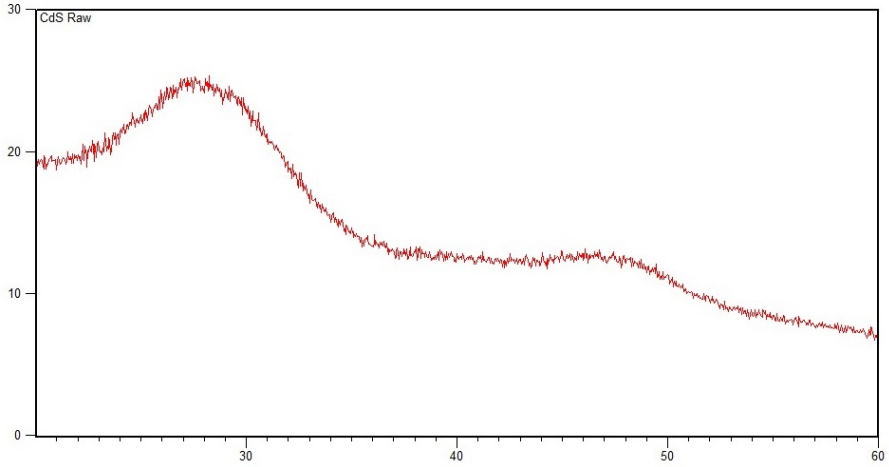


**Figure S3. 2.** PXRD of OA@CdS-MM post-synthesis.

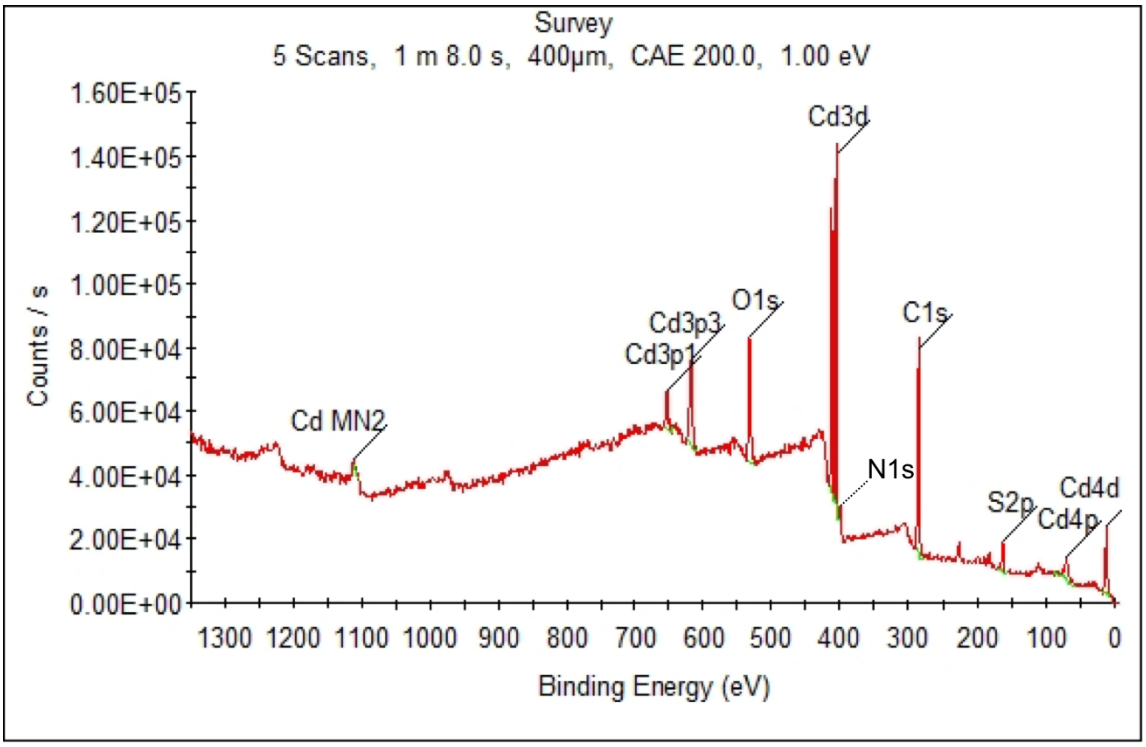


**Figure S3. 3.** XPS survey spectrum of OA@CdS-MM.

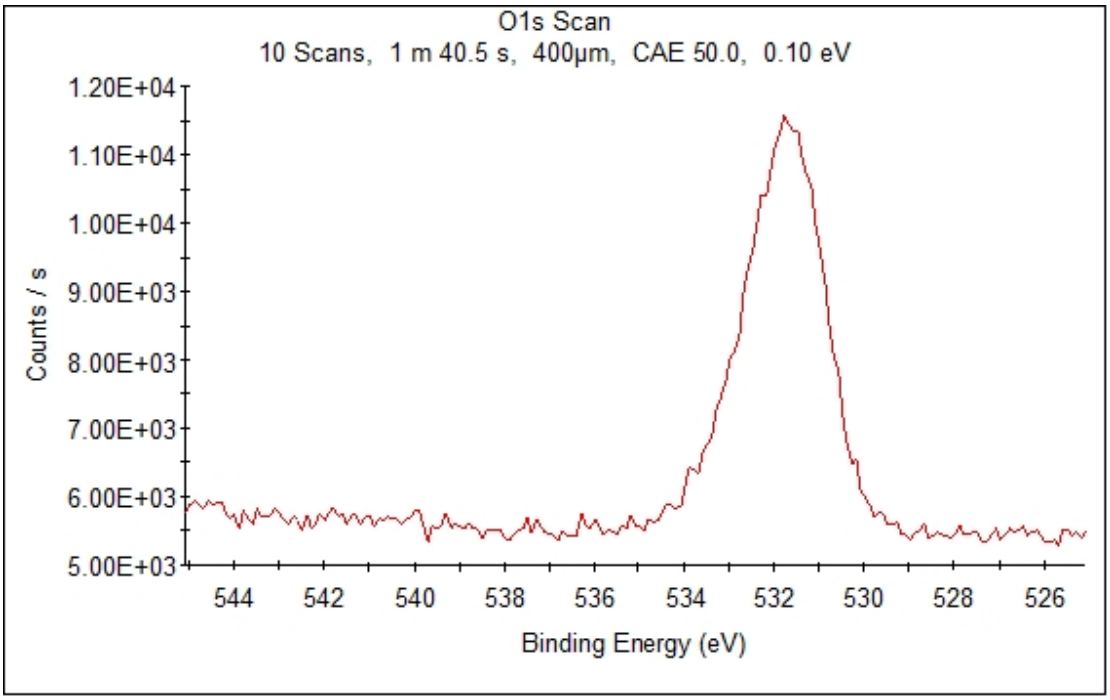


**Figure S3. 4.** XPS O 1s spectrum of OA@CdS-MM, centered about 531.8 eV.

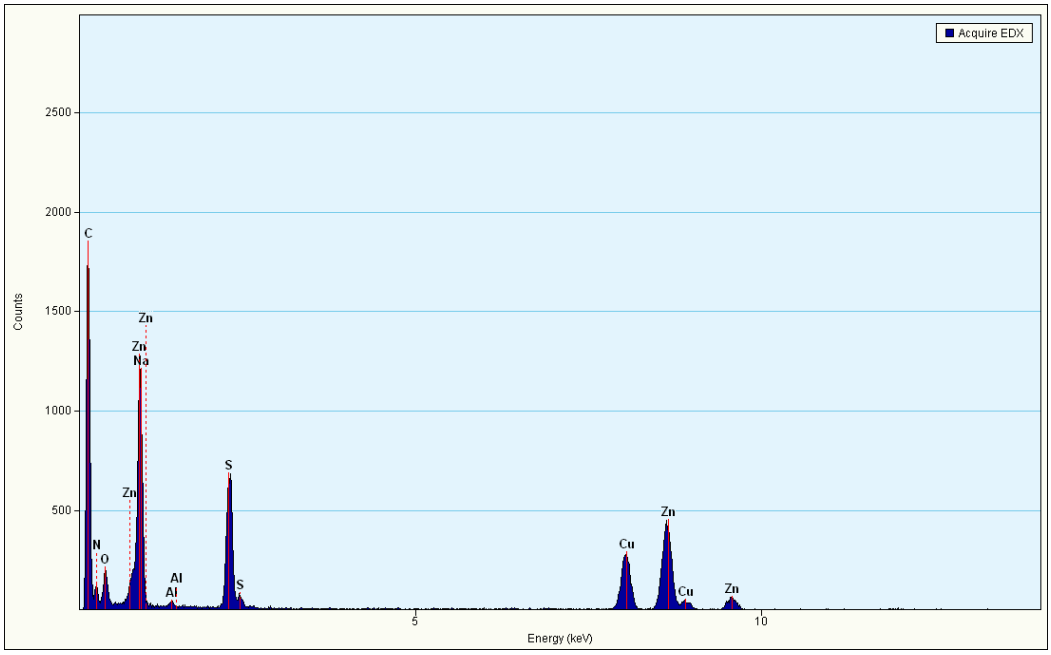


**Figure S3. 5.** EDS Survey of OA@ZnS-MM.

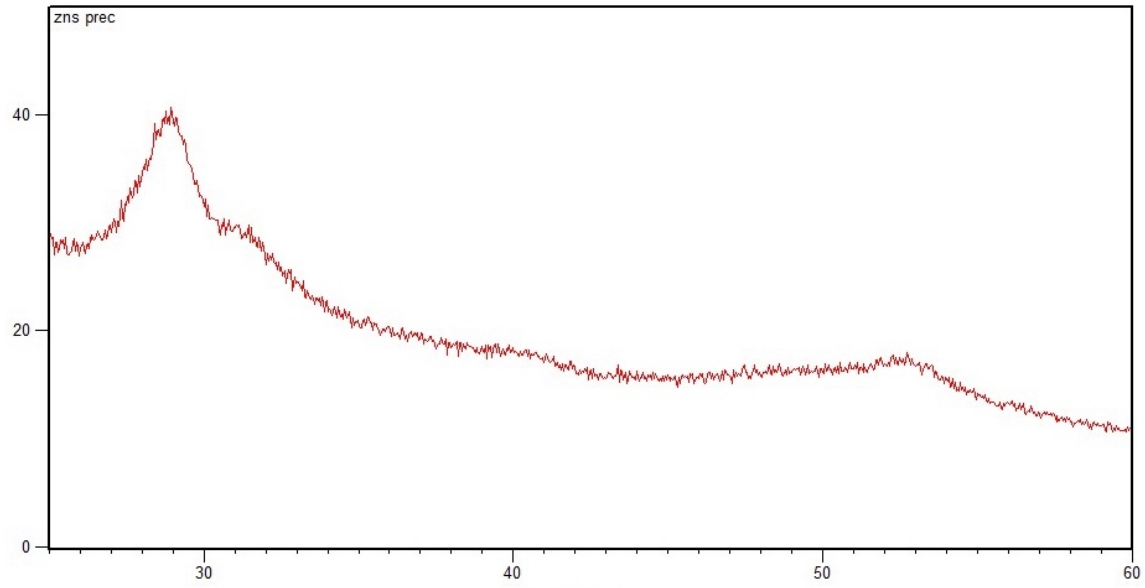


**Figure S3. 6.** PXRD pattern of OA@ZnS-MM post-synthesis.

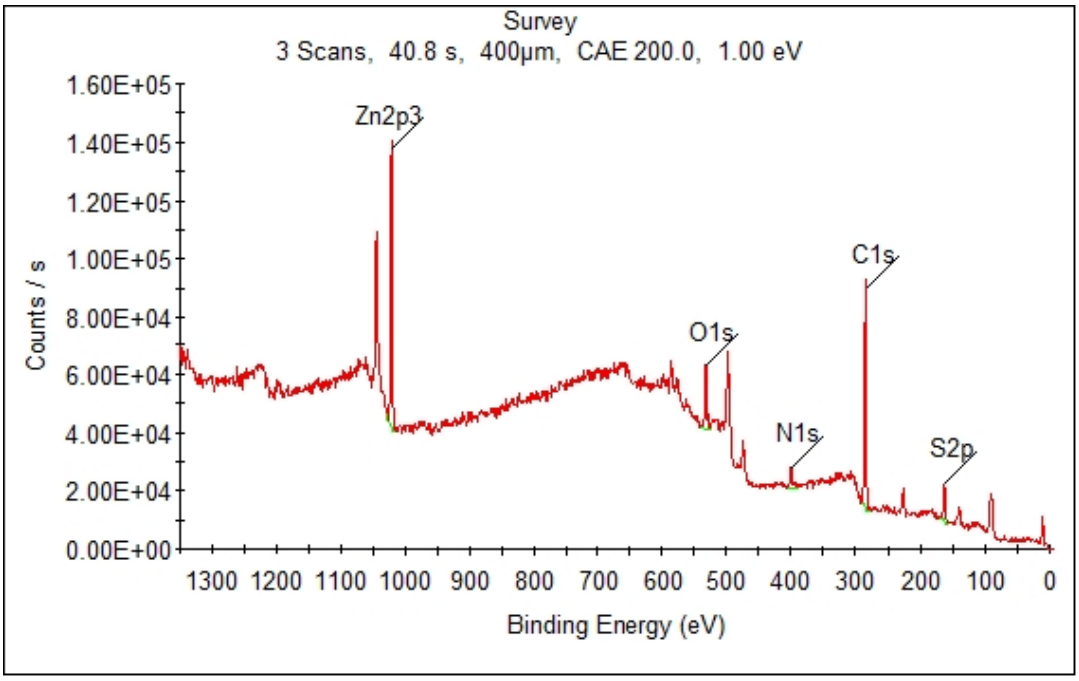


**Figure S3. 7.** XPS survey spectrum of OA@ZnS-MM.

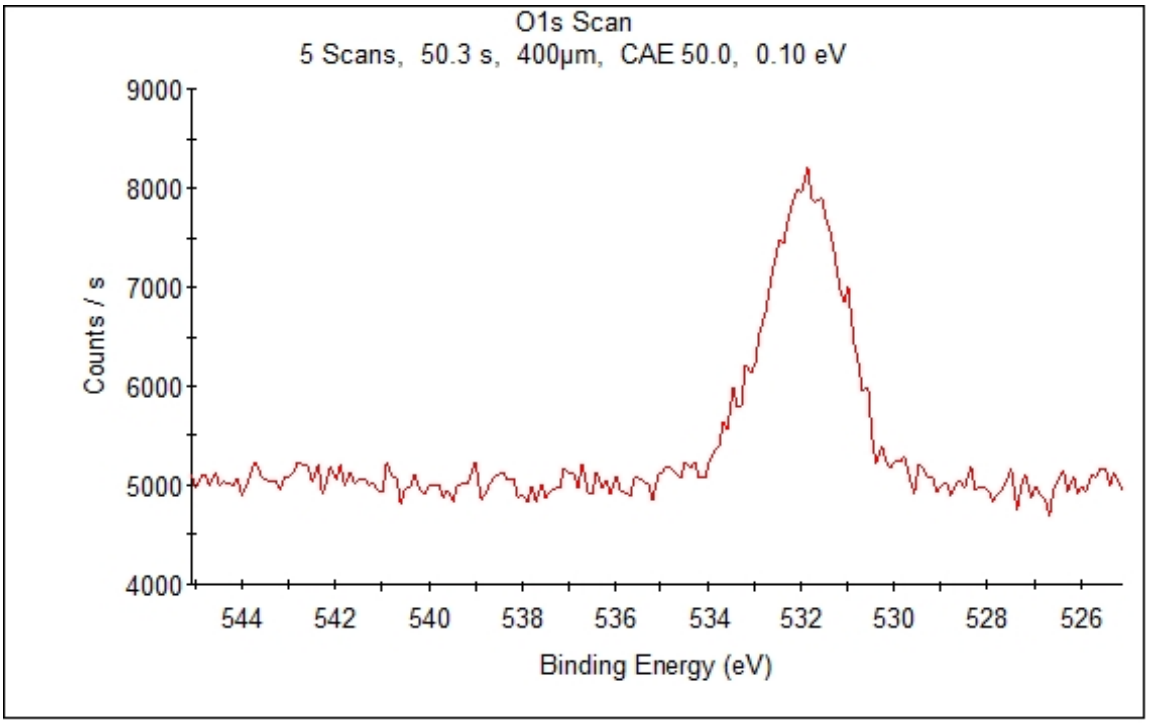


**Figure S3. 8.** XPS O1s spectrum of OA@ZnS-MM, centered about 531.9 eV.

# Chapter 4 Solid-state mechanochemical ω-functionalization of poly (ethylene glycol)

**Abstract**

---

Poly (ethylene glycol) (PEG) is a linear polymer with a wide range of applications in chemical manufacturing, drug development and nanotechnology. PEG derivatives are being increasingly used to covalently modify small molecule and peptide drugs, as well as bioactive nanomaterials in order to improve solubility in biological serum, reduce immunogenicity, and enhance pharmacokinetic profiles. Herein we present the development of mechanochemical procedures for PEG functionalization without the need for bulk solvents, offering a cleaner and more sustainable alternative to the existing solution-based PEG procedures. The herein presented mechanochemical procedures enable rapid and solvent-free derivatization of PEG with tosyl, bromide, thiol, carboxylic acid or amine functionalities in good to quantitative yields and with no polymer chain oligomerization, proving the versatility of the method.

---

## 4. 1 Introduction

Poly (ethylene glycol) (PEG) is a linear polyether polymer with highly hydrophilic properties. Whereas PEG functionalization is restricted to its terminal functionalities, derivatization of these sites is essential for its use in pharmaceutical and material design. Specifically, modification of bioactive substrates with PEG is well established in drug development, and is also becoming important in the purification of proteins and nucleic acids[1]. Since the first demonstration of PEGylated proteins with altered immunogenicity[2,3], PEG has been heavily investigated for affording biologically active molecules with superior pharmacokinetic profiles and increased solubility in aqueous media[4,5,6]. A wide variety of modern PEGylated drugs take advantages of these properties: Mucagen (2004), Cimzia (2008) and Puricase1 (2010) are but a few examples[7]. On the other end, PEG is also being used to stabilize nanomaterials, allow their stable suspension in aqueous media, and interface to them with biological systems.[8,9,10] Besides for its effects on solubility, PEG also creates a hydrodynamic barrier around the conjugate nanomaterial, allowing for reduced immunogenicity,[11] leading to significant improvements in blood circulation half-lives, decrease in clearance rates, and prolonged pharmacological effects[12,13,14]. Derivatives of PEG are often used to perform conjugation reactions on small molecule drugs, proteins, or bioactive nanomaterials[15]. Other methods include chelation or ligand-exchange reactions at metal-based nanomaterials with $\omega$-functionalized PEG polymers[16,17,18].

The two most common methods for accessing $\omega$-functionalized PEG derivatives are solution-based through either ring-opening polymerization of ethylene oxide unites or modification of commercially available, parent hydroxyl-terminated PEG[19]. The latter route is milder, more accessible and offers more fine control over the polymer molecular weight. However, in both cases, the methods for PEG $\omega$-functionalization rise concerns in terms of environmental impact, given that these reactions typically require dilute conditions under inert atmosphere, warranting large amounts of solvents and time[1,19,20]. High dilution during derivatization is a requirement of solvent-based syntheses to avoid unwanted chain lengthening

caused by intermolecular reactions[21]. Having in mind the vocal demands of pharmaceutical industry for the development of cleaner, more efficient synthetic techniques[22], we now explore the possibility of accessing PEG derivatives in the solid-state. The use of mechanochemistry to achieve both supramolecular[23] and covalent[24] synthesis and modification of active pharmaceutical ingredients (APIs) is an emergent area that was recently reviewed.[25] In particular, solvent-free polymerization methods have been recently developed to access polyimines[26], polylactides[27] poly(phenylene vinylene)[28] and polyolefins[29]. There has been however limited effort towards the functionalization of premade polymers. Recently, Yan and coworkers used ball milling to deacetylate chitin to afford chitosan[30].

We now provide a proof-of-principle demonstration of mechanochemical ω-functionalization of α-protected methyxo-PEG (mPEG) with -COOH, -OTs, -$NH_2$, -Br, and –SH functionality, leading to rapidly and cost-effective synthesis of these important derivatives in good to quantitative yields under aerobic conditions, using methoxypoly(ethylene glycol) of average molecular weights $M_n$ = 750 Da and $M_n$ =2000 Da ($mPEG_{750}$ and $mPEG_{2000}$, respectively). We chose these derivatives because of their versatile functionalities for accessible covalent conjugation onto various substrates and metal-based nanomaterials.

## 4. 2 Results and Discussion

For this study, we focused on the functionalization of mPEG, which allows the simple mono-functionalization of the polymer, for useful applications to drug development or nanomaterials. To establish the generality of the method, we used mPEGs of two different, commercially available molecular weights, n=750 and 2000 Da ($mPEG_n$). In all the examples we explored in this study, reaction progress was determined $^1$H-NMR yields, where yields were determined by integration of peaks attributed to the methylene hydrogens geminal to the ω-functionality of mPEG, namely hydroxyl, for the starting material, and the functionality introduced in the reaction explained below, for the products. *p*-Xylene was used as an internal standard for $^1$H NMR analysis, and the methoxy-end of mPEG (singlet at 3.38 ppm) served to

confirm conversions. Prudence was given to confirming inter-chain reactions did not occur by confirming mass balance in all cases.

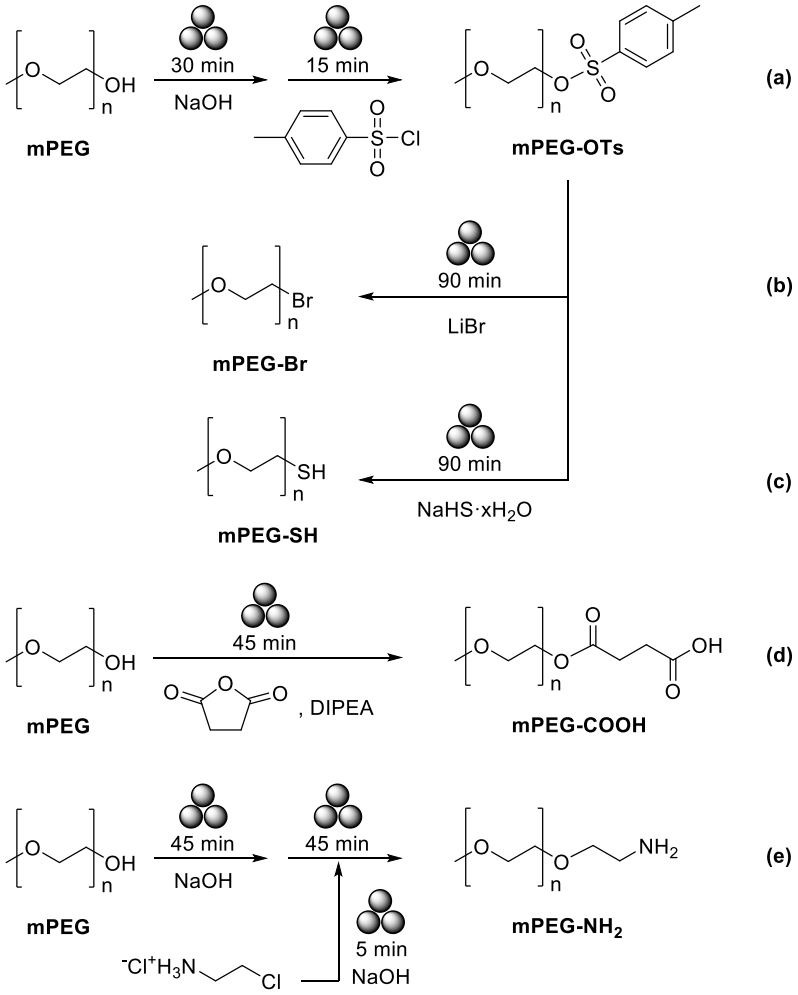


**Scheme 4. 1.** Developed syntheses for accessing: (a) $mPEG_x$-OTs, (b) $mPEG_x$-Br, (c) $mPEG_x$-SH, (d) $mPEG_x$-COOH, and (e) $mPEG_x$-$NH_2$. mPEG of $M_n$ = 750 and 2000 Da were investigated as precursors. All milling reactions were performed at an operating frequency of 30 Hz.

We first explored the possibility of introducing a *p*-methylsulfonato (tosyl) moiety at the termination of mPEG by ball-milling. Namely, the tosyl moieties are known as excellent leaving groups, making tosylated mPEG ($mPEG_x$-OTs) useful synthons for accessing further PEG derivatives. For this, we conducted a two-step one-pot reaction involving milling first the mPEG reactant with a base, followed by addition of p-toluenesulfonyl chloride (TsCl) and further milling (Scheme 4.1-a, Table 1). $mPEG_{750}$ was used to survey and optimize the tosylation reaction

conditions. Milling of only mPEG with TsCl led to a poor conversion of 6 % (Table 4.1, entry 1). However, addition of 1 equivalent of weak base, such as $K_2CO_3$ and N,N-Diisopropylethylamine (DIPEA) led to $^1$H-NMR yields of 21 %, and 17% respectively (Table 4.1, entry 2-3). Switching to NaOH as the base led to a sharp increase of mPEG conversion to 81%. The highest conversions were obtained by using mPEG, NaOH and TsCl in respective stoichiometric ratios of 1:1.2:1.5 (Table 4.1, entry 4). These conditions functioned similarly to the higher molecular weight $mPEG_{2000}$ (Table 4.1, entry 5). In the $^1$H-NMR spectra of these samples, the triplet of the terminal methylene moieties in the mPEG starting material at 3.72 ppm is replaced by a new one at 4.15 ppm, consistent with tosylation of the terminal group (Figure 4.1)[20]. The functionalization of mPEG was also corroborated by the observed shift in the $^1$H NMR signals of the tosylate group protons from 7.92 (2H) and 7.49 (2H) in TsCl to 7.79 and 7.34 ppm, in mPEG-OTs (Figure S4.1)[20].

| **Entry** | **mPEG M.W** | **base (eq)** | **TsCl (eq)** | **Time (min)** | **$^1$H-NMR Yield** |
|---|---|---|---|---|---|
| **1** | 750 | --------- | 1.2 | 45 | 6% |
| **2** | 750 | $K_2CO_3$ (1.0) | 1.2 | 45 | 21% |
| **3** | 750 | DIPEA (1.0) | 1.2 | 45 | 17% |
| **4** | 750 | NaOH (1.2) | 1.5 | 15 | 81% |
| **5** | 2000 | NaOH (1.2) | 1.5 | 15 | 80% |

**Table 4. 1.** Surveyed reactions for mechanochemical derivatization of mPEG with tosylate functionality. TsCl = p-toluenesulfonyl chloride; CEA = chloroethylamine HCl; M.W = molecular weight. All reactions were ball-milled at an operating frequency of 30 Hz.

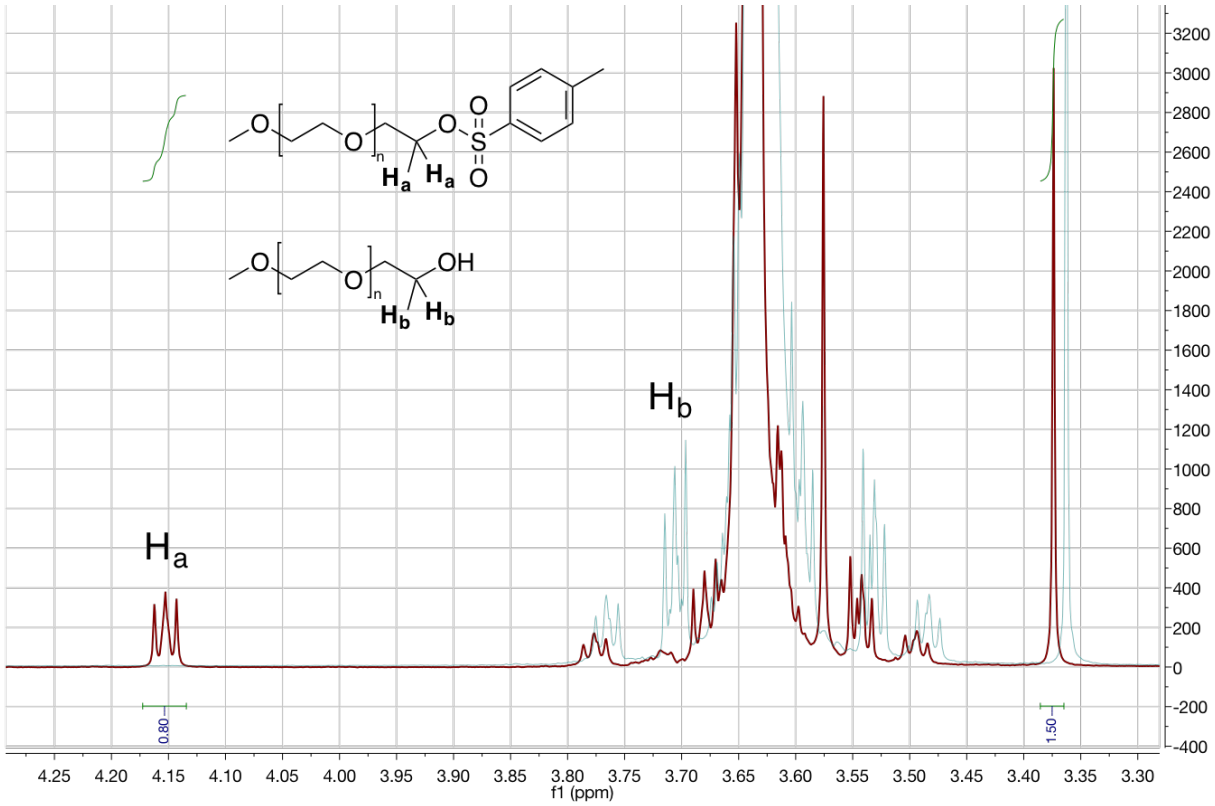


**Figure 4. 1.** $^{1}$H-NMR of sample $mPEG_{2000}$-OTs (table 1, entry 5) in $CDCl_3$ showing mPEG end group shift after tosylation.

Employing NaOH as a base yielded the best results with both molecular weight (MW) mPEGs. NaOH is a strong base, thus favoring deprotonation of mPEG over weaker bases to facilitate subsequent tosylation. The deprotonation step (Scheme 4.1-b) also generates water locally, which may have led to liquid-assisted grinding (LAG) conditions and facilitated the interaction and mobility of substrates[31,32,33], and allowed the substrates to better interact *in situ*. Given that DIPEA did not afford high yields albeit being liquid and having a $pK_a$ of 3.02, smaller than the one of mPEG ($pK_a$=4.5-4.8), it suggests that solvation may play a role in promoting the reaction. Interestingly TsCl is prone to hydrolysis in presence of water, yet it did not seem to affect the high reactivity observed with NaOH, likely because the generated, strongly nucleophilic, alcoholate would react even faster.

Progress of reactions in entries 4 and 5 in Table 4.1 was probed every 15 minutes at the second step (Scheme 4.1-a) in order to follow the reaction progress. After 15 minutes milling, the reaction was complete, as almost identical $^{1}$H-NMR yields were obtained for up to 75 min milling for both $mPEG_{750}$ and $mPEG_{2000}$.

| **Entry** | **Product** | **Time of milling (min)** | **$^{1}$H-NMR Yield** |
|---|---|---|---|
| **1** | $mPEG_{750}$-Br | 90 | 58% |
| **2** | $mPEG_{2000}$-Br | 90 | 65% |
| **3** | $mPEG_{750}$-SH | 90 | 48%[a] |
| **4** | $mPEG_{2000}$-SH | 90 | 69%[a] |
| **5** | $mPEG_{750}$-COOH | 45 | 99% |
| **6** | $mPEG_{2000}$-COOH | 45 | 90% |
| **7** | $mPEG_{750}$-$NH_2$ | 45 | 42% |
| **8** | $mPEG_{2000}$-$NH_2$ | 45 | 63% |

**Table 4. 2.** Surveyed reactions of mechanochemical derivatization to afford mPEG-Br, -SH, -COOH and –$NH_2$ derivatives. Reaction conditions: **[6-7]** mPEG-OTs, LiBr (3 eq); **[8-9]** mPEG-OTs, $NaHS{\cdot}xH_2O$ (2 eq assuming 3 $H_2O$); **[10-11]** mPEG, DIPEA (0.2 eq), succinic anhydride (1.2 eq); **[12-13]** mPEG, NaOH (1.2 eq), CEA-HCl/NaOH (1.2 eq). All reactions were ball-milled at an operating frequency of 30 Hz. [a] Corresponding disulfides were also observed as minor side product

The mechanochemically prepared tosylated polymers provide an entry into the synthesis of other mPEG derivatives by mechanochemistry, through ball milling reaction with additional nucleophiles. The synthesis of terminally brominated mPEG (mPEG-Br) derivatives achieved by milling of mPEG-OTs with LiBr (Scheme 4.1-b). Analysis of the milled reaction mixture by $^{1}$H NMR revealed the appearance of a new triplet resonance centered at about 3.45 ppm in $CDCl_3$, consistent with the methylene germinal to Br in mPEG–C$\underline{H_2}$-Br (Figure S4.2)[34,35]. $^{1}$H NMR yields of 58% and 65% were obtained for reactants $mPEG_{750}$ and $mPEG_{2000}$, respectively (Table 4.2, entry 1-2). 2D-HSQC was performed to validate terminal bromo functionality showing a cross-peak at

($^{1}$H, $^{13}$C) = (3.45 ppm, 30.10 ppm) (Figure S4.3). These results are exciting given that PEG bromination is often performed under harsh conditions either *via* radical intermediates or using bromo acyl-halides, which introduces unnecessary ester groups instead of direct bromine substitution onto the polymer chain[34,36,37].

Next, we explored the thiolation by milling the mPEG-OTs with NaHS·x$H_2O$ for 90 min (Table 4.2, entry 3-4) as reagent, which afforded $^{1}$H NMR conversions of 55% and 78% for Mn = 750 and 2000 Da, respectively. In this reaction, thiol was obtained a major product, with a small portion of disulfide forming. Yield of 48% -SH + 7% -S-S- and 69% -SH + 9% -S-S- were measured for Mn = 750 and 2000 Da, respectively. In the $^{1}$H NMR spectra, the mPEG-SH was clearly identified by a triplet at 2.86 ppm, characteristic of methylene hydrogens germinal to thiol, while the corresponding peak of mPEG-S-S-mPEG appeared as 2.72 ppm (Figure S4.4)[20]. The formation of the disulfide derivatives is explained by the reaction being performed under aerobic conditions[20].

To access mPEG-carboxylate (mPEG-COOH) under milling condition, native mPEG was reacted directly with succinic anhydride in the presence of catalytic amounts of DIPEA (Scheme 4.1-d; Table 4.2, entry 5-6). Quantitative yields (>99%) of the $mPEG_{750}$-COOH were obtained after only 45 min of milling (Figure S4.5)[38]. The end hydroxyl group of mPEG at 3.72 disappeared and was replaced by a peak as 4.23 ppm after carboxy- functionalization, further proving that the reaction was successful. Starting material succinic anhydride featured a singlet at 3.01 ppm, while the open structure resulting from reaction with mPEG is characterized by two triplets centered at 2.54 and 2.62 ppm (Figure S4.6)[38]. The reaction was readily adaptable to $mPEG_{2000}$ reactant, in 90% yield according to $^{1}$H-NMR spectroscopy.

Finally, we explored the possibility of accessing mPEG-$NH_2$ polymers by using chloroethylamine hydrochloride (CEA) as an aminating agent (Scheme 4.1-e). For this purpose, both mPEG and CEA were reacted separately mechanochemically with NaOH to afford the deprotonated mPEG and CEA free base, respectively. CEA was milled with NaOH briefly for only

5 min to avoid polymerization of the free base before reaction with mPEG. The milled products were then mixed and milled for 45 minutes, leading to a yield of 42% and 63% (for Mn = 750 and 2000 Da, respectively), according to $^{1}$H NMR spectroscopy (Table 4.2, Entries 7-8). Analysis by $^{1}$H NMR revealed a new triplet at 2.98 ppm the methylene hydrogens germinal to $NH_2$ (Figure S4.7)[20,39]. 2D-HSQC was performed to validate the addition of this functionality at the terminus of mPEG, showing a cross-peak at ($^{1}$H, $^{13}$C) = (3.98 ppm, 43.63 ppm) (Figure S4.8)[20,39].

Importantly, in all the samples studied for this reaction, complete mass balance was obtained, using an external standard and the $^{1}$H-NMR signal of the terminal methoxy group of mPEG. This allowed to established that unfunctionalized polymers were all recovered after reaction as unreacted mPEG and not as mPEG dimers resulting from the intermolecular coupling of two chains. Interestingly, in solvent-based synthesis, dilute conditions are typically required to avoid intermolecular reactions between chains leading to unwanted chain lengthening during the derivatization process. Our results show that solvent-free conditions for the post-functionalization of native PEG is a good avenue to address this limitation of conventional methods. It may be more favorable to achieve the kinetically-favorable end-products with our method, whereby the molecular precursors are more likely to diffuse and react in the solid-state preferentially over inter-chain reactions.[21] This is a particularly appealing aspect of herein demonstrated transformations, as solvent-based PEG derivatization often require hours for completion[19,40]. Finally, our method is advantageous over solvent-based on, as it eliminates the need for inert atmosphere.

## 4. 3 Concluding Remarks

We have demonstrated the efficient and selective synthesis of various PEG derivatives rapidly under mechanochemical conditions, without using any bulk solvent. The short times required to achieve reaction completion (45-90 minutes), combined with excellent selectivity to avoid reactant oligomerization in the absence of bulk solvent is, to the best of our knowledge, unprecedented.

## 4. 4 References


(1) Li, J.; Kao, W. J. *Biomacromolecules* **2003**, *4*, 1055–1067.

(2) Abuchowski, A.; Mccoy, J. R.; Palczuk, N. C.; Es, T. V. A. N.; Davis, F. F. *J. Biol. Chem.* **1976**, *252* (11), 3582–3586.

(3) Abuchowski, A.; Es, T. V; Palczuk, N. C.; Davis, F. F. *J. Biol. Chem.* **1977**, *252* (11), 3578–3581.

(4) Gref, R.; Minamitake, Y.; Peraccia, M. T.; Trubetskoy, V.; Torchilin, V.; Langer, R. *Science* **1994**, *263*, 1600–1603.

(5) Gref, R.; Domb, A.; Quellec, P.; Blunk, T.; Müller, R. H.; Verbavatz, J. M.; Langer, R. *Adv. Drug Deliv. Rev.* **1995**, *16* (2–3), 215–233.

(6) Gref, R.; Lück, M.; Quellec, P.; Marchand, M.; Dellacherie, E.; Harnisch, S.; Blunk, T.; Müller, R. H. *Colloids Surfaces B Biointerfaces* **2000**, *18* (3–4), 301–313.

(7) Li, W.; Zhan, P.; De Clercq, E.; Lou, H.; Liu, X. *Prog. Polym. Sci.* **2013**, *38* (3–4), 421–444.

(8) Juliano, R. L. *Adv. Drug Deliv. Rev.* **1988**, *2* (1), 31–54.

(9) Stolnik, S.; Illum, L.; Davis, S. S. *Adv. Drug Deliv. Rev.* **1995**, *16* (2–3), 195–214.

(10) Leroux, J.-C.; Allémann, E.; De Jaeghere, F.; Doelker, E.; Gurny, R. *J. Control. Release* **1996**, *39* (2–3), 339–350.

(11) Moghimi, M. S.; Hunter, C. A.; Murray, C. J. *Pharmacol. Rev.* **2001**, *53* (2), 283–318.

(12) Hrkach, J. S.; Peracchia, M. T.; Bomb, A.; Lotan, N.; Langer, R. *Biomaterials* **1997**, *18* (1), 27–30.

(13) Klibanov, A. L.; Maruyama, K.; Beckerleg, A. M.; Torchilin, V. P.; Huang, L. *Biochim. Biophys. Acta - Biomembr.* **1991**, *1062* (2), 142–148.

(14) Gombotz, W. R.; Guanghui, W.; Horbett, T. A.; Hoffman, A. S. *J. Biomed. Mater. Res.* **1991**, *25* (12), 1547–1562.

(15) Veronese, F. M.; Pasut, G. *Drug Discov. Today* **2005**, *10* (21), 1451–1458.

(16) Na, H. Bin; Lee, I. S.; Seo, H.; Park, Y. Il; Lee, J. H.; Kim, S.-W.; Hyeon, T. *Chem. Commun.* **2007**, 0, 5167-5169.

(17) Gentili, D.; Ori, G.; Comes Franchini, M. *Chem. Commun.* **2009**, 5874–5876.

(18) Smolensky, E. D.; Park, H. Y. E.; Berquó, T. S.; Rie, V.; Pierre, C. *Contrast Media Mol. Imaging*

**2011**, *6*, 189–199.

(19) Thompson, M. S.; Vadala, T. P.; Vadala, M. L.; Lin, Y.; Riffle, J. S. *Polymer* **2008**, *49* (2), 345–373.

(20) Mahou, R.; Wandrey, C. *Polymers* **2012**, *4* (4), 561–589.

(21) Loiseau, F. A.; Kuok, K.; Hii, M.; Hill, A. M. *J. Org. Chem.* **2004**, *69*, 639–647.

(22) Dunn, P. J. *Chem. Soc. Rev.* **2012**, *41* (4), 1452–1461.

(23) Delori, A.; Friščić, T.; Jones, W. *CrystEngComm* **2012**, *14* (7), 2350.

(24) Bonnamour, J.; Métro, T. X.; Martinez, J.; Lamaty, F. *Green Chem.* **2013**, *15* (5), 1116.

(25) Tan, D.; Loots, L.; Friščić, T. *Chem. Commun.* **2016**, *52* (50), 7760–7781.

(26) Klok, H. A.; Genzer, J. *ACS Macro Lett.* **2015**, *4* (6), 636–639.

(27) Ohn, N.; Shin, J.; Kim, S. S.; Kim, J. G. *ChemSusChem* **2017**, *10*, 1–6.

(28) Ravnsbæk, J. B.; Swager, T. M. *ACS Macro Lett.* **2014**, *3* (4), 305–309.

(29) Jakobs, R. T. M.; Ma, S.; Sijbesma, R. P. *ACS Macro Lett.* **2013**, *2* (7), 613–616.

(30) Chen, X.; Yang, H.; Zhong, Z.; Yan, N. *Green Chem.* **2017**, *19* (12), 2783–2792.

(31) Friščić, T.; Jones, W. *Cryst. Growth Des.* **2009**, *9* (3), 1621–1637.

(32) Michalchuk, A. A. L.; Tumanov, I. A.; Konar, S.; Kimber, S. A. J.; Pulham, C. R.; Boldyreva, E. V. *Adv. Sci.* **2017**, 1700132, 1–7.

(33) Shyam Karki; Tomislav Friščić; William Jones, and; Motherwell, W. D. S. *Mol. Pharm.* **2007**, *4* (3), 347–354.

(34) Zhou, H.; Chen, Y.; Plummer, C. M.; Huang, H.; Chen, Y. *Polym. Chem.* **2017**, *8* (14), 2189–2196.

(35) Wang, J.; Sun, P.; Zheng, Z.; Wang, F.; Wang, X. *Polym. Degrad. Stab.* **2012**, *97*, 2294–2300.

(36) Xie, C.; Yang, C.; Zhang, P.; Zhang, J.; Wu, W.; Jiang, X. *Polym. Chem.* **2015**, *6* (10), 1703–1713.

(37) Liu, L.; Zhang, M.; Zhao, H. *Macromol. Rapid Commun.* **2007**, *28* (9), 1051–1056.

(38) Ishii, T.; Yamada, M.; Hirase, T.; Nagasaki, Y. *Polym. J.* **2005**, *37* (3), 221–228.

(39) Goswami, L. N.; Houston, Z. H.; Sarma, S. J.; Jalisatgi, S. S.; Hawthorne, M. F. *Org. Biomol. Chem.* **2013**, *11* (7), 1116–1126.

(40) Harris, J. M.; Struck, E. C.; Case, M. G.; Steven Paley, M.; Yalpani, M.; Van Alstine, J. M.;

Brooks, D. E. *J. Polym. Sci.* **1984**, *22*, 341–352.

## 4. 5 Appendix - Supporting Information

### 4.5. 1 Materials and Instrumentation

Poly (ethylene glycol) methyl ether ($M_n$ - 750 & 2000 Da) ($mPEG_x$), p-toluenesulfonyl chloride (TsCl, $\geq 98\%$), diisopropylamine (DIPEA, $\geq 99\%$), succinic anhydride (97%), sodium hydrosulfide hydrate ($NaHS \cdot xH_2O$), lithium bromide (LiBr, $\geq 99\%$), chloroethylamine hydrochloride (CEA, 99%) and p-Xylene (anhydrous, $\geq 99\%$) were purchased from Sigma Aldrich. Sodium hydroxide pellets (NaOH, 97%) were purchased from ACS reagents. Potassium carbonate ($K_2CO_3$ anhydrous, $\geq 99\%$) was purchased from EMD Millipore. 10 mL Teflon jars and 10 mm Zr balls were obtained from FORM-TECH Scientific. The milling reactions were performed using a Retsch Mixer Mill 400 at an operating frequency of 30 Hz. $^1$H- and 2D-HSQC spectra were recorded using a Bruker AV500 operating at 500 MHz.

### 4.5. 2 Methods

**Synthesis of $mPEG_{750}$-OTs:** 150.0 mg mPEG ($M_n$ - 750 g/mol) and 9.6 mg NaOH (1.2 eq) were loaded in a 10 mL Teflon jar with one 10 mm Zr ball and milled for 30 min at 30 Hz with a drop of p-xylene as an internal standard. Alternatively, 27.64 mg $K_2CO_3$ (1.0 eq) was added as the base. 57.20 mg TsCl (1.5 eq) was then added to the reaction vessel and milled for 15-45 min at 30 Hz. The crude product was then dissolved in $CDCl_3$ and filtered through a Celite/cotton plug.
$^1$H-NMR: $\delta$ 7.33 (d, *J* = 8.1 Hz); 4.14 (t, *J* = 5.1 Hz)

**Synthesis of $mPEG_{2000}$-OTs:** 150.0 mg mPEG ($M_n$ - 2000 g/mol) and 3 - 4.5 mg NaOH (1.0 – 1.5 eq) were loaded in a 10 mL Teflon jar with one 10 mm Zr ball and milled for 30 min at 30 Hz with a drop of p-xylene as an internal standard. 21.45 mg TsCl (1.5 eq) was then added to the reaction vessel and milled for 15-45 min at 30 Hz. The crude product was then dissolved in $CDCl_3$ and filtered through a Celite/cotton plug. $^1$H-NMR: $\delta$ 7.34 (d, *J* = 8.1 Hz); 4.15 (t, *J* = 4.8 Hz)

**Synthesis of mPEG$_{750}$-Br:** 150.0 mg PEG$_{955}$-OTs and 40.92 mg LiBr (3 eq) were loaded in a 10 mL Teflon jar with one 10 mm Zr ball and milled for 90 min at 30 Hz with a drop of p-xylene as an internal standard. The crude product was then dissolved in $CDCl_3$ and filtered through a Celite/cotton plug. $^1$H-NMR: $\delta$ 3.37 (s); 3.47 (t, *J* = 6.3 Hz); 3.50 (t, *J* = 5.8 Hz); 3.69 (t, *J* = 5.8 Hz); 3.80 (t, *J* = 6.3 Hz).

**Synthesis of mPEG$_{2000}$-Br:** 150.0 mg PEG$_{2155}$-OTs and 18.13 mg LiBr (3 eq) were loaded in a 10 mL Teflon jar with one 10 mm Zr ball and milled for 90 min at 30 Hz with a drop of p-xylene as an internal standard. The crude product was then dissolved in $CDCl_3$ and filtered through a Celite/cotton plug. $^1$H-NMR: $\delta$ 3.36 (s); 3.45 (t, *J* = 6.3 Hz); 3.79 (t, *J* = 6.4 Hz). 2D-HSQC: $\delta$ (3.47, 30.10) corresponding to -O-$CH_2\underline{CH_2}$-Br

**Synthesis of mPEG$_{750}$-SH:** 150.0 mg PEG$_{955}$-OTs and 44 mg $NaHS \cdot xH_2O$ (2 eq assuming 3 $H_2O$) were loaded in a 10 mL Teflon jar with one 10 mm Zr ball and milled for 90 min at 30 Hz with a drop of p-xylene as an internal standard. The crude product was then dissolved in $CDCl_3$ and filtered through a Celite/cotton plug. $^1$H-NMR: $\delta$ 2.72 (t, *J* = 6.9 Hz); 2.86 (t, *J* = 6.8 Hz); 3.35 (s); 3.48 (t, *J* = 5.8 Hz); 3.76 (t, *J* = 5.9 Hz).

**Synthesis of mPEG$_{2000}$-SH:** 150.0 mg PEG$_{2155}$-OTs and 16.5 mg $NaHS \cdot xH_2O$ (2 eq assuming 3 $H_2O$) were loaded in a 10 mL Teflon jar with one 10 mm Zr ball and milled for 90 min at 30 Hz with a drop of p-xylene as an internal standard. The crude product was then dissolved in $CDCl_3$ and filtered through a Celite/cotton plug. $^1$H-NMR: $\delta$ 2.72 (t, *J* = 6.9 Hz); 2.86 (t, *J* = 6.7 Hz); 3.36 (s); 3.48 (t, *J* = 5.8 Hz); 3.76 (t, *J* = 5.8 Hz).

**Synthesis of mPEG$_{750}$-COOH:** 150.0 mg of mPEG ($M_n$ – 750 g/mol), 5.2 mg DIPEA (0.2 eq) and 24.0 mg succinic anhydride (1.2 eq) were loaded in a 10 mL Teflon jar with one 10 mm Zr ball and milled using a Retsch Mixer Mill 400 in air for 45 min at 30 Hz. A drop of p-xylene was added to the reaction vessel as an internal standard. The crude product was then dissolved in $CDCl_3$ and

filtered through a Celite/cotton plug. $^{1}$H-NMR: $\delta$ 4.21 (t, *J* = 4.9 Hz); 2.62 (t, *J* = 7.0 Hz); 2.54 (t, *J* = 7.0 Hz)

**Synthesis of mPEG$_{2000}$-COOH:** 150.0 mg of mPEG ($M_n$ – 750 g/mol), 5.2 mg DIPEA (0.2 eq) and 24.0 mg succinic anhydride (1.2 eq) were loaded in a 10 mL Teflon jar with one 10 mm Zr ball and milled using a Retsch Mixer Mill 400 in air for 45 min at 30 Hz. A drop of p-xylene was added to the reaction vessel as an internal standard. The crude product was then dissolved in $CDCl_3$ and filtered through a Celite/cotton plug. $^{1}$H-NMR: $\delta$ 4.21 (t, *J* = 4.9 Hz); 2.62 (t, *J* = 7.0 Hz); 2.54 (t, *J* = 7.0 Hz)

**Synthesis of mPEG$_{750}$-NH2:** 150.0 mg of mPEG ($M_n$ – 750 g/mol) and 9.6 mg NaOH (1.2 eq) were loaded in a 10 mL Teflon jar with one 10 mm Zr ball and milled for 45 min at 30 Hz. In a separate jar, 27.84 mg CEA-HCl (1.2 eq) and 9.6 mg NaOH were loaded in a 10 mL Teflon jar with one 10 mm Zr ball and milled for 5 min at 30 Hz. The contents of the first step were added to the second jar with a drop of p-xylene as an internal standard, and the reaction was milled for 45 min at 30 Hz. The crude product was then dissolved in $CDCl_3$ and filtered through a Celite/cotton plug. $^{1}$H-NMR: $\delta$ 2.97 (t, *J* = 5.6 Hz); 3.35 (s); 3.47 (t, *J* = 5.9 Hz); 3.75 (t, *J* = 5.9 Hz).

**Synthesis of mPEG$_{2000}$-NH2:** 150.0 mg of mPEG ($M_n$ – 750 g/mol) and 3.6 mg NaOH (1.2 eq) were loaded in a 10 mL Teflon jar with one 10 mm Zr ball and milled for 45 min at 30 Hz. In a separate jar, 10.44 mg CEA-HCl (1.2 eq) and 3.6 mg NaOH were loaded in a 10 mL Teflon jar with one 10 mm Zr ball and milled for 5 min at 30 Hz. The contents of the first step were added to the second jar with a drop of p-xylene as an internal standard, and the reaction was milled for 45 min at 30 Hz. The crude product was then dissolved in $CDCl_3$ and filtered through a Celite/cotton plug. $^{1}$H-NMR: $\delta$ 2.98 (t, *J* = 5.6 Hz); 3.35 (s); 3.47 (t, *J* = 5.9 Hz); 3.76 (t, *J* = 5.9 Hz). 2D-HSQC: $\delta$ (2.98, 46.63) corresponding to -O-$CH_2\underline{CH_2}$-$NH_2$

### 4.5. 3 Additional Figures

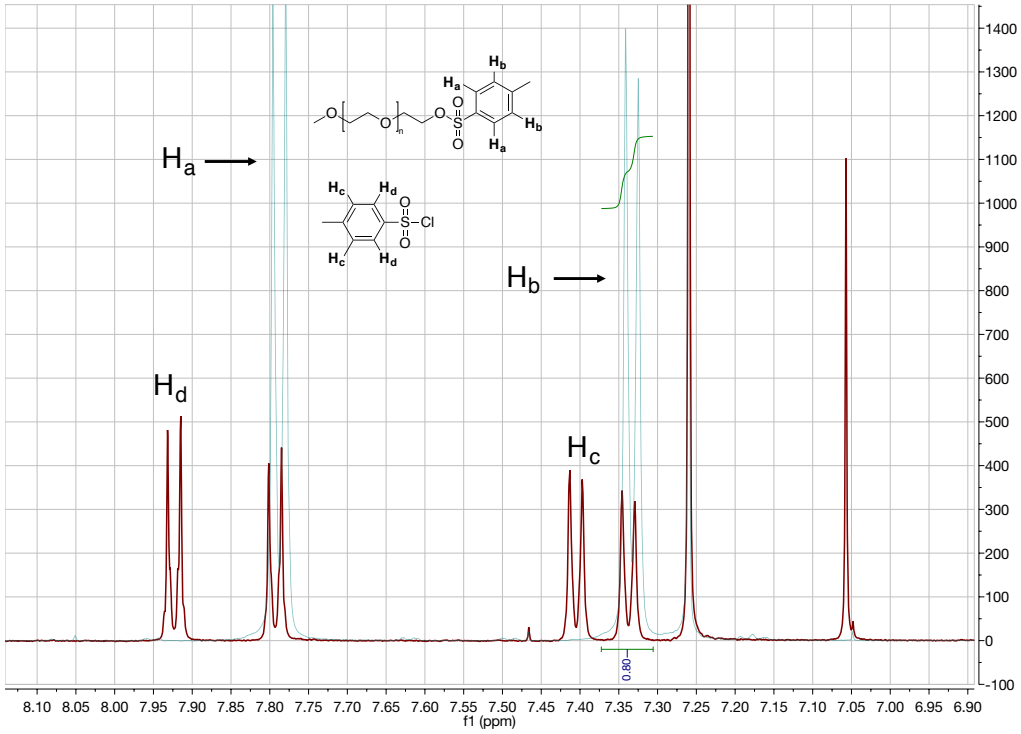


**Figure S4. 1.** Comparison of tosylated PEG (red) and TsCl starting material (blue). Some TsCl starting material can be seen in the product spectrum.

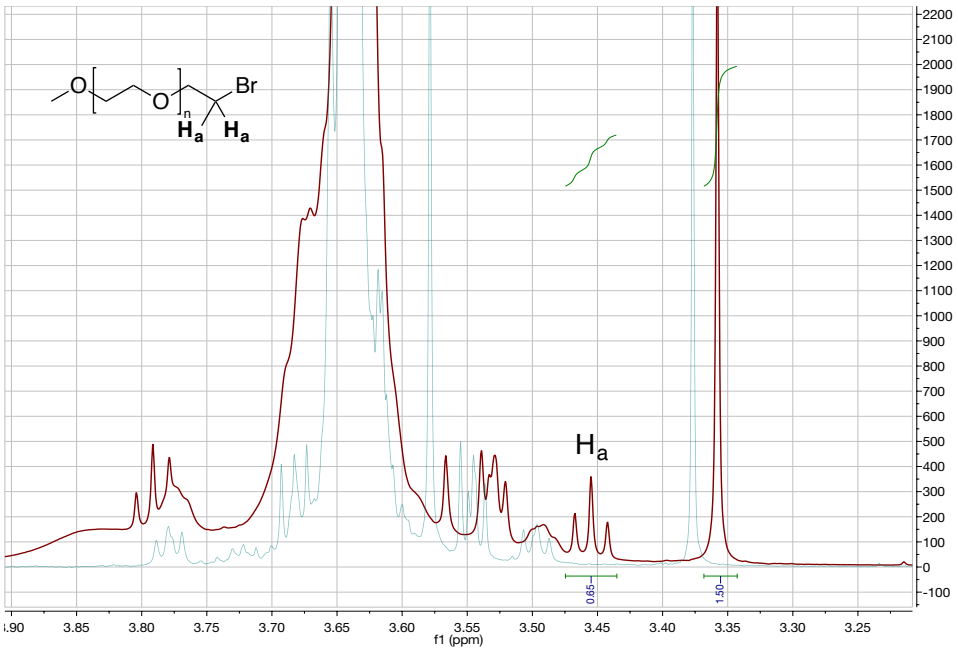


**Figure S4. 2.** $^{1}$H-NMR of synthesized mPEG$_{2000}$-Br showing appearance of triplet centered at 3.45 ppm corresponding to -O-CH$_2$C<u>H$_2$</u>-Br.

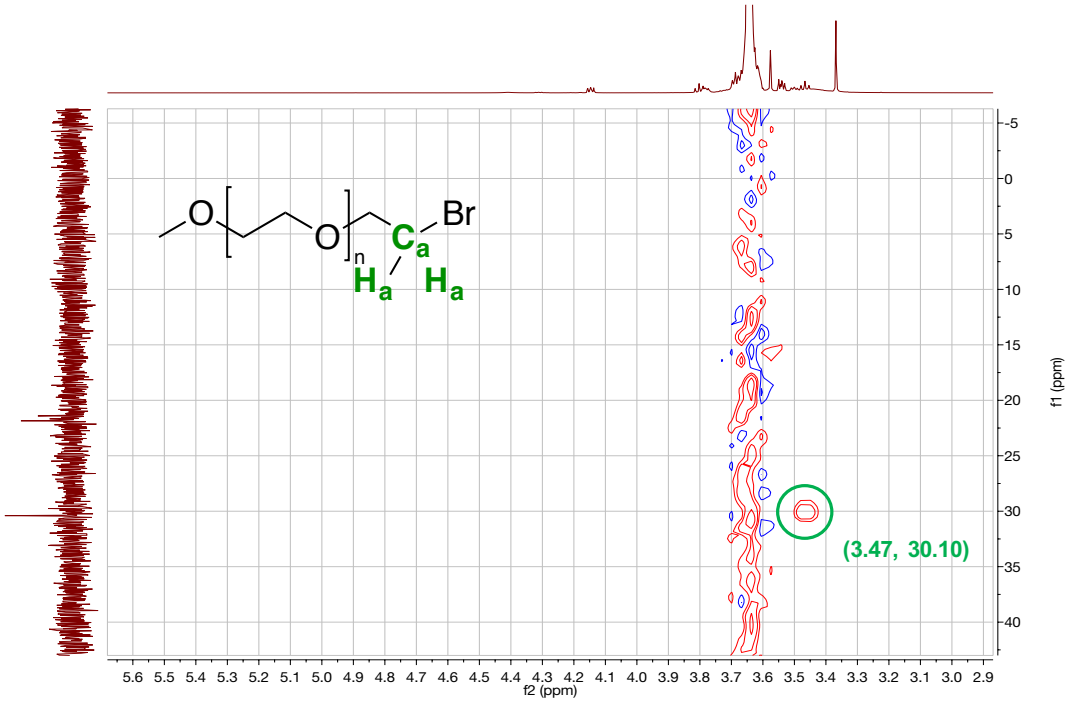


**Figure S4. 3.** 2D-HSQC of synthesized $mPEG_{2000}$-Br showing appearance of correlated peak at (x,y) = (3.47, 30.10) corresponding to -O-$CH_2$$\underline{CH_2}$-Br.

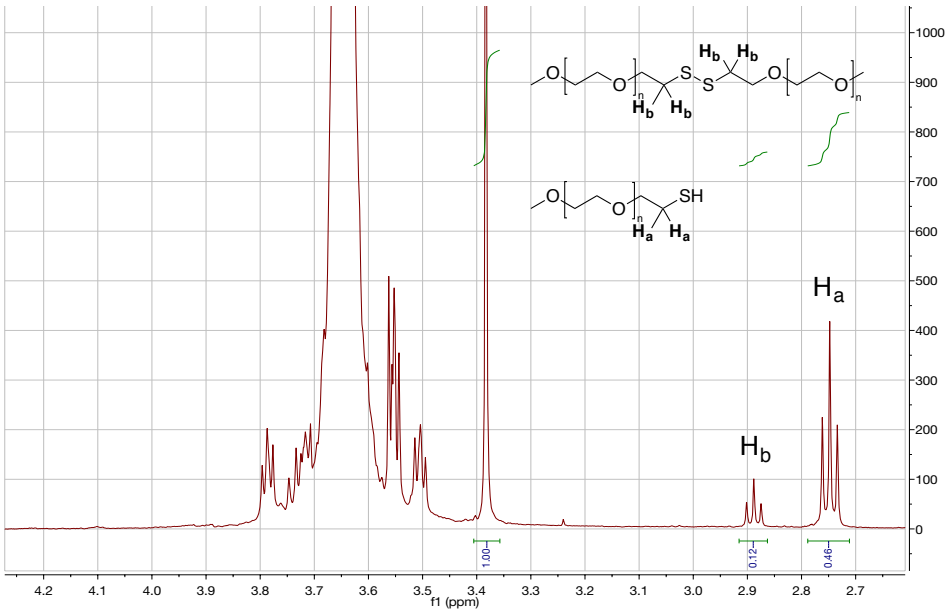


**Figure S4. 4.** $^1$H-NMR of synthesized $mPEG_{2000}$-SH showing appearance of two triplet centered at 2.72 and 2.86 ppm corresponding to -O-$CH_2$$\underline{CH_2}$-SH and -O-$CH_2$$\underline{CH_2}$-S-S-$\underline{CH_2}$$CH_2$-O-, respectively.

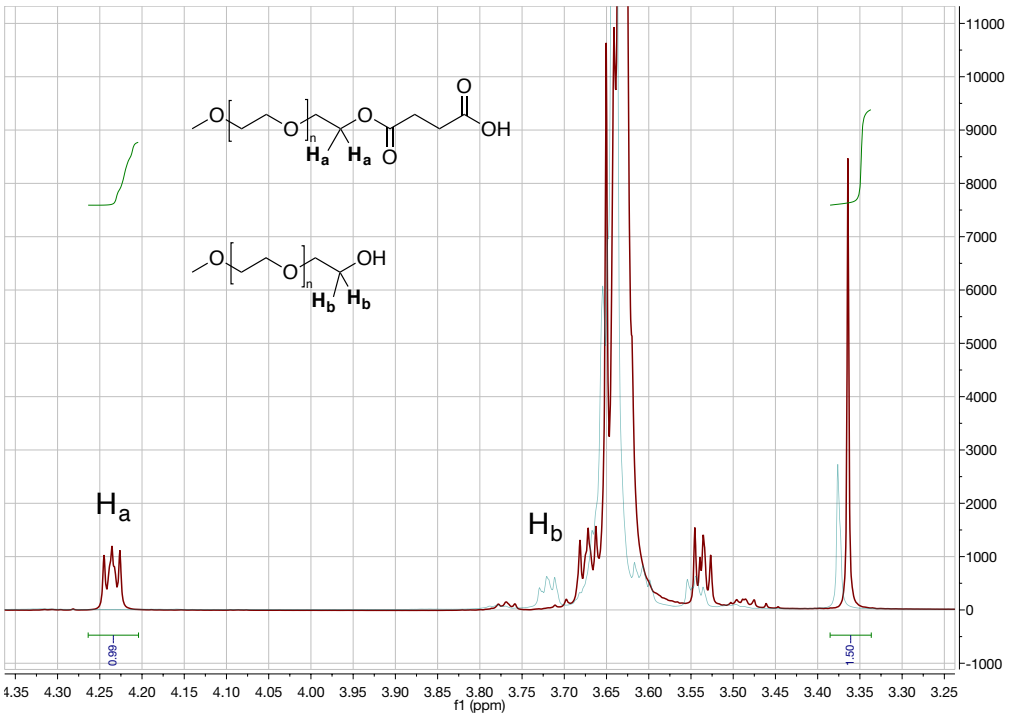


**Figure S4. 5.** $^{1}$H-NMR of mPEG$_{750}$-COOH in $CDCl_3$ showing mPEG end group shift from 3.72 to 4.23 ppm.

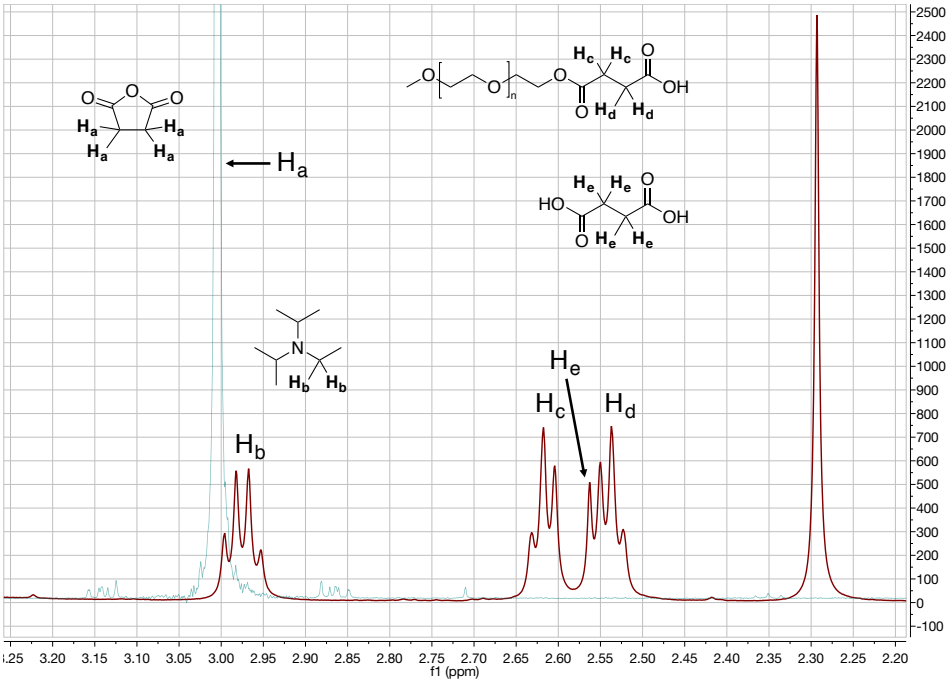


**Figure S4. 6.** $^{1}$H-NMR showing appearance of conjugated PEG-COOH (red) and succinic anhydride starting material (blue). Free succinate and DIPEA can be seen in the spectrum.

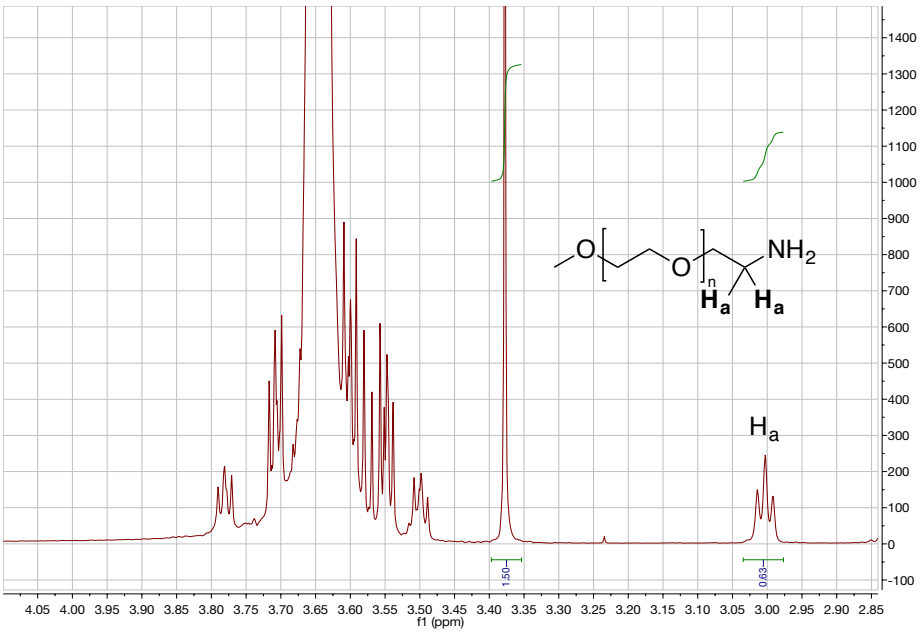


**Figure S4. 7.** $^{1}$H-NMR of synthesized mPEG$_{2000}$-NH$_2$ showing appearance of a triplet centered at 2.98 ppm corresponding to -O-CH$_2$C<u>H$_2$</u>-NH$_2$.

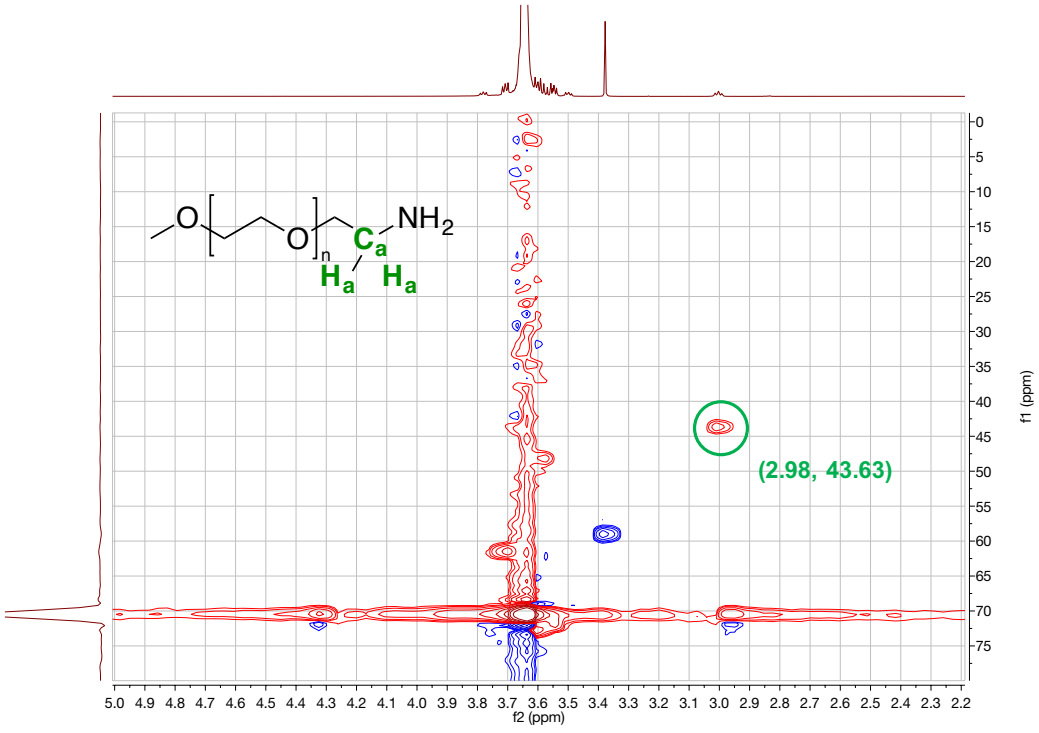


**Figure S4. 8.** 2D-HSQC of synthesized mPEG$_{2000}$-Br showing appearance of correlated peak at (x,y) = (2.98, 43.63) (red) corresponding to -O-CH$_2$C<u>H$_2$</u>-NH$_2$.

# Chapter 5 Concluding Remarks and Future Work

In Chapter 2 and 3 for this thesis, we have shown that monodisperse metal sulfide nanoparticles (M = Bi, Cd, Zn) can be induced to spontaneously self-assemble after mechanical activation. These assemblies are systematically robust and employ nominal solvent (mostly in the hydrated precursor form) in yielding the final products.

In Chapter 2, we see that varying the amount of ligand used, milling time, and method of milling systematically failed to affect the size of the final NPs, which is very interesting from an energetic standpoint in nucleation and growth kinetics. Given that the nanoparticles (NPs) produced were highly monodisperse in nature and the materials assemble during the aging process in all cases, it advocates that the bulk of the reaction is not mediated by sporadic mechanisms such as defect formation or amorphization, which are not uniform processes within the reaction vessel, would occur during milling, and would yield a more polydisperse product. That being said, these mechanisms may aid in the dissolution of the precursors into the LAG solvent where reaction may take place.

Solvent seemed to play a significant role in our systems whereby a catalytic amount of solvent *in situ* promoted the assembly pathways of said precursors into NPs. In Chapter 2, the assembly of AHA@$Bi_2S_3$-MM NPs using the solid ligand sodium 6-aminohexanoate was successful only when small amounts of water were added to the reaction vessel. While this ligand has a high solubility in water, it would nevertheless saturate the nominal amount added, including from the hydrated bismuth precursor. It would be reasonable to assume that solvation-desolvation of the starting materials influenced the reaction pathway. Under previous work using bismuth chloride - a non-hydrated salt - as a precursor, with oleylamine as a ligand, bismuth sulfide could not be achieved under milling conditions, supporting the need for solvation of the starting materials in question. However, to confirm this notion, a reaction with bismuth chloride in the presence of catalytic amounts of water should indicate if indeed water was necessary for this reaction to proceed, and this would still need to be performed. Through this mechanism, precursors would

be stimulated to dissociate into molecular units - either by reaching a critical size through mechanical attrition and/or being appreciably soluble in the liquid introduced – and then allowed to react in the solvated phase. A metastable suspension would form post-assembly, which can later desolvate and push the reaction forward in this way[1].

Using oleylamine as a ligand, we achieved the smallest NPs of $Bi_2S_3$ ever reported. Very small NPs were also obtained in Chapter 3 as shown by TEM imaging and their largely blue-shifted optical properties. Previous work in our group with Au found that ultra-small NPs could be obtained under complete solid-state conditions[2]. It is very possible that these assemblies proceed via a distinct pathway than that of solution-based methods, when in solid-state. However, with the assumption that solvent is playing a major role, it can be rationalized as such: firstly, the nominal solvent would be continuously supersaturated allowing smaller critical radii to nucleate NP growth[3]. At this stage, NP growth would eventually be impeded by ligand binding to their surface. However, given that this is performed under solid-state and therefore with reduced ligand mobility and monomer diffusion *in situ*, the NPs may cease to grow early on with bias to kinetic influence. For similar reasons, there may also be limited opportunity for Oswald ripening or aggregation to occur, which explains their surprisingly stable nature at this size regime. It would be interesting to see if this method can be adaptable to other binary systems.

Prudence must be taken when defining a mechanochemical reaction that proceeds through mechanical activation. The definition provided for mechanical activation so far describes it as a change in the physical properties of a given material that proceeds *via* four steps: accumulation of defects, amorphization, formation of metastable intermediaries and chemical reaction[4,5]. Provided that the mechanochemical processes operate in the theorized fashions aforementioned, it suggests that mechanical activation plays a role in some cases in allowing solid-state reactions to occur *in situ*. Within the context of the herein research presented, these definitions need to be more specifically defined. The reason is as follows: if structural changes in the precursors associated with milling are what allow mechanochemical reactions to proceed, this assumes that reactions that are mainly dependent on intimate mixing of the reagents (for

example, grinding the reagents gently together using a mortar and pestle) would not fall under the dogma of mechanical activation. However, given that absorption of mechanical energy takes place in this case, it should justly so, albeit not in line with theoretical aspects of what makes mechanical activation pertinent to allowing many solid-state reactions to occur. Regardless of the time it takes to achieve significant yields, if mechanical input allows the spontaneous reaction of the starting materials after the grinding is stopped, it seems to nicely fit under the convenient name of "mechanical activation", but may not necessarily be a result of introducing physical anomalies any more than reducing particle size for enough surface lability or spontaneous lattice failure into molecular constituents (assuming the precursors would otherwise go unreactive in a heterogeneous ensemble). Aging the reaction after gentle but homogeneous mixing of starting materials would give a nice indication that it proceeds via this mechanism, if the product can be obtained in realistic time. Where the reaction can be performed under gentle mortar and pestle grinding, this alludes to either it being dependent on intimate mixing of the reagents or intrinsically having low energy barriers that can be overcome by the energy input of manual grinding, though the latter would suggest it can be performed via thermal input and not *exclusively* via a mechanical one. We strongly suspect that under this mechanism - at least within the context of nanomaterial assembly - a mobile component would be necessary to provide a lower-energy well where lattice breakdown supersedes particle aggregation.

Empirical evidence from Chapter 2 and ratified by Chapter 3 suggests that the nature of the ligand used had the most influence on the product size obtained. Interestingly, while the size of the NPs obtained in Chapter 2 and 3 with oleylamine as a ligand varied depending on the metal precursor, the standard deviation of the NP sizes did not change significantly between methods. This may point to uniform ripening of the NPs in the reaction medium, albeit within a longer time scale. Given the ligands used were in excess in all cases, it may be that the ligand controls the fate of the reaction by promoting an energy minimum that is uniformly distributed across the sample. This also endorses the notion that ligand mobility is limited in solid-state, constraining the system below a certain size regime. Furthermore, all reactions in Chapter 2 and 3 did not require inert atmospheric conditions, which is not often the case in metal-sulfide syntheses. Once

again, it is possible that this reaction promotes kinetically favorable products to form, given that metal oxides are generally the more thermodynamically favorable end product.

PXRD could not identify strongly crystalline regions of the samples in all cases. Typically, nanocrystals are annealed post-synthesis to afford a more crystalline material. However, introducing heat to the system could very well affect the structure of the produced material and was therefore avoided to maintain product integrity in Chapter 3, since CdS and ZnS can adopt two main crystal forms depending on the reaction conditions and thermal input. Clear lattice fringes could be seen via TEM in all cases, suggesting that the inconclusive results on the phases of the materials produced is most likely due to the small NP sizes obtained, leading to broadening of the PXRD diffractograms.

We define the methods of synthesis presented in Chapter 2 and 3 as part of mechanical activation, whereby the energy supplied by mechanical perturbation stimulates the spontaneous assembly of these precursors overtime (i.e. aging the reaction), as opposed to the direct absorption of mechanical energy to surpass associated energy barriers and reach the final product. The reasons are as follows: (i) the nanoparticles form only after aging and not after milling; (ii) the method of grinding (ball milling or manual grinding) or grinding time is shown to not affect the product integrity (Chapter 2); (iii) changing the amount of ligand is shown to not affect the size distribution of the product obtained (Chapter 2) and (iv) the relative ratios of metal and sulfur in the produced nanomaterials are equivalent even though the sulfur precursor was added in excess, suggesting a complementary association of ions during the aging process.

In the future, we would like to explore different paths. Firstly, given the success of using PEG-$NH_2$ as a ligand in situ, it would be interesting to characterize the product obtained using only PEG-$NH_2$ as a ligand and later determine its efficacy as a contrast agent. The benefits would be twofold: first, it would develop the notion of PEGylating in situ without the need for coupling or ligand exchange reactions post synthesis. Varying the PEG:total-ligand ratio may also allow for general control of NP size obtained, depending on their application of interest. While we chose

contrast agents for our purposes, the unprecedented size of the NPs obtained and increased surface-to-volume ratio may provide a superior material for its application that are dependent on this property. It would also be interesting to determine their optical properties in the UV-Visible range and determine if they show any quantum confinement effects as well. Regarding the ZnS and CdS NP syntheses, we would like to explore the possibility of accessing water-soluble NPs *in situ* by employing a different ligand. We would also like to determine the quantum yield of the products for direct comparison with known literature. Finally, it would be interesting to confirm their bench-top stability presented (suggested from the UV-Vis and photoluminescence spectroscopy results) through transmission electron microscopy imaging.

## 5.1 References


(1) Braga, D.; Giaffreda, S. L.; Grepioni, F.; Chierotti, M. R.; Gobetto, R.; Palladino, G.; Polito, M.; Mathre, D. J.; Dormer, P. G.; Euler, D. H.; Ball, R. G.; Ye, Z.; Wang, Y.; Santos, I. *CrystEngComm* **2007**, *9* (10), 879.

(2) Rak, M. J.; Saadé, N. K.; Friščić, T.; Moores, A. *Green Chem.* **2014**, *16* (1), 86–89.

(3) Van Embden, J.; Mulvaney, P. *Langmuir* **2005**, *21* (22), 10226–10233.

(4) Baláž, P.; Achimovičová, M.; Baláž, M.; Billik, P.; Cherkezova-Zheleva, Z.; Criado, J. M.; Delogu, F.; Dutková, E.; Gaffet, E.; Gotor, F. J.; Kumar, R.; Mitov, I.; Rojac, T.; Senna, M.; Streletskii, A.; Wieczorek-Ciurowa, K. *Chem. Soc. Rev.* **2013**, *42* (18), 7571.

(5) Boldyrev, V. V.; Tkáčová, K. *J. Mater. Synth. Process.* **2000**, *8* (3/4), 121–132.